Sprayable Biofilm

–

Agarose Hydrogel as 3D Matrix for Enhanced Productivity in Bioelectrochemical Systems

Vom Promotionsausschuss der
Technischen Universität Hamburg

zur Erlangung des akademischen Grades

Doktorin der Naturwissenschaften (Dr. rer. nat.)

genehmigte Dissertation

von

Melanie Tabea Knoll

aus

Germersheim

2023

Gutachter:	Prof. Dr. rer. nat. Johannes Gescher
	Prof. Dr. rer. nat. Andreas Liese
Vorsitzender des Prüfungsausschusses:	Prof. Dr.-Ing. Martin Kaltschmitt
Tag der mündlichen Prüfung:	29.09.2023

DOI:	https://doi.org/10.15480/882.8898
Handle:	https://hdl.handle.net/11420/44463
ORCiD:	https://orcid.org/0000-0003-1009-3055

Abstract

The ongoing climate crisis highlights the need to rethink the way humanity consumes and produces resources. Bioelectrochemical systems (BES) offer the possibility of producing sustainable electricity. In these systems, electroactive microorganisms catalyze the conversion of chemical into electrical energy and vice versa. The microorganisms can utilize biological waste streams as substrate and transfer their respiratory electrons on the BES electrode, generating electricity in a sustainable manner. To facilitate this electron transfer, the organisms colonize the electrode surface in the form of a biofilm. The biofilm-electrode interaction is a key factor that can limit sufficient space-time-yield required for industrial applications. Providing the organisms with an artificial scaffold that enhances this interaction compared to the naturally formed biofilm matrix can significantly improve current production. In this work, such a hybrid biomaterial was established by embedding the electroactive model organism *Shewanella oneidensis* in an agarose hydrogel.

The BES application of the novel biohybrid material resulted in a 2-fold increase in current production in the start-up phase compared to the natural system. With the addition of riboflavin-functionalized carbon nanofibers or a second electroactive organism known for excellent BES performance, namely *Geobacter sulfurreducens*, the biomaterial was engineered to achieve a 10-fold improvement in current production, demonstrating the customizability of the biomaterial. Further, this synthetic biofilm was introduced into the BES by spraying. Thereby, a novel inoculation technique was successfully established for the effortless application of biomaterials that will facilitate scalability for industrial upscaling. In addition, the implementation of this biohybrid material in a BES-biogas system resulted in the same maximum current density as in the natural system, omitting the one-week pre-cultivation phase and therefore significantly reducing the start-up time. Finally, the detachment of the biomaterial showed that the material determines whether a partial or total detachment occurred and revealed the maximum number of electrons that can be supplied before the material degrades. The latter is an important parameter for the potential application of the biomaterial in bioelectrosynthesis, a process in which organisms grow on the cathode as a source of electrons and energy and where the biomaterial could have similar beneficial effects on productivity.

Zusammenfassung

Der fortschreitende Klimawandel verdeutlicht die Notwendigkeit eines Umdenkens in Bezug auf die anthropogene Ressourcennutzung. Bioelektrochemische Systeme (BES) ermöglichen eine nachhaltige Stromerzeugung durch den Einsatz elektroaktiver Mikroorganismen als Katalysatoren für die Umwandlung von chemischer in elektrische Energie. Die Organismen können Abfallströme als Substrat nutzen und ihre Atmungselektronen auf die BES-Elektrode übertragen und so auf nachhaltige Weise Strom erzeugen. Um diese Elektronenübertragung zu erleichtern, besiedeln die Organismen die Elektrodenoberfläche in Form eines Biofilms. Dabei ist die Biofilm-Elektroden Interaktion der Schlüsselfaktor in der Anwendung von BES. Durch die Bereitstellung eines synthetischen Gerüsts in Form eines Hydrogels, das die natürliche Biofilm-Matrix ersetzt, kann die Interaktion und damit die Stromerzeugung verbessert werden. In dieser Arbeit wurde ein solches Biomaterial durch die Einbettung des elektroaktiven Organismus *Shewanella oneidensis* in ein Agarose-Hydrogel hergestellt.

Die BES-Anwendung des neuartigen Biomaterials führte in der Startphase zu einer Verdoppelung der Stromproduktion im Vergleich zum natürlichen System. Durch Zugabe von Riboflavin-funktionalisierten Kohlenstoff-Nanofasern oder *Geobacter sulfurreducens*, einem weiteren elektroaktiven Organismus, konnte das Biomaterial so funktionalisiert werden, dass eine 10-fach verbesserte Stromproduktion erreicht wurde. Außerdem wurde das Biomaterial auf die Elektrode aufgesprüht, wodurch eine neue Inokulationstechnik für die einfache Applikation von Biomaterialien etabliert wurde, die eine Hochskalierung für die industrielle Anwendung ermöglicht. Weiterhin resultierte die Anwendung des Biomaterials in einem gekoppelten BES-Biogassystem in der gleichen maximalen Stromproduktion wie das natürliche System, wobei die einwöchige Vorkultivierungsphase entfiel und somit die Inbetriebnahme erheblich verkürzt wurde. Die induzierte Ablösung des Biomaterials zeigte weiterhin, dass das Elektrodenmaterial entscheidend für den Grad der Ablösung ist und die maximale Anzahl an Elektronen, die zugeführt werden können bevor eine Ablösung des Biomaterials eintritt, wurde bestimmt. Dies ist ein wichtiger Aspekt für Anwendungen in der Bioelektrosynthese, einem Prozess, bei dem Organismen auf der Kathode als Elektronen- und Energiequelle wachsen und bei dem die Anwendung des hier entwickelten Biomaterials ebenfalls positive Auswirkungen auf die Produktivität haben könnte.

Table of Contents

Table of Figures

Table of Figures

List of Tables

Abbreviations

AD	anaerobic digestion
BES	bioelectrochemical system
CNFs	carbon nanofibers
CPE-K	conjugated polyelectrolyte
ddH_2O	double-distilled water
DET	direct electron transfer
E	redox potential
EAB	(exo)electroactive bacteria
EET	extracellular electron transfer
EIS	electrochemical impedance spectroscopy
EPS	extracellular polymeric substances
IF	improvement factor
M	molar concentration [mol L^{-1}]
MEC	microbial electrolysis cell
MES	microbial electrochemical system
MESC	microbial electrosynthesis cell
MET	mediated electron transfer
MFC	microbial fuel cell
OCT	optical coherence tomography
$OD_{600\ nm}$	optical density with λ = 600 nm
PBS	phosphate buffered saline
PEDOT:PSS	poly(3,4-ethylenedioxythiophene):poly(styrenesulfonate)
PEEK	polyetheretherketon
PMBVF	poly(2-methacryloyloxyethyl phoshorylcholin-*co*-*n*-butyl metha-crylate-*co*-*p*-vinylphenylboronic acid-*co*-vinylferrocene)
RFP	red fluorescent protein
SEM	scanning electron microscopy
SHE	standard hydrogen electrode
VFA	volatile fatty acids

1 INTRODUCTION

Humanity is exhausting natural resources faster than the Earth can replenish them. The so-called Earth Overshoot Day marks the exact day in each year on which mankind's demand for resources exceeds the biocapacity of the planet. While this day occurred on December 25th in 1971, last year's Overshoot Day was already on July 28th (Global Footprint Network, 2022), which underlines the importance of rethinking the way we produce and consume. Thus, economic valorization has to align with ecological guidelines to achieve the required sustainability. This is especially true for the electricity sector, as this resource is central to modern life and essential for the necessary shift to clean energy. While global electricity demand was still at around 7 petawatt hours in 1980, it has risen to a new record high of about 23 petawatt hours in 2019 (International Energy Agency, 2019). The rapid increase of 0.5 petawatt hours per year in the last 20 years is especially significant (Figure 1).

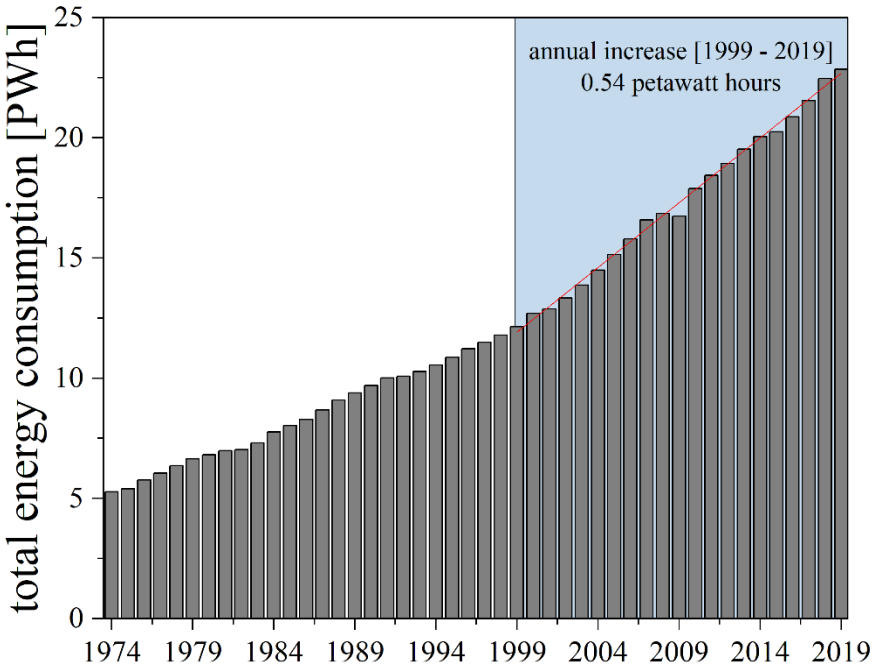

Figure 1: Global energy demand from 1974 to 2019. While annual energy demand was reported to be around 7 petawatt hours in 1980, this value is rising rapidly to around 23 petawatt hours in 2019. The annual increase of 0.54 petawatt hours in the last 20 years was particularly significant. This underlines the need for more efficient power generation technologies (modified from International Energy Agency, 2019).

As a result, more efficient technologies that meet this increasing demand and allow for sustainable electricity production must be developed and established. In addition to renewable energy sources such as wind, water and solar power, biotechnology likewise offers possibilities for harnessing renewable sources in the interests of sustainability. One such biotechnological process involves bioelectrochemical systems (BES) in which chemical energy is converted into electrical energy - and vice versa. This enables previously unexploited biological waste streams to be unlocked as resources and utilized to generate electricity. Further, this interdisciplinary technology, operating at the interface of biology and electrochemistry, enables the conversion of these waste substrates into industrially relevant chemicals, in some cases even generating electricity only as a by-product. For this purpose, microorganisms are used as biocatalysts and the direct interaction of these organisms with the electrode is crucial for the nature of the process. This thesis focuses on improving this interaction by means of synthetic biology and thus on improving BES technology as a whole. In the following chapters, the BES technology is introduced with its biochemical background and a focus on the interface between microorganism and electrode surface, before the synthetic approach chosen for this thesis is outlined.

1.1 **Bioelectrochemical systems**

The conversion of chemical energy into electrical energy and vice versa can be realized in BES. In general, these systems consist of an anode at which oxidation takes place and a cathode at which reduction takes place. When this conversion is catalyzed by microbial organisms, the systems are referred to as microbial electrochemical systems (MES). The first report of microbial conversion of chemical into electrical energy dates back to 1911 (Potter, 1911). Only twenty years later was this phenomenon confirmed by Cohen, who reported the first MES with a voltage of 35 V at a current of 0.2 mA (Cohen, 1931). In the following years, the development of industrial applications for MES stagnated due to low performance and practicability at that time (Schröder, 2011). However, with the climate change-driven motivation to develop alternative energy production and conversion methods, the importance of this technology has become evident since the turn of the century (Schröder, 2011).

1.1.1 **Basics of bioelectrochemical processes**

To understand the basic principles of BES, it is essential to be aware of the direct link between microbial metabolism and electric current. The metabolic reactions of all life are coupled to redox reactions to promote countless biochemical processes (Canfield *et al.*, 2005). A redox reaction is the type of chemical reaction during which a substrate changes its oxidation state by donating or accepting electrons to a reactant. Whether a chemical species can accept or donate electrons is described by the electrode or redox potential E. Microorganisms carry out their metabolism by transferring electrons from a species with a lower E (electron donor) to a species with a higher E (electron acceptor). The energy gained by this redox reaction, more precisely the change in Gibbs free energy (ΔG), can be calculated from the redox potential of donor and acceptor (ΔE), the number of electrons transferred in the redox reaction (n) and Faraday's constant (F; Equation 1).

$$\Delta G = - n F \Delta E \quad \text{with } \Delta E = E_{acceptor} - E_{donor} \qquad (1)$$

This results in the amount of work that can be gained for microbial metabolism by shuttling electrons from the donor to the acceptor. When an external electron acceptor is reduced, such as oxygen or nitrate, this process is called respiration and energy is mostly gained via oxidative phosphorylation. In contrast, fermentation generates energy mostly by substrate level phosphorylation (Canfield *et al.*, 2005). In a MES, so-called electroactive microbes can either utilize the anode as external electron acceptor (exoelectrogenic organisms) or the cathode as electron donor (electrotrophic organisms) to drive their metabolism (Logan and Rabaey, 2012). In this process, the microorganisms catalyse the oxidation or reduction reactions that occur at the anode or cathode. For this catalysis to take place, the organisms colonise the electrode surface in the form of a biofilm (see section 1.2.3). Several variants of MES that enable this catalysis are discussed in section 1.1.2. It should be noted that although microorganisms are referred to as biological catalysts in MES, this is not entirely correct, as ohmic losses due to electron transfer from microorganisms to anode or cathode are to be expected. This is evident when considering, for example, acetate degradation in MES. If acetate is converted by microorganisms under oxic conditions, the energy gain can be calculated in accordance with Equation 1. Four electrons are transferred from acetate as donor

(E_{donor} = -0.3 V) to oxygen (O_2) as acceptor ($E_{acceptor}$ = 0.8 V), whereby the redox potentials for donor and acceptor can be taken from literature (e.g. Thauer *et al.*, 1977). With a potential difference ΔE of 1.1 V, correspondingly -425 kJ/mol are released by this redox reaction, which are available to the organism. In a BES, however, this amount can never be generated as current, since the electrode transfer of chemical species via microorganisms to the anode and cathode takes place spatially separated, which leads to potential and corresponding energy losses (Rabaey and Verstraete, 2005). In addition, the microorganisms naturally use part of the energy gained for their anabolism, i.e. the process in which cell components are synthesized, and this also reduces the amount of energy that can be generated as electricity in BES (Canfield *et al.*, 2005). Accordingly, BES technology enables the (partial) utilization of previously inaccessible microbial metabolic processes in the context of electrochemistry to convert chemical energy into electrical energy and vice versa, thus creating new process flows in the context of sustainability.

1.1.2 **Variants of bioelectrochemical systems**

MES are usually divided into anodic and cathodic systems, whereby the localization of the microbial catalyst is decisive. In anodic MES, the exoelectrogenic microorganisms oxidize organic and/or inorganic substrates as electron donors and transfer their respiratory electrons to the anode as external electron acceptors. This external electron transfer (EET) is specific for each organism and the molecular mechanisms are discussed in section 1.2.2. Simultaneously, protons are generated due to the oxidation reaction in the anode chamber that migrate to the cathode to maintain the charge balance. Mostly to prevent O_2 diffusion to the anode chamber, anode and cathode compartment are often separated by a proton or anion exchange membrane, whereas the latter is considered more efficient due to lower internal resistance (Sleutels *et al.*, 2009). The electrons flow through an external circuit to the cathode, whereby MES technology can be further differentiated into microbial electrolysis cells (MECs) and microbial fuel cells (MFCs).

In a MEC, the electrons flow through an external power supply circuit to the cathode (Figure 2, B). Due to the additional power supply, the cathodic potential is sufficient to reduce protons at the cathode and hydrogen (H_2) is produced (Liu *et al.*, 2005; Rozendal *et al.*, 2006b). Hence, the current production in MECs directly correlates with H_2 production at the

cathode (Kadier *et al.*, 2019). Remarkably, H_2 production using MEC requires less energy input (E = 0.2 – 0.8 V) compared to conventional electrolysis from H_2O (E > 2.1 V) and the catalysis of the microorganisms in this BES supports thermodynamically unfavorable reactions to value-added products (Zhang and Angelidaki, 2014). Contrary to MECs, the electrons in MFCs flow from the anode through an external resistor, while a terminal electron acceptor, in most cases O_2, is reduced on the cathodic side (Figure 2, B). The resulting voltage leads to the generation of electricity. However, if no oxygen or similar electron acceptor is present in the cathodic compartment, electricity is not generated. This establishes a link between MFCs and MECs, since in the latter, current generation in the absence of an electron acceptor in the cathode compartment is forced by applying small voltages (E > 0.2 V) as mentioned above, which leads to the reduction of protons and accordingly to the formation of hydrogen (Logan *et al.*, 2008).

In cathodic MES, however, the electron flow is reversed in such a way, that a reductive current can power a biological process on the cathodic side (Figure 2, C). Here, the electrotrophic microorganisms utilized the cathode as electron donor. Power is utilized for the electrolysis of H_2O in the anode compartment, providing the electrons for the organisms in the cathode compartment. Compared to MECs, cathodic MES require a higher energy input to achieve the electrolysis of H_2O at the anode, however, the acceptance of electrons at the cathode is carried out directly via reverse EET processes or mediated via H_2 (Rabaey and Rozendal, 2010; Lovley, 2011). Due to the biotic catalysis of the reduction reaction at the cathode, the corresponding energy input is therefore lower compared to abiotic H_2O electrolysis due to lower required potential differences. In most cases, the fixation of CO_2 in these so-called microbial electrosynthesis cell (MESC) is catalyzed either alongside with the reduction of O_2 or directly with CO_2 as the final electron acceptor for the production of biomass or multicarbon compounds (Nevin *et al.*, 2010; Rabaey and Rozendal, 2010).

In both anodic and cathodic MES, the interaction of the microorganisms with the electrode, and in particular the transfer of electrons to and from the electrode, is crucial. There is a large number of MES variants, each specified for the application objective they are to fulfil, and reactor systems built for precisely those optimized applications are described in detail elsewhere (Krieg *et al.*, 2014; Kadier *et al.*, 2016; Mohanakrishna *et al.*, 2017; Bhargavi *et al.*, 2018). Since this thesis revolves around the improvement of anodic MES processes,

cathodic MES will not be discussed in the following. Accordingly, reviews addressing the application and recent advances of MESC are referenced here (Lovley and Nevin, 2013; ElMekawy *et al.*, 2016; Jourdin and Burdyny, 2021; Bakonyi *et al.*, 2023).

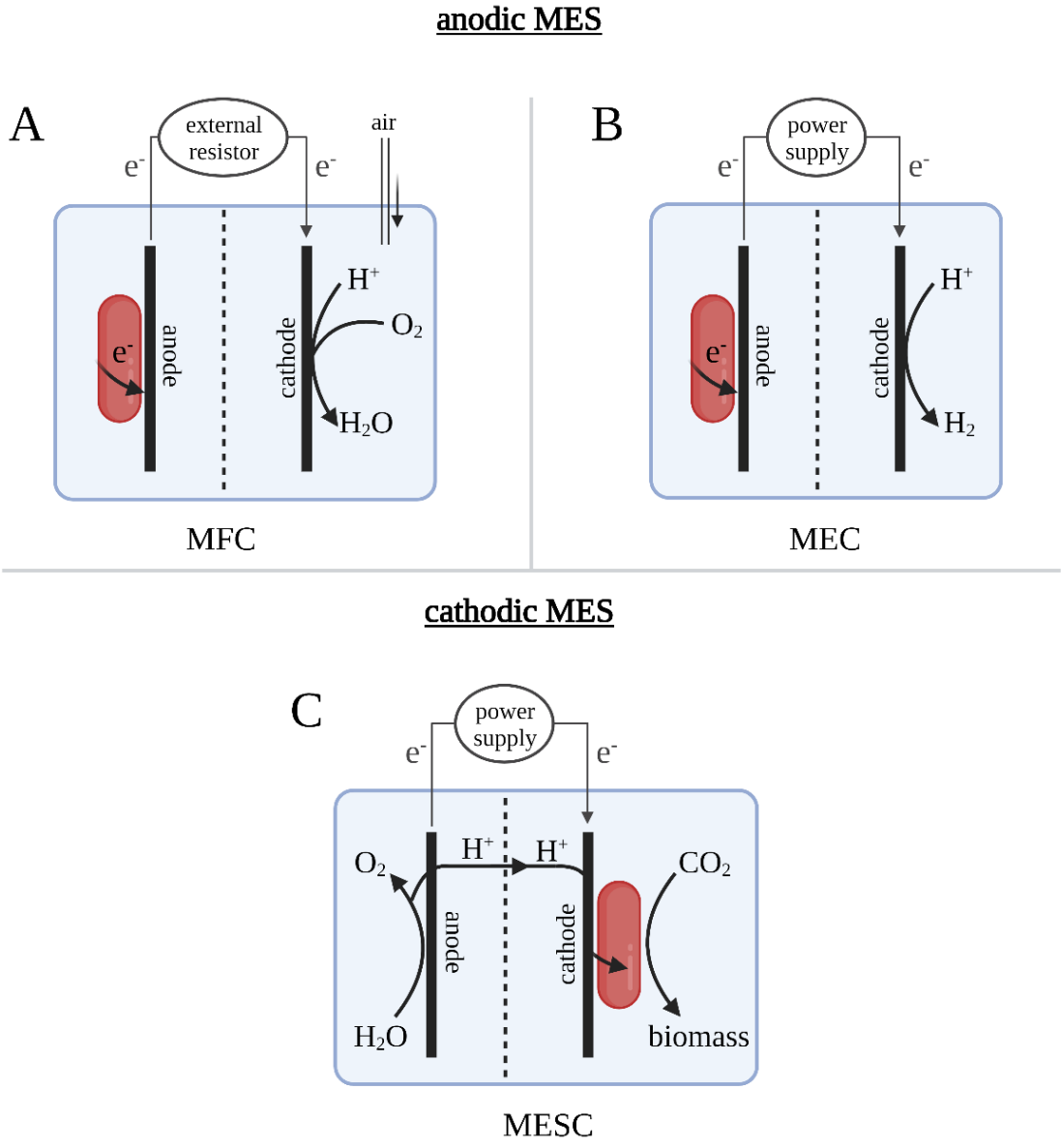

Figure 2: Microbial electrochemical systems utilizing the microbial catalysis of anodic oxidation (anodic MES) or cathodic reduction (cathodic MES). In anodic MES, the microbes transfer their respiratory electrons to the anode as the terminal electron acceptor. The electrons flow through an external resistor (microbial fuel cell, MFC) or an additional power supply circuit (microbial electrolysis cell, MEC) to the cathode, where the reduction of either O_2 or protons takes place. The additional power supply in MEC allows for the formation of H_2 on the cathode. In cathodic MES, microbes use the cathode as an electron donor for the reduction of CO_2 to produce biomass or multicarbon compounds. For this purpose, a reduction current provided by an additional current source enables the electrolysis of H_2O in the anode compartment (modified from Klein *et al.*, 2023).

1.2 Interaction of exoelectrogenic organisms with BES electrodes

The interaction, and in particular the transfer of electrons to or from an electrode, provides the basis of BES technology, and the performance of BES is directly linked to the efficiency of this interaction. To illuminate this in more detail, the following chapter gives a brief insight into the molecular mechanism of EET for the exoelectrogenic organisms *Shewanella oneidensis* and *Geobacter sulfurreducens* studied in this thesis and their interaction with the BES electrode through biofilm formation. However, there is an enormous number of electroactive organisms (Logan, 2009; Koch and Harnisch, 2016; Logan *et al.*, 2019) and the molecular mechanisms behind EET are being intensively researched for each of them (Light *et al.*, 2018; Paquete, 2020; Edel *et al.*, 2022).

1.2.1 Basic mechanisms of extracellular electron transfer

As already mentioned, the first electrical potential generated by microorganisms was already reported back in 1911 (Potter, 1911). However, the molecular mechanisms that enable this conversion of chemical to electrical energy were not uncovered until much later, when exoelectrogenic organisms of the genus *Shewanella* and *Geobacter* were isolated that were shown to perform EET (Lovley and Phillips, 1988; Myers and Nealson, 1988). In nature, the ability to perform EET enables the utilization of abundant insoluble minerals such as iron and manganese oxides as electron acceptors. This allows exoelectrogenic organisms to thrive in an ecological niche where O_2 as an electron acceptor is limited or absent, and still obtain energy from respiration processes. In general, there are three different ways for organisms to transfer their electrons to an electrode (Figure 3). First, electron transfer can be facilitated via produced soluble electron shuttles, which is referred to as mediated electron transfer (MET). Second and thirdly, direct electron transfer (DET) is performed either by short-range transfer using redox-active molecules, namely *c*-type cytochromes, located on the cell surface or long-range transfer using conductive cell appendages including pili and/or nanowire filaments (Lovley, 2012).

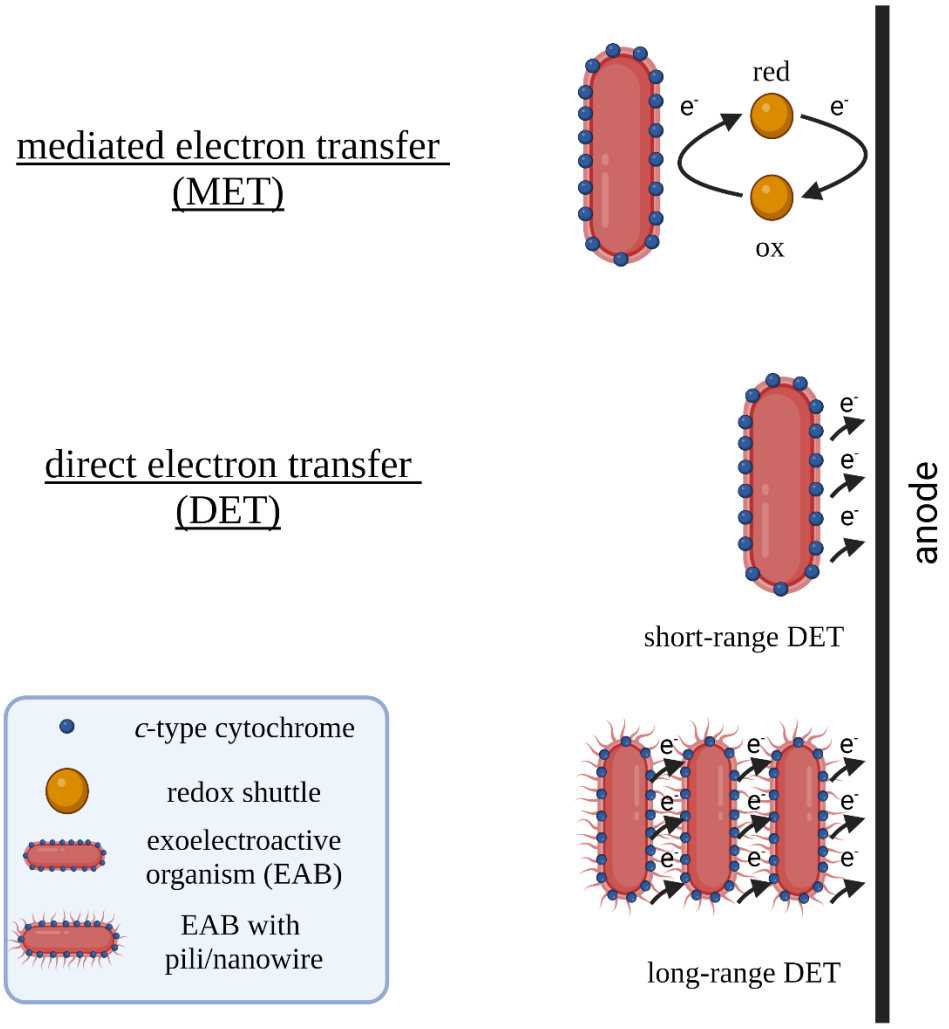

Figure 3: Mechanisms of extracellular electron transfer (EET). Three possibilities for EET are known to be performed by exoelectroactive bacteria (EAB). Electron transfer can be facilitated using soluble redox shuttles, that are reduced by the organism and regenerated at the anode (mediated electron transfer, MET). Direct electron transfer (DET) can be performed via redox-active molecules (*c*-type cytochrome) located in the outer membrane of EAB (short-range DET) or via conductive cell appendages including pili and/or nanowires (long-range DET; modified from Lovley, 2012).

For short-range DET, spatial proximity between the *c*-type cytochrome and the insoluble electron acceptor of no more than 10 Å is required for direct electron hopping (Neal *et al.*, 2003; Kerisit *et al.*, 2007). This means that for short-range DET in BES, the organisms must adhere directly to the electrode surface or to each other for direct cell-to-cell electron transfer, which means that only a limited number of bacteria can colonize the electrode. The layer of cells is therefore limited in the amount of current it can generate due to the limited area of the electrode surface (Lovley, 2012). Long-range DET, on the other hand, is facilitated by

conductive pili and/or nanowires. These cell appendages form an electronic network that enables electron transfer across multiple cell layers (Reguera *et al.*, 2006). Accordingly, conductive biofilms (see section 1.2.3) formed by organisms capable of long-range DET have been found to result in higher current densities (current generated per electrode area) in BES systems than organisms capable of only short-range DET. The best studied organisms for EET are *S. oneidensis* and *G. sulfurreducens*, both of which were employed in this thesis which is why their molecular mechanisms for EET is discussed in the following section.

1.2.2 **Molecular background for EET in *S. oneidensis* and *G. sulfurreducens***

S. oneidensis MR-1 is a Gram-negative, facultative anaerobic γ-proteobacterium (Venkateswaran *et al.*, 1999) first noted for its ability to reduce manganese oxide after its isolation from Oneida Lake in New York State, USA (Myers and Nealson, 1988). Meanwhile, *G. sulfurreducens* PCA was isolated from the sediment of a hydrocarbon-contaminated ditch in Oklahoma and associated with the dissimilatory reduction of metal ions (Caccavo *et al.*, 1994). As already mentioned, both organisms were later applied in BES due to their ability to perform EET.

The respiratory electrons are collected in the quinone pool and subsequently transferred to the tetraheme cytochrome CymA in *S. oneidensis* (Gescher *et al.*, 2008; McMillan *et al.*, 2012; Figure 4, A) or to the nonaheme cytochromes ImcH and CbcL in *G. sulfurreducens* (Zacharoff *et al.*, 2016; Figure 4, B). For the onward transport of electrons, the gap between the inner and outer membrane must be passed by the electrons via the periplasm. This is facilitated by a network of soluble *c*-type cytochromes, namely FccA and STC or PpcA in the case of *S. oneidensis* and *G. sulfurreducens*, respectively (Lloyd *et al.*, 2003; Fonseca *et al.*, 2013; Sturm *et al.*, 2015). Electron transport across the outer membrane occurs via electron conduits consisting of an integral β-barrel protein and two *c*-type cytochromes located at the inside and the outside of the outer membrane. In *S. oneidensis*, this electron conduction is carried out by MtrABC (Hartshorne *et al.*, 2009), while in *G. sulfurreducens* several different conduits are found. However, ExtABCD was found to be the main conduit for the EET performed in BES (Otero *et al.*, 2018). In contrast to *S. oneidensis*, where the EET chain terminates with MtrC and the secondary outer membrane cytochrome OmcA, *G. sulfurreducens* was shown to have conductive nanowires that allow EET over several

micrometers in length. The conductivity of the nanowires has long been attributed to pili filaments decorated with *c*-type cytochromes, however the molecular nature of the nanowires has been a matter of controversy in the literature (Filman *et al.*, 2019; Lovley and Walker, 2019; Wang *et al.*, 2019; Gu *et al.*, 2021). Although pili filaments free of other proteins or metals have been reported to exhibit considerable conductivities (Adhikari *et al.*, 2016; Lovley, 2017), recently the long-suspected pili filaments were crystallized in their atomic structure and found to be polymerized cytochromes (Wang *et al.*, 2023). Interestingly, both terminal reductases of *S. oneidensis* and *G. sulfurreducens* were found to contain flavin as a cofactor (Okamoto *et al.*, 2013; Okamoto *et al.*, 2014; Xu *et al.*, 2016).

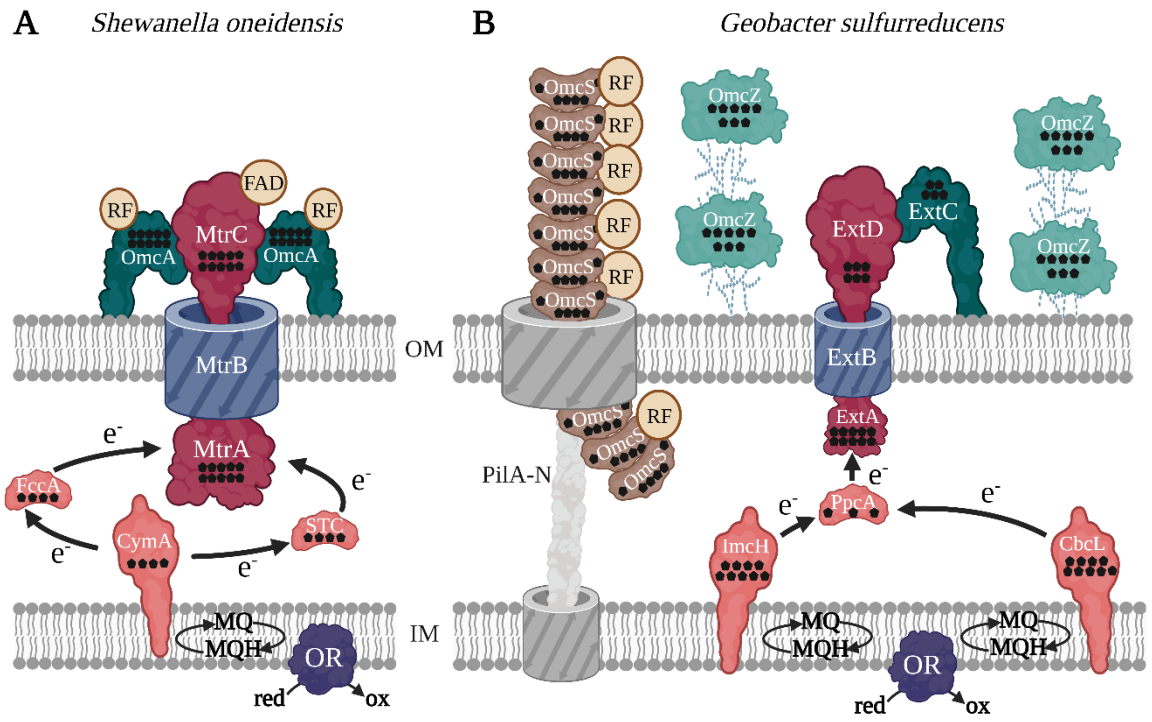

Figure 4: Molecular mechanism of EET in *Shewanella oneidensis* (A) and *Geobacter sulfurreducens* (B). IM: inner membrane, OM: outer membrane, ♦: number of heme cofactors in *c*-type cytochrome, OR: oxidoreductase, FAD: flavin adenine dinucleotide, RF: riboflavin. A) EET in *S. oneidensis*. Electrons are transferred through the periplasm via CymA, FccA and STC to the MtrABC complex. RF and FAD act as co-factors and MtrC and OmcA are the outer membrane cytochromes that facilitate EET to insoluble electron acceptors. B) EET in *G. sulfurreducens*. ImcH and CbcL are the inner membrane cytochromes that transfer their electrons to the soluble cytochrome PpcA. The pre-dominant complex ExtABCD facilitates EET across the outer membrane and conductive type IV pili decorated with cytochromes OmcS/OmcZ allow EET over several micrometers in length (modified from Edel *et al.*, 2022 and Klein *et al.*, 2023).

For *S. oneidensis*, the production of electron shuttles in the form of flavins could be demonstrated (Canstein *et al.*, 2008; Okamoto *et al.*, 2014). Flavins of *S. oneidensis* are reduced by the outer membrane cytochromes MtrC or OmcA and MET between bacterium and electrode can be carried out. Although short-range DET by means of these *c*-type cytochromes is also possible for *S. oneidensis* (Baron *et al.*, 2009), it has been shown that the presence of flavins significantly increases the current production (Jiang *et al.*, 2010). Thus, MET processes contributed to the major part of current production by this organism in BES. In contrast, *G. sulfurreducens* was found to exhibit conductive pili/nanowires, which enables this organism to perform long-range DET over greater distances (up to 20 µm; Lovley and Holmes, 2020) compared to *S. oneidensis*. With this in mind, and as will be discussed in the next section, it seems reasonable that the attachment and colonization of the BES electrode differs significantly between the two model organisms.

1.2.3 **Biofilm formation of exoelectrogenic model organisms**

Microorganisms are grown and studied in the laboratory using planktonic cell culture, in which individual cells are cultured in a liquid media suspension. In nature, however, most microorganisms grow in aggregated forms which accumulate at interfaces and are called biofilms (Wingender *et al.*, 1999) . In general, a biofilm describes a self-produced matrix of extracellular polymeric substances (EPS) in which the organisms are embedded (Flemming and Wingender, 2010). This EPS matrix is formed by polysaccharides, proteins, nucleic acids and lipids which form a three-dimensional scaffold. Further, the cells embedded in this network are interconnected and transiently immobilized on the interface at which a biofilm is formed (Flemming *et al.*, 2016). The formation of a biofilm usually starts with the adherence of free-living, planktonic cells to the corresponding surface. Next, the attached organisms start to proliferate and produce the EPS matrix. After the maturation of the matrix, the cells are irreversibly attached to the surface, however, dispersion of single, then again free-living cells has been reported (Sauer *et al.*, 2002; O'Toole *et al.*, 2003; Sauer *et al.*, 2022). With regard to biotechnological applications, biofilms offer the possibility of immobilizing a large number of cells in a small volume (Morgan-Sagastume *et al.*, 2008). Dynamic nutrient exchange between the different biofilm layers, simplified cellular communication and higher resistance to harsh environmental conditions are facilitated by

biofilm growth (Costerton *et al.*, 1995; Donlan, 2002; Flemming *et al.*, 2016). However, as height of the biofilm increases, diffusion limitations may occur (Renslow *et al.*, 2010) and the lower layers of the biofilm may not be adequately supplied with nutrients.

Against this background, electroactive bacteria (EAB) are shown to proliferate in BES on the anode and cathode in the form of a biofilm at the interface of the electrode. While biofilms studied in BES have first been described to have insulating characteristics (Herbert-Guillou *et al.*, 1999; Dheilly *et al.*, 2008), the findings of long-range DET via nanowires in *G. sulfurreducens* biofilms introduced the concept of conductive biofilms (Lovley, 2011; Malvankar *et al.*, 2011). Accordingly, biofilms in which many cell layers simultaneously contribute to current production with a biofilm thickness of up to 100 µm have been reported (Franks *et al.*, 2010; Torres *et al.*, 2010; Malvankar *et al.*, 2012). Hence, the conductivity of an anodic biofilm can be directly linked to the total current generated by the biofilm-forming organisms (Malvankar and Lovley, 2012). With increasing biofilm thickness, short-range DET therefore becomes less relevant, as only a limited number of cells are in direct contact with the electrode, whereas long-range DET enables electron transfer even in biofilms with greater thickness. Further, MET is limited above a certain biofilm height due to diffusion limitations in multilayered biofilms, which prevent optimal use of the redox shuttles.

Consequently, *G. sulfurreducens* is reported to produce higher current densities in BES compared to *S. oneidensis*. The latter was shown to form rather thin biofilms on a BES electrode (Biffinger *et al.*, 2009) that further were less conductive compared to *G. sulfurreducens* biofilms (Malvankar and Lovley, 2012). This can be attributed to the aforementioned characteristic of *S. oneidensis* to rely mainly on MET and short-range DET, both of which limit biofilm height and consequently current output by diffusion limitations or physical proximity requirements. Although the overall current performance of *G. sulfurreducens* naturally exceeds that of *S. oneidensis*, the genetic accessibility of the latter organism still makes it an excellent candidate for BES applications. This allows modification of the genetic background and custom optimization for improved application properties of this organism. In addition, the oxygen tolerance and the possibility to expand the substrate spectrum of *S. oneidensis* using genetic engineering are advantages that support the industrial use of the organism. The comprehensive knowledge of the molecular mechanisms of *S. oneidensis* compared to all other exoelectrogenic organisms further

facilitates the modification of the EET process in *S. oneidensis* for easier optimization. Therefore, intensive research has been carried out to improve the overall performance of *S. oneidensis* biofilms using genetic engineering and synthetic biology (see section 1.4). The aim of this research is to connect as many cells as possible to the electrode in order to improve the overall current performance and enable an industrial application of this organism. In the following chapter, the most common applications of BES are first highlighted before possible optimization strategies to improve the performance of *S. oneidensis* are introduced.

1.3 Application of bioelectrochemical systems

To highlight the relevance of MES technology, the range of application examples will be discussed in this section. The most common application of MES is their intended use in wastewater treatment (Figure 5, A). Wastewater is produced in practically all industrial processes, and the conventional treatment of industrial, but also municipal, wastewater requires enormous amounts of energy. However, it is known that the residual energy contained in wastewater exceeds the amount needed for its treatment by a factor of 2 to 4 (Koul *et al.*, 2022). MFCs and also MECs are applied in conventional wastewater plants to enable the degradation of organic compounds into CO_2, water and energy. Besides the removal of organics, the recovery and production of value-added compounds such as bioplastics, biosurfactants and biofuels is realized in MES and various types of wastewater have been suggested as substrates for this conversion (Pandey *et al.*, 2016; Ding *et al.*, 2017; Hiegemann *et al.*, 2019; Koul *et al.*, 2022).

For example, one of these substrates is utilized in coupled systems, exploiting MECs for anaerobic digestion processes. Anaerobic digestion (AD) describes the process of decomposition of organic material by microbes in an oxygen-deficient environment to produce a mixture of gases (biogas), mainly methane (CH_4) and CO_2 (Achinas *et al.*, 2020). Thereby, CO_2 reduces the quality of the biogas as a biofuel, and several biogas upgrading processes are used to remove CO_2 from the gas mixture. The introduction of a MEC system within AD processes was shown to boost substrate degradation or stabilize methane production (Cerrillo *et al.*, 2018; Yu *et al.*, 2018). The latter is due to the introduced cathode and the corresponding influence of the additional H_2 supply on methane production. CH_4 can be converted directly from CO_2 and H_2, the latter of which can be provided

bioelectrochemically. Thus, it has been reported that the addition of BES in AD processes could increase the CH_4 content up to 98 % (Bo *et al.*, 2014). The increase in substrate degradation can be attributed to the additional removal of volatile fatty acids (VFA) such as acetate, butyrate and propionate. While the accumulation of VFA in AD processes may indicate process instability, the additional electron acceptor in the form of the MEC anode offers the possibility of enhanced removal of volatile fatty acids (Cerrillo *et al.*, 2016).

The most obvious application for MEC is the use of this technology for H_2 formation (Figure 5, B). In this context, the importance of H_2 as an alternative and particularly clean biofuel for the transport sector instead of fossil fuels should be emphasized (Schrope, 2001). As already mentioned, H_2 can be produced in MEC with much lower energy input compared to conventional H_2 production processes including electrolysis from water. Conventional H_2 production can also be achieved using fermentation technology, however, the efficiency of this so-called dark fermentation in terms of H_2 production remains relatively low (< 15 %, Angenent *et al.*, 2004). The substrates are mainly converted into undesired by-products, mainly VFA, which, as mentioned above, can indeed be utilized in MFC for current (Freguia *et al.*, 2010) and in MEC for H_2 production (Yang *et al.*, 2015b). Accordingly, MES technology should be considered in combination with dark fermentation processes as well to maximize H_2 production. Besides this, various substrates including non-fermentable organic acids, lignocellulosic biomass besides wastewater from both domestic and industrial origins have been utilized for the production of H_2 using MEC (Kadier *et al.*, 2014).

Another application example for anodic MES technology is their use as biosensors (Figure 5, C). Biosensors are generally defined as devices capable of providing (semi-)quantitative analytical information using a biological recognition element that is in direct spatial contact with an electrochemical transduction element (Thevenot *et al.*, 1999). When an analyte is metabolized by the microorganisms in an MFC, an electrical output is generated in relation to the concentration of that compound, enabling the use of MFCs as transducers in biosensors (Sun *et al.*, 2015). MFC biosensors have been established for the detection of fermentable compounds such as arabinose (Golitsch *et al.*, 2013), toxicants (Stein *et al.*, 2012), biochemical oxygen demand (Chang *et al.*, 2004), VFA content in AD processes (Kaur *et al.*, 2013) among others (Yang *et al.*, 2015a; Ivars-Barceló *et al.*, 2018). Through electrochemical analyses such as cyclic voltammetry, it was even possible to distinguish between the

individual VFA species and their respective concentrations (Kaur *et al.*, 2013), which provides insight into the monitoring capabilities of these biosensors.

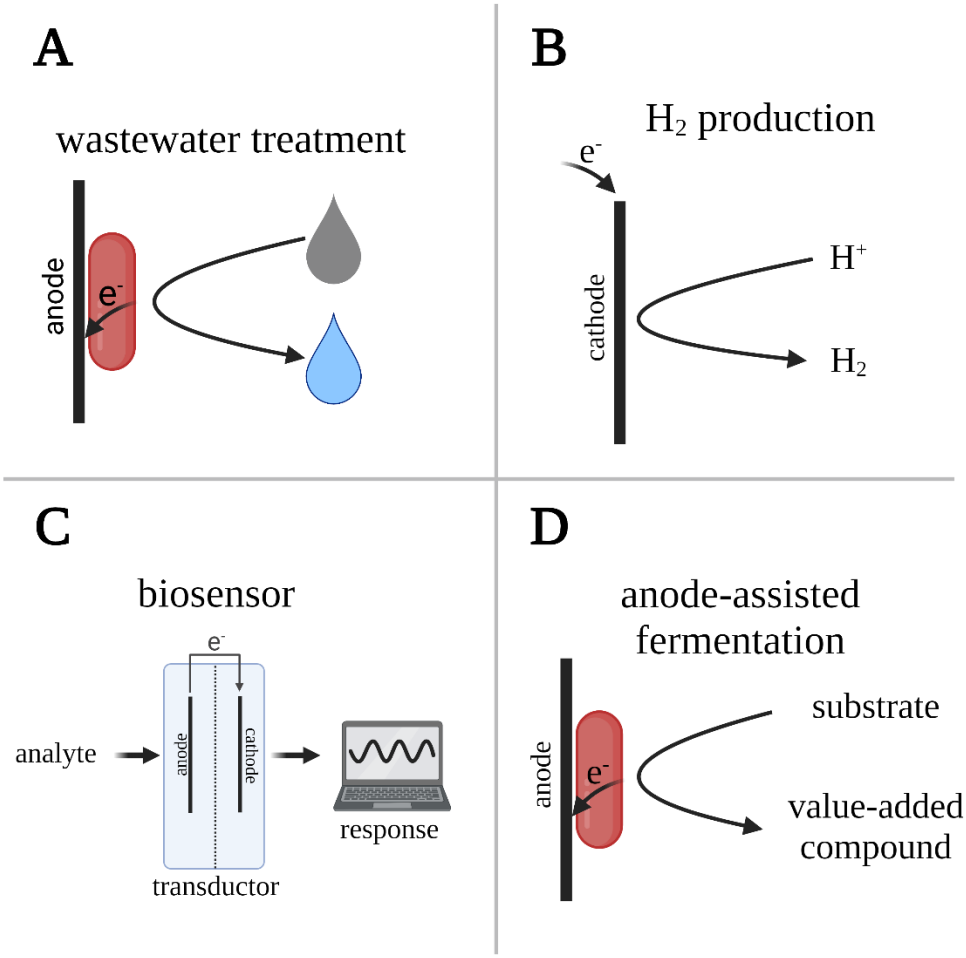

Figure 5: Applications of MES technology. A) Wastewater treatment. MFCs and also MECs are applied in conventional wastewater plants to enable the degradation of organic compounds into CO_2, water and energy. Besides the removal of organics, the recovery and production of value-added compounds such as bioplastics, biosurfactants and biofuels is realized in MES. B) Hydrogen production. H_2 can be produced in MEC with much lower energy input compared to conventional H_2 production processes including electrolysis from water. C) Biosensor. When an analyte is metabolized by the microorganisms in an MFC, an electrical output is generated in relation to the concentration of that compound, enabling the use of MFCs as transducers in biosensors. MFC biosensors have been established for the detection of fermentable compounds, toxicants and biochemical oxygen demand among others. D) Anode-assisted fermentation. To overcome the thermochemical limitations of anaerobic fermentations, the possibility to introduce an additional electron acceptor for the organisms to dissipate a surplus of electrons is offered by BES. This enables the formation of value-added products that in total have a higher oxidation state than the given substrate, and the anode-assisted fermentation for ethanol and acetoin, two platform chemicals of industrial relevance, was demonstrated.

Further application of MES technology is facilitated in the anode-assisted fermentation of value-added compounds (Figure 5, D). In most anaerobic fermentation processes, redox imbalances are observed that limit the efficiency of converting the given substrate into the desired product (Humphrey and Lee, 1992). To overcome the stoichiometric limitations of anaerobic fermentations, the possibility to introduce an additional electron acceptor for the organisms to dissipate a surplus of electrons is offered by BES (Palma-Delgado *et al.*, 2020). This enables the fermentation of value-added products that in total have a higher oxidation state than the given substrate, and the anode-assisted fermentation of e.g., ethanol (Flynn *et al.*, 2010; Sturm-Richter *et al.*, 2015) and acetoin (Bursac *et al.*, 2017; Förster *et al.*, 2017; Beblawy *et al.*, 2020) from glycerol and glucose, an otherwise unbalanced process, could be successfully established. For all these applications, the optimized interaction of microbes with the electrode surface is essential to achieve the space-time yields required for industrial application processes.

1.4 Optimizing the microbe-electrode interaction

As stated before, the interaction of microorganism with the electrode is of upmost importance for unlocking BES technology for industrial applications. The efficiency of this interaction is linked in the balance between connecting as many cells as possible to the electrode for optimized electron transfer and the mass transfer in biofilms due to diffusion limitations of substrates and products. For the model organism *S. oneidensis*, the increase in biofilm thickness and more so conductivity as well as the improvement of EET processes are therefore the focus of research on the microbe-electrode interface. There are a variety of approaches to improving the microbe-electrode interaction, which can essentially be divided into four different categories (Klein *et al.*, 2023; Figure 6). All of these approaches aim to improve the biofilm formation, EET throughout the biofilm via improved conductivity and lower resistance of biofilm and electrode material, provision of more attachment sites and larger electrode surface area for optimized adhesion processes and an improved biocompatibility between electrode and bacteria.

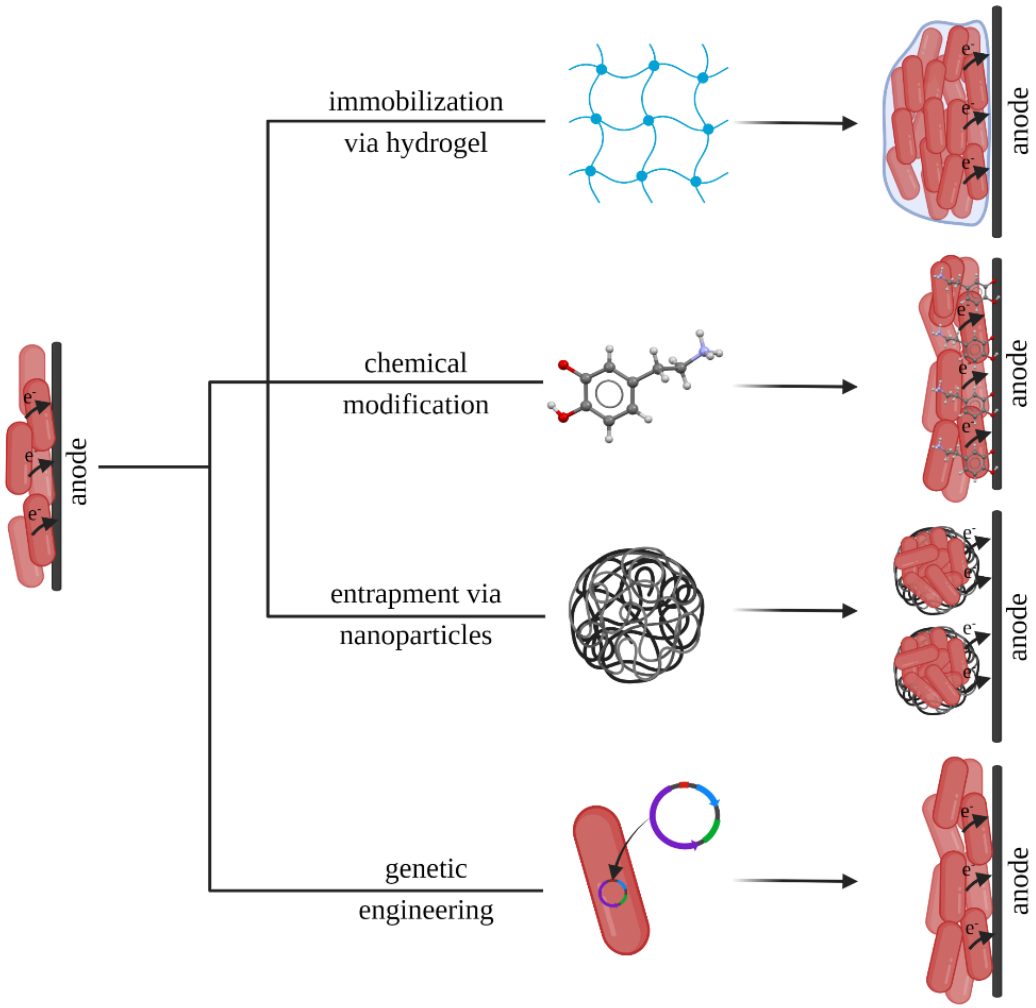

Figure 6: Strategies for optimization of the microbe-electrode interaction. The interaction between biofilm and electrode is altered by genetic engineering or synthetic biology using modifications based on pre-treatment with chemical compounds, nanoparticles or hydrogels. These improvements aim to improve biofilm formation, higher biofilm conductivity and therefore improve EET throughout the biofilm as well as better adhesion processes due to more attachment sites, larger electrode surface area and lower electrical resistance. Further, biocompatibility between bacterial and electrode material is introduced (according to Klein *et al.*, 2023).

One optimization approach focusses on the utilization of genetic engineering. These genetic alterations focus either on genes improving biofilm formations and/or conductivity or improving EET processes. For example, the overexpression of *cymA* (Figure 4, A) led to a performance improvement in MFCs due to an increase in EET (Vellingiri *et al.*, 2019). In addition, Edel and colleagues produced an *S. oneidensis* strain that exhibited enhanced biofilm formation due to the overexpression of *speC* (Edel *et al.*, 2021). This gene encodes the ornithine decarboxylase, which is naturally induced by the presence of riboflavin, and the strain overexpressing *speC* produces a higher current density when applied in a MEC due to

the increased biofilm formation. However, the molecular mechanisms of EET and anaerobic biofilm formation have not yet been fully unraveled, even for the model organism *S. oneidensis*, which is why further basic research in this field is vital for optimization using genetic engineering. An overview about recent advances regarding genetic engineering is found in multiple reviews (Sydow *et al.*, 2014; Li *et al.*, 2018; Philipp *et al.*, 2020; Bird *et al.*, 2021; Klein *et al.*, 2023).

Another approach to improve microbe-electrode interactions is the usage of synthetic biology by means of altering the electrochemical characteristics of this interface. The aim is to change the electrochemical properties of the electrode surface or the cell surface in order to improve the adhesion and attachment processes of the organisms, which are necessary for the formation of the catalytic biofilm. Moreover, the altered electrochemical properties of the cell and electrode surface are reported to have a direct impact on microbial metabolism in a way that increases EET compared to unmodified biofilms (Chen *et al.*, 2018; Savla *et al.*, 2020). There are many studies on the optimal electrode material (Kumar *et al.*, 2013; Hindatu *et al.*, 2017; Kerzenmacher, 2017; Li *et al.*, 2017; Nosek *et al.*, 2020; Park *et al.*, 2022), which postulate mostly carbon-based (i.e., graphite derivatives) or metal-based (i.e., stainless steel) BES electrodes. Both carbon and metal-based systems have advantages and disadvantages, which are to be balanced out by the pre-treatment of electrodes and cells with nanoparticles or enhancing chemical compounds.

For example, Yu and colleagues demonstrated that *in situ* polymerization of polydopamine or FeS nanoparticles on single *S. oneidensis* cells led to the formation of single-cell current collectors that exhibited an improved power output in BES by up to 16-fold (Yu *et al.*, 2020). The treatment with polydopamine, which was shown to improve riboflavin production of *S. oneidensis* (Wang *et al.*, 2021), and the nanoparticles thereby resulted in an additional connection to the inner membrane electron pool. The positive effects of nanoparticles have also been shown before to boost BES performance due to an increase in bacterial metabolism and in turn an increase in EET processes as mentioned above (Chen *et al.*, 2018; Savla *et al.*, 2020). Further, Cao and colleagues reported the modification of a carbon paper electrode with reduced graphene oxide and silver nanoparticles that boosted power output of *S. oneidensis* 13-fold (Cao *et al.*, 2021). The beneficial effect of reducing the diameter of the electrode material from the micro- to the nanoscale for optimized biofilm formation of

S. oneidensis has been postulated previously (Sanchez *et al.*, 2015) and the addition of silver nanoparticles and reduced graphene oxide therefore resulted in an improved electrode structure that optimally extracted metabolic electrons (Cao *et al.*, 2021). At this point, a tabular overview of recent advances in the pre-treatment of cells or electrodes is referred to (Klein *et al.*, 2023).

Immobilization of bacteria using (conductive) polymer structures, i.e. hydrogels, likewise facilitated the improvement of BES performance. In general, hydrogels are defined as water-swollen polymeric material that maintain a distinct three-dimensional structure and exhibit excellent biocompatibility (Wichterle and Lím, 1960). When found to be non-degradable by microorganisms, they are suitable to replace the naturally formed EPS matrix in biofilms and their use as an artificial biofilm model has been proposed (Strathmann *et al.*, 2000). In addition, they have been described as the first biomaterials rationally developed for human use, as they mimic the basic processes of living systems, and their applications range from implants to nanomaterials (Kopeček and Yang, 2007). While their application especially in the medical field for tissue engineering is already established, the utilization of biomaterials consisting of electroactive bacteria and hydrogels for the application of conductive, artificial biofilms in BES is relatively new. Coating the electrode surface with polymer hydrogels to achieve optimal cell adhesion properties resulted in improved current output (Liu *et al.*, 2011; Jiang *et al.*, 2015; Liu *et al.*, 2015), however, the number of cells directly connected to the electrode was still limited in these studies.

Recognizing the potential to maximize electron transfer efficiency by embedding the exoelectrogenic organisms directly into the conductive 3D scaffold of a poly(3,4-ethylenedioxythiophene):poly(styrenesulfonate) (PEDOT:PSS) hydrogel, Zajdel and colleagues reported the successful fabrication of a multilayer conductive bacterial composite film containing viable *S. oneidensis* cells (Zajdel *et al.*, 2018). This hybrid biomaterial resulted in a 20-fold increase in current compared to the naturally formed biofilm. In addition, Freyman and colleagues have demonstrated the possibility of manufacturing a 3D printable biomaterial from *S. oneidensis* cells embedded in an alginate hydrogel with integrated carbon particles, which could be used as a ready-to-use bioanode (Freyman *et al.*, 2019). While the application of these biomaterials for biosensing appears feasible at the microscale, the complicated manufacturing process as well as the toxic monomers from which some of the

hydrogels are formed could hinder the use of these biomaterials for various industrial applications, including wastewater treatment and the production of value-added compounds, that would require biomaterial upscaling. In addition, for large-scale industrial application, a process must be provided that enables the easy application of the hybrid biomaterials. Electropolymerization, as required for the production of PEDOT:PSS biomaterials, for example, would not be practicable, and another application strategy must be developed that opens up the possibility of covering large electrode areas with the corresponding hybrid biomaterial.

1.5 Aim of this thesis

BES technology offers the opportunity to contribute to the necessary transition to clean energy production in terms of sustainability. However, the performance of BES still has to increase significantly to enable industrial application of this technology. To improve the performance of BES current production by the model organism *S. oneidensis*, it was the aim to optimize the interface between this microbe and the electrode surface. To this end, a novel biomaterial that would be suitable for upscaling was developed from *S. oneidensis* and a biocompatible and readily available hydrogel. Agarose was chosen as the basis for the 3D matrix of the biomaterial due to its excellent biocompatibility, low economic impact, easy availability and thus the possibility of upscaling.

The novel biohybrid material was characterized in terms of the interplay of cell concentration and material height with current density and its physical accessibility was investigated to verify the suitability of the artificial matrix as a substitute for the natural matrix formed by *S. oneidensis*. Following the initial characterization of the synthetic biofilm, it was a second objective to develop spraying as a scalable technology for easy application of the biomaterial. As the hybrid biomaterial was found to result in improved electricity production compared to the naturally formed biofilm of *S. oneidensis*, the subsequent aim was to functionalize the engineered biomaterial to further increase the current output. In the next step, the optimized biomaterial was to be tested for its performance in an application scenario. To this end, a coupled MEC-biogas system was selected and the effects on electricity production for synthetic and natural biofilm were observed over 35 days. In a final step, the possibility of detaching the hybrid biofilm material should be investigated, as the recovery of the biomaterial could be essential in future application processes.

2 MATERIALS AND METHODS

2.1 Microbial methods

2.1.1 Microorganisms

Strains used in this study are listed in Table 1.

Table 1: Strains with relevant genotype used in this study.

Strain no.	Relevant genotype	Reference
JG 493	*S. oneidensis* MR-1 71982::barcode synthetic sequence	Dolch *et al.*, 2016
JG 1697	*S. oneidensis* MR-1 pMK-RQ-Ara_RFP Kanamycin resistance; ColE1 ori	Hu *et al.*, 2020
JG 407	*G. sulfurreducens* PCA wildtype	Caccavo *et al.*, 1994

2.1.2 Growth conditions of anodic organisms

All media were prepared with ddH_2O (PURELAB®, ELGA LabWater, Celle, Germany) and autoclaved (DX-65 and VE-150, Systec, Linden, Germany) after preparation at 121 °C for 20 min. Temperature sensitive reagents including antibiotics, vitamins and reducing agents were sterile filtered (Filtropur S, pore size 0.2 µm, Sarstedt, Nümbrecht, Germany) and added after autoclaving to the media under sterile conditions. For the cultivation of strain JG 1697 kanamycin (50 µg ml^{-1}) was added to select for stable plasmid propagation and arabinose (1 mM) was introduced to the medium to induce the *rfp* gene. Anoxic media was treated with 2 min of vacuum (diaphragm vacuum pump VP 86, VWR, Radnor, PA, USA) followed by 2 min of gas flushing with a mixture of 80 % N_2 and 20 % CO_2. To ensure that oxygen was excluded, a minimum of 15 cycles of this anaerobization process was performed.

2.1.2.1 Cultivation of *S. oneidensis*

The cultivation of *S. oneidensis* started from a cryo culture (see section 2.1.2.4) which was plated onto LB agar (Table 2) and incubated under oxic conditions at 30 °C (Incubator I, Memmert, Schwabach, Germany). Cultures in liquid LB media (Table 2) were then inoculated with single colonies from these plates and incubated under oxic conditions over night shaking at 180 RPM at 30 °C as well (New Brunswick Innova® 44, Eppendorf, Hamburg, Germany).

Table 2: LB media used for oxic cultivation of *S. oneidensis* cells. For liquid medium, no agar was added.

Component	**Amount L^{-1}**
Tryptone	10 g
Yeast extract	5 g
NaCl	5 g
Agar [2 %]	20 g

2.1.2.2 Cultivation of *G. sulfurreducens*

For the cultivation of *G. sulfurreducens*, the BES culture media (Table 3) was modified to contain 20 mM sodium acetate instead of 20 mM sodium lactate as electron donor as well as 20 mM fumaric acid as electron acceptor. The pH was adjusted to 7.0 and the media were treated as described above (see section 2.1.2) to ensure anoxic conditions. Liquid cultivation of *G. sulfurreducens* was started by inoculating this medium with the total volume of a thawed cryo culture (see section 2.1.2.4). After incubation at 30 °C for a minimum of 2 days, this culture was kept at room temperature for a maximum of 4 weeks before a new culture was started. Two days before a BES experiment, 5 % of the cell suspension from this running culture was transferred to fresh cultivation medium to ensure that the cells were harvested in their exponential growth phase.

2.1.2.3 Cultivation under BES condition

For the cultivation of *S. oneidensis* as well as the co-cultivation of *S. oneidensis* and *G. sulfurreducens* under BES condition, the BES culture media containing 20 mM sodium lactate as electron donor and no additional electron acceptor was prepared accordingly (Table 3). The pH was adjusted to 7.0 and the medium was treated as described above (see section 2.1.2) to ensure anoxic conditions.

Table 3: BES cultivation media for anodic organisms. The media was used for the cultivation of *S. oneidensis* as well as the co-cultivation of *S. oneidensis* and *G. sulfurreducens*.

Component	**Amount L^{-1}**
Salt solution (Table 4)	100 mL
$NaHCO_3$	1.8 g
Na_2CO_3	0.5 g
$MgCl_2$ * 6 H_2O	0.2 g
Sodium-D,L-lactate, 60% syrup	3.8 g
Trace element solution 1 (Table 5)	10 mL
Selenite tungstate solution (Table 6)	1 mL
Complement after autoclaving	
Vitamin solution (Table 7)	10 mL
10% Yeast extract	10 mL
0.2 M Sodium ascorbate	1 mL
0.4 M $CaCl_2$ * 2 H_2O	1 mL

Table 4: Salt solution with 10x concentration.

Component	**Amount L^{-1}**
KH_2PO_4	4.2 g
K_2HPO_4	2.2 g
NH_4Cl	2.0 g
KCl	3.8 g
NaCl	3.6 g

Table 5: Trace element solution 1 with 100x concentration.

Component	**Amount L^{-1}**
Nitrilotriacetic acid	2.1 g
$MnCl_2$ * 4 H_2O	0.1 g
$FeSO_4$ * 7 H_2O	0.3 g
$CoCl_2$ * 6 H_2O	0.2 g
$ZnSO_4$ * 7 H_2O	0.2 g
$CuCl_2$ * 2 H_2O	0.3 g
$AlK(SO_4)_2$ * 12 H_2O	5 mg
H_3BO_3	5 mg

Table 6: Selenite tungstate solution with 1000x concentration.

Component	**Amount L^{-1}**
NaOH	0.5 g
Na_2SeO_3	3 mg
$Na_2WO_4 * 2 H_2O$	4 mg

Table 7: Vitamin solution with 100x concentration.

Component	**Amount L^{-1}**
Folic acid	2 mg
Pyridoxine hydrochloride	10 mg
Thiamine hydrochloride	5 mg
Riboflavin	5 mg
Calcium D,L-pantothenate	5 mg
Nicotinic acid	5 mg
Vitamin B_{12}	0.1 mg
p-Aminobenzoic acid	5 mg
D,L-α-Lipoic acid	5 mg
Biotin	2 mg

2.1.2.4 Conservation of strains

The long-term preservation of the bacteria used in this study was implemented by producing cryo cultures. For this purpose, 1 mL cell suspension in the exponential growth phase was mixed with 0.5 mL sterile glycerol and immediately frozen in liquid N_2. Storage took place at -80 °C.

2.1.3 Chemicals and enzymes

Unless otherwise stated, the chemicals used in this work were obtained from AppliChem (Darmstadt, Germany), Carl Roth (Karlsruhe, Germany), Merck (Darmstadt, Germany), Thermo Fisher Scientific (Waltham, MA, USA) or VWR (Radnor, PA, USA).

2.1.4 Synthesis of agarose biofilms

The here established synthetic biofilm consisted of an agarose hydrogel and bacterial cells that were embedded in this hydrogel and was fabricated according to Knoll *et al.* (2022). For this, the amount for a 1.8 % (w/v) low melt agarose (ROTI®Garose low melt, Roth, Karlsruhe, Germany) solution was weighed into a hungate tube. Low melt agarose was used instead of standard agarose as the gelling temperature of the low melt polymer is ≤ 28 °C instead of 38 °C. This allowed for an embedding of cells at physiological temperatures into the still liquid hydrogel. Before autoclaving of the low melt agarose solution, 75 % of the final volume were added using double-distilled water (ddH_2O) to the agarose polymer. Due to the heating in the sterilization process, the polymer dissolved and the hydrogel solution could be stored at room temperature indefinitely.

Right before the start of an experiment, the agarose solution was heated up to ≥ 85 °C to liquify the hydrogel and then tempered to exactly 37 °C (Cultura M mini-incubator, Merck, Darmstadt, Germany). Further, *S. oneidensis* and *G. sulfurreducens* cells were cultivated as described above (see section 2.1.2.1 and 2.1.2.2) and harvested by centrifugation for 10 min at 6000 g (SORVALL® RC-5C Plus, Thermo Fisher Scientific, Waltham, MA, USA). The cells were resuspended using a 1:10 dilution of the salt solution (Table 4), followed by two more cycles of centrifugation and resuspension. This washing of the cell suspension ensured that any traces of electron acceptors were removed before inoculation of the BES reactor. In

the last resuspension step, a small volume of about 5-10 mL of salt solution was used to obtain a concentrated cell suspension. After washing, the cells were kept on ice.

For the characterization of the synthetic biofilms using *S. oneidensis*, cell densities were determined corresponding to the optical density at 600 nm (OD_{600}; see section 2.1.4.1). For the co-cultivation of *S. oneidensis* and *G. sulfurreducens* the optical density measured using a spectrophotometer (GENESYS™ 20, Thermo Fisher Scientific, Waltham, MA, USA) was taken as reference value. Cell densities and OD_{600} were extrapolated to the total volume of the BES batch reactor, meaning that the defined number of cells corresponded with the reactor volume, not the gel volume. All experiments that included co-cultivation were inoculated with a total OD_{600} of 0.5 with a *S. oneidensis* to *G. sulfurreducens* ratio of 10:1, meaning *S. oneidensis* cells were inoculated with an OD_{600} of 0.45 and *G. sulfurreducens* of 0.05, respectively. For the synthesis of the synthetic biofilm, 25 % of the final gel volume with the defined cell number according to OD_{600} or calculated cell density was taken from the cell suspension on ice and inoculated into the 37 °C tempered, liquid agarose hydrogel.

This biofilm-hydrogel suspension was then inoculated either by spraying (see section 2.1.4.3) or pouring it directly into the mould of the working electrode of the BES batch reactor (see section 2.3.3.1). During both application techniques the hydrogel would start to cool down below the gelling temperature and a 3D matrix with embedded cells was introduced into the BES reactor. To compare naturally formed biofilms with the synthetic approach, a planktonic control was performed in which the same number of cells as described for the synthetic biofilm was introduced directly into the media via syringe. Cultivation in the BES batch reactor took place at 30 °C if not stated otherwise (Incudrive H, Schuett-Biotec, Göttingen, Germany).

2.1.4.1 Cell density of agarose biofilms

The cell density of the synthetic biofilm is defined as the cell number per mL gel. To determine the cell number, *S. oneidensis* was cultivated in LB liquid media overnight as describe above (see section 2.1.2.1). The cells were then harvested in the same manner as for the synthesis of synthetic biofilms (see section 2.1.4). The OD_{600} of the suspension was adjusted to 0.5 and a Neubauer counting chamber (BLAUBRAND® Neubauer Improved, chamber depth 0.1 mm, Brand, Wertheim, Germany) was used to count the cell number

per mL. Therefore, an optical cell density of 0.5 referred to a cell concentration of 1.28 x 10^6 cells per mL (data not shown). Five different cell densities were tested for their current production to characterize the synthetic biofilm using *S. oneidensis* (see section 3.1.1). For all other studies except the migration behaviour and the SEM analysis experiment the cell density was kept at 3.98 x 10^7 cells per mL gel.

2.1.4.2 Addition of enhancing supplements

To improve the performance of the synthetic biofilm, two different additives were used to change the properties of the hydrogel itself. For this, only 50 % of the final volume was added to the agarose before autoclaving. As 25 % of the final volume of the hydrogel consisted of the riboflavin solution, a 7.4 µM concentrated stock solution was prepared in ddH_2O and sterile filtered before use. The final concentration was 1.85 µM according to Arinda *et al.* (2019). The riboflavin solution was adjusted to 37 °C and added to the liquid hydrogel at the same temperature under sterile conditions. Afterwards the cells were added as described above (see section 2.1.4). As a second additive, carbon nanofibers (CNFs) were functionalized with riboflavin to introduce hydrophilicity (Toshimitsu *et al.*, 2019). For this, 0.2 % (w/v) CNFs were weighed into a 1.5 mL reaction tube. 1 mL of 2-propanol was added to the CNFs, followed by 10 min of ultrasonication (USR 18 ultrasonic bath, VWR, Radnor, PA, USA). In the next step, 2-propanol was evaporated at 80 °C (ThermoMixer® C, Eppendorf, Hamburg, Germany) for 1 hour. The dried CNFs were resuspended in the 7.4 µM riboflavin stock solution and ultrasonication was performed at room temperature for 1 h. Again, 25 % of the final volume consisted of these riboflavin-functionalized CNFs which were added as described for the riboflavin-spiked hydrogel.

2.1.4.3 Spraying of agarose biofilms

The synthetic biofilms were introduced into the BES reactor with two different techniques. First, the still liquid biofilm was poured into the mould of the BES batch reactor as described above (see section 2.1.4). Secondly, a novel spray technique was developed in this thesis. To spray the synthetic biofilm including the ones with additives (see section 2.1.4.2) the still liquid hydrogel cell suspension was drawn into a syringe. This syringe was attached to a custom-made, autoclaved spray applicator (Figure 7) using Luer hose connectors (ROTILABO® Luer hose connector, inner Ø 1.6 mm, Roth, Karlsruhe, Germany). The still

liquid biofilm was manually pushed towards the Y-tube connector (ROTILABO® hose connectors, inner Ø 1.6 mm, Roth, Karlsruhe, Germany) to which it was connected via silicone tubes (ROTILABO® silicone tube, inner Ø 1.5 mm, Roth, Karlsruhe, Germany). To the other side of this connector, a stream of N_2 gas with a maximum pressure of 0.5 bar corresponding to an acceleration < 50 kilopascals was sterilized via sterile filter. When the liquid biofilm and the gas flow met in the Y-tube connector, a spray mist was formed which was directed onto the electrode surface with a canula (19Gx1 ¼ 1.1 x 30 mm Sterican®, B. Braun, Melsungen, Germany). During the spray process, the synthetic biofilm started to solidify. The solid synthetic hydrogel was therefore sticking onto the electrode material that it was sprayed on, more specifically the graphite felt in the BES batch reactor and the graphite plate in the BES flow cell reactor. As a negative control, a sprayed cell suspension without the addition of agarose was sprayed in the same manner as described for the hydrogel cell suspension (see section 3.2.1). Further, synthetic biofilms with embedded *S. oneidensis* and *G. sulfurreducens* cells were sprayed either in an anaerobic chamber (vinyl anaerobic chamber, Coy Laboratory Products, Grass Lake, MI, USA) or under a constant stream of argon gas that was sterilized using a sterile filter.

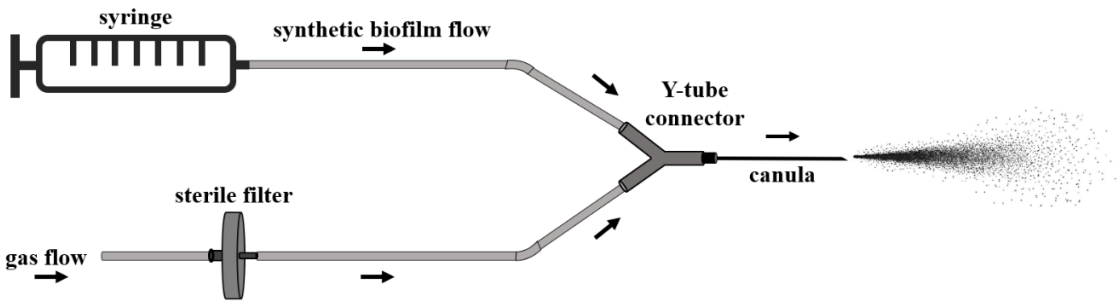

Figure 7: Design of spray applicator. The liquid hydrogel cell suspension was drawn into a syringe which was attached to the autoclaved spray applicator via Luer hose connectors. The synthetic biofilm was manually pushed towards the Y-tube connector, where a spray mist was formed due to the sterilized N_2 gas flow connected to the other side of the Y-tube connector. This spray mist was directed onto the electrode surface via the attached canula.

2.1.5 **Operational conditions for coupled MEC-biogas system**

In the coupled MEC-biogas system, the performance of naturally grown biofilms (planktonic) was compared to the performance of synthetic biofilms (sprayed). For this, the BES batch reactors (see section 2.3.3.1) were inoculated with a mixed culture of *S. oneidensis* and *G. sulfurreducens* with a ratio of 10:1 as described above (see section 2.1.4). For the naturally grown biofilms, the cell suspension was directly inoculated into the media and one week of pre-cultivation in the BES media (Table 3) at 35 °C took place. After this pre-cultivation phase, a second reactor was inoculated with a synthetic biofilm (see section 2.1.4). On the same day, the addition of biomass consisting of 40 % fresh silage mixture and 60 % active biogas community (see section 2.1.5.1 and 2.1.5.2) was started. For one week, 1/7 of the working volume of the BES batch reactor (250 mL) was drawn from the system via a syringe and replaced by the same volume of biomass mixture every day. After 7 days, the addition of biomass was stopped and the process was switched to batch conditions, monitoring current production at all times. Each day, 1 mL samples were drawn for total organic carbon analysis. After 35 days of cultivation, the MEC-biogas reactors were stopped, and samples of the electrode material and the planktonic phase were taken for subsequent metagenomic analysis. However, due to time limitations the results of this metagenome analysis as well as total organic carbon analysis are not discussed in this thesis.

2.1.5.1 Establishment of active biogas community

The application of the synthetic biofilm was studied in a coupled MEC-biogas system. For this, a community that actively produced biogas was started from cow manure. Roughly 5 L of cow manure from a local cow farm (Beckers Hofladen, Karlsruhe, Germany) was diluted 1:1 with tab water. After mixing, the cow manure mixture was filtered with a 1 x 1 cm mesh and transferred into a 10 L bottle. This mixture was flushed with N_2 for 30 min before incubation took place at 35 °C. Gas production was monitored regarding the total gas volume (MilliGascounter, Dr.-Ing. Ritter Apparatebau, Bochum, Germany) and the methane and CO_2 content (BCP-CO_2 and BCP-CH_4, BlueSens gas sensor, Herten, Germany). After roughly 8 days of incubation, methane and CO_2 formation could be detected (see appendix, Figure S2). This active biogas community was fed with a mixture containing maize silage (see section 2.1.5.2) every 1 to 3 months to ensure long-term availability of an active biogas community.

2.1.5.2 Feed solution based on maize silage

For the establishment of an active biogas community and for the coupled MEC-biogas system, a feed solution based on maize silage was prepared. The corresponding components (Table 8) were first dissolved in a small amount of ddH_2O of around 200 mL. This silage mixture was shredded at high speed in a food blender (HR2094 aluminium blender, Philips, Amsterdam, Netherlands). Further, the mixture was then filtered first with a 5 x 5 mm V4A stainless steel mesh (Drahtgewebe-Shop, Bergisch Gladbach, Germany) and then, again, with a 2 x 2 mm V4A stainless steel mesh (Drahtgewebe-Shop, Bergisch Gladbach, Germany) to exclude fibers of the size ≥ 2 mm. For the active biogas community, 10 % of the total volume was taken from the bottles and replaced by this fresh feed solution. In the coupled MEC-biogas system, 40 % of the feed solution was mixed with 60 % of the active biogas community (see section 2.1.5).

Table 8: Feed solution based on maize silage for active biogas community.

Component	**Amount L^{-1}**
Maize silage	80 g
100 mM Na_2CO_3	25 mL
Trace element solution 2 (Table 9)	0.1 mL

Table 9: Trace element solution 2.

Component	**Amount L^{-1}**
HCl, 7.7 M	10 mL
$FeCl_2 * 4 H_2O$	1.5 g
$ZnCl_2$	70 mg
$MnCl_2 * 4 H_2O$	0.1 g
H_3BO_3	6 mg
$CoCl_2 * 6 H_2O$	0.19 g
$CuCl_2 * 2 H_2O$	2 mg
$NiCl_2 * 6 H_2O$	24 mg
$Na_2MoO_4 * 2 H_2O$	36 mg

2.2 Analytical methods

2.2.1 Fluorescence microscopy for analysis of migration behaviour of embedded cells

To monitor the behaviour of cells regarding their migration after embedding into the agarose hydrogel (see section 3.1.2), a red fluorescent protein (RFP) tagged *S. oneidensis* strain (Table 1, Hu *et al.*, 2020) was used. The distribution of cells in the gel was monitored at three different time points, namely 0 h, 24 h and 48 h. For this, the synthetic biofilm was poured onto the graphite felt (see section 2.1.4) with a cell density of 0.79 x 10^7 cells per mL gel (see section 2.1.4.1). For each time point, the graphite felt with the attached synthetic biofilm was dismantled from the BES system and cut into 10 x 2 mm pieces with a scalpel (Cutfix®, B. Braun, Melsungen, Germany). Using a 630-fold magnification immersion lens of a fluorescence microscope (Leica DM5500B, Leica Microsystems, Wetzlar, Germany), the cross section between the poured synthetic biofilm and the electrode material was analysed.

LAS AF software (version 2.6, Leica Microsystems, Wetzlar, Germany) and ImageJ (version 1.53c, Schindelin *et al.*, 2012) were used for imaging and image analysis.

2.2.2 **Scanning electron microscopy analysis of agarose biofilm**

Scanning electron microscopy (SEM) was used to visualize the synthetic biofilm including the agarose fibers of the hydrogel and the cells attached to these fibers. For this, *S. oneidensis* cells were cultivated in LB liquid media overnight (see section 2.1.2.1). The cells were harvested via centrifugation at 6000 g for 10 min (centrifuge 5430, Eppendorf, Hamburg, Germany). Phosphate buffered saline (PBS) solution (Table 10) was used to resuspend the cell pellet. This process of centrifugation and resuspension was repeated twice. In the last resuspension step, formaldehyde was added to the PBS solution with a final concentration of 4 %. After fixation for 1 h at 4 °C, the cells were centrifuged at 6000 g for 10 min twice and the pellet was resuspended with ddH_2O to exclude any traces of formaldehyde. The 1.8 % agarose hydrogel was prepared as described above (see section 2.1.4) and the fixed cells were again embedded in the 37 °C tempered solution to obtain a synthetic biofilm with a cell density of 0.79 x 10^7 cells per mL gel (see section 2.1.4.1). 10 µL of the still liquid synthetic biofilm was put on a silicon wafer and the sample was frozen at -80 °C for at least 1 h. Then, lyophilisation at -80 °C was performed overnight (alpha 1-2, Martin Christ Gefriertrocknungsanlagen, Osterode am Harz, Germany). Thereafter, the sample was coated and analysed using a scanning electron microscope (Leo 1530 Gemini, Carl Zeiss, Jena, Germany) at the Laboratory for Electron Microscopy (LEM) at the Karlsruhe Institute of Technology (KIT).

Table 10: Phosphate buffered saline (PBS) solution.

Component	**Amount L^{-1}**
NaCl	8 g
KCl	0.2 g
Na_2HPO_4	1.44 g
KH_2PO_4	0.24 g
37 % formaldehyde [4 %]	108 mL

2.2.3 **Optical analysis of hydrogel detachment process**

Synthetic biofilm detachment was induced by applying negative current (see section 2.3.2) to a sprayed hydrogel to the BES flow cell reactor (see section 2.3.3.2). For this, 5 mL of a 1.8 % agarose hydrogel was sprayed (see section 2.1.4) once onto graphite felt and once onto a graphite plate. After not more than 1 min, BES media without lactate (Table 3) was poured on top of the hydrogel to prevent dehydration. The flow cell was closed with the polycarbonate window and metal top and the system was completely filled with media (~ 50 mL). The flow cell was mounted horizontally onto a metal rack, allowing for the analysis via optical coherence tomography (OCT) as shown by Hackbarth *et al.* (2020). OCT is a non-invasive imaging method that allows the visualization of 3D structures including biofilms. Thereby, a light beam is reflected and scattered by the sample to be observed and subsequently interferes with the light beam of a reference (Wagner and Horn, 2017). This interference is captured by a detector and analysed to obtain a three-dimensional representation of the sample. Since the light is able to penetrate the sample to a certain degree, a depth profile can be created at each scanned point (A-scan in Z-direction). If such a depth profile is then recorded along a defined axis, a 2D view of the biofilm is obtained (B-scan in XZ-direction). Many such two-dimensional "lines", consecutively one after the other, finally result in a 3D image of the biofilm (C-scan in XYZ direction; Wagner and Horn, 2017).

To visualize the detachment, OCT C-scans were used for a before and after picture of the 3D structure of the agarose hydrogel. Further, B-scans were filmed using the Windows Xbox Game Bar (version 5.823.1271.0) to give a 2D view of the detachment process. The OCT device (Ganymede II – LSM04, Thorlabs, Dauau, Germany) was therefore mounted onto the metal rack to visualize the back part of the BES flow cell. As the detachment process was visible without optical magnification as well, a video recording of the hydrogel was made using a mobile phone camera (Samsung S20 FE, version 13.1.00.50, Samsung Electronics, Suwon, South Korea). Therefore, the mobile phone was fixed onto the metal rack to visualize the front part of the BES flow cell. The videos of the OCT images and the mobile phone camera were then displayed side by side and compared for the different applied currents. For video processing the Microsoft video software (version 2023.10030.7003.0) and the AnyMP4 video converter ultimate (version 8.5.20) were used.

2.2.4 **Statistical analysis of anodic current**

Current data was normalized to the surface area of the working electrode. In the BES batch reactor (see section 2.3.3.1) this corresponded to 16 cm^2 of projected surface area and in the BES flow cell reactor to 20 cm^2, respectively. Current density (I) is therefore calculated by dividing the total current (i) by the projected surface area (A) of the working electrode (Equation 2).

$$I = \frac{i}{A} \tag{2}$$

Further, the mean current density ($\bar{I}$) for the entire duration of the experiments was determined by dividing the integrated current density (I) and the experimental time (t), which was 24 h unless otherwise stated (Equation 3).

$$\bar{I} = \frac{\int_0^t I \, dt}{t} \tag{3}$$

Biological triplicates (n = 3) were performed for all experiments, unless explicitly stated otherwise. Therefore, empirical mean ($\overline{x}$) of each sample (x_i) is given based on the number of experiments (n) as the arithmetical mean of each experiment (Equation 4).

$$\overline{x} = \frac{\sum_{i=1}^{n} x_i}{n} \tag{4}$$

Further, standard deviation of each experiment ($\sigma_{\overline{x}}$) was calculated based on the empirical mean ($\overline{x}$) of each sample (x_i) and the number of experiments (n) and is given in the form of error bars (Equation 5).

$$\sigma_{\overline{x}} = \sqrt{\frac{\sum_{i=1}^{n} (x_i - \overline{x})^2}{n - 1}} \tag{5}$$

If stated, statistical significance was determined using an unpaired *t*-test. The *p*-value is marked with * for $p < 0.1$, ** for $p < 0.05$ and *** for $p < 0.01$. In addition, a normalised improvement factor (IF) is given for the comparison of the performance of spray inoculation and planktonic inoculation after the start-up phase (see section 0, Figure 16). For this purpose, the mean current density after 24 h of the planktonic inoculation experiment was set to an IF of 1 (corresponds to no improvement) and all other calculated mean current densities were normalised to this value by division. Further, the hourly incline in improvement was calculated from the IF. For this, the IF was described as linear function and a trendline was calculated. Based on this, the gradient of that trendline was divided by 24 so an hourly inline (h^{-1}) could be given. For all above mentioned calculations either Microsoft Excel (version 2021) or Origin Lab (version 2021b) was used. All of the figures in this thesis have been created using either BioRender.com or Origin Lab.

2.3 Electrochemical methods

2.3.1 Chronoamperometric measurements

In this study, chronoamperometric measurements were performed to analyse the performance of the synthetic biofilm in terms of current generation. For this purpose, the potential at the working electrode was set to -0.199 V against Ag/AgCl, which corresponds to 0 V against the standard hydrogen electrode (SHE). The generated current was monitored over time with a measurement interval of 60 s. Potentiostats such as DropSens µSTAT 8000 (Metrohm, Herisau, Switzerland), MultiEmStat (PalmSens, Houten, Netherlands) and Interface 1000B/1000E/1010E/5010E (Gamry, Philadelphia, PA, USA) were used to set the specific potential at the working electrode.

2.3.2 Chronopotentiometric measurements

For the detachment of the synthetic biofilm, chronopotentiometric measurements were performed. In this electrochemical method, a constant current is applied to the system while the potential is monitored using an Interface 1000B potentiostat (Gamry, Philadelphia, PA, USA). To detach the synthetic biofilm, negative currents ranging from -10 mA to -100 mA decreasing in increments of 10 mA were applied. This corresponds to an applied current density between -0.5 and -5 mA cm^{-2} in the utilized flow cell (see section 2.3.3.2). Each current density was applied for 1 min while the detachment process was monitored (see section 2.2.3).

2.3.3 Bioelectrochemical setup

2.3.3.1 Bioelectrochemical system for biofilm characterization

A three-electrode batch reactor was used for all BES experiments except the biofilm detachment experiment as described before (Golitsch, 2016; Knoll *et al.*, 2022). This reactor had a working volume of 250 mL and consisted of a battery glass sealed by a polycarbonate lid and base (Figure 8). The top part included six openings into which components made of polypropylene, polytetrafluorethylene or polyamide were inserted. These were closed with septa and served as sampling ports, for the gas supply of the system and for the insertion of

the three electrodes. To ensure anoxic conditions, a constant stream of N_2 gas was supplied at all times through one of these ports.

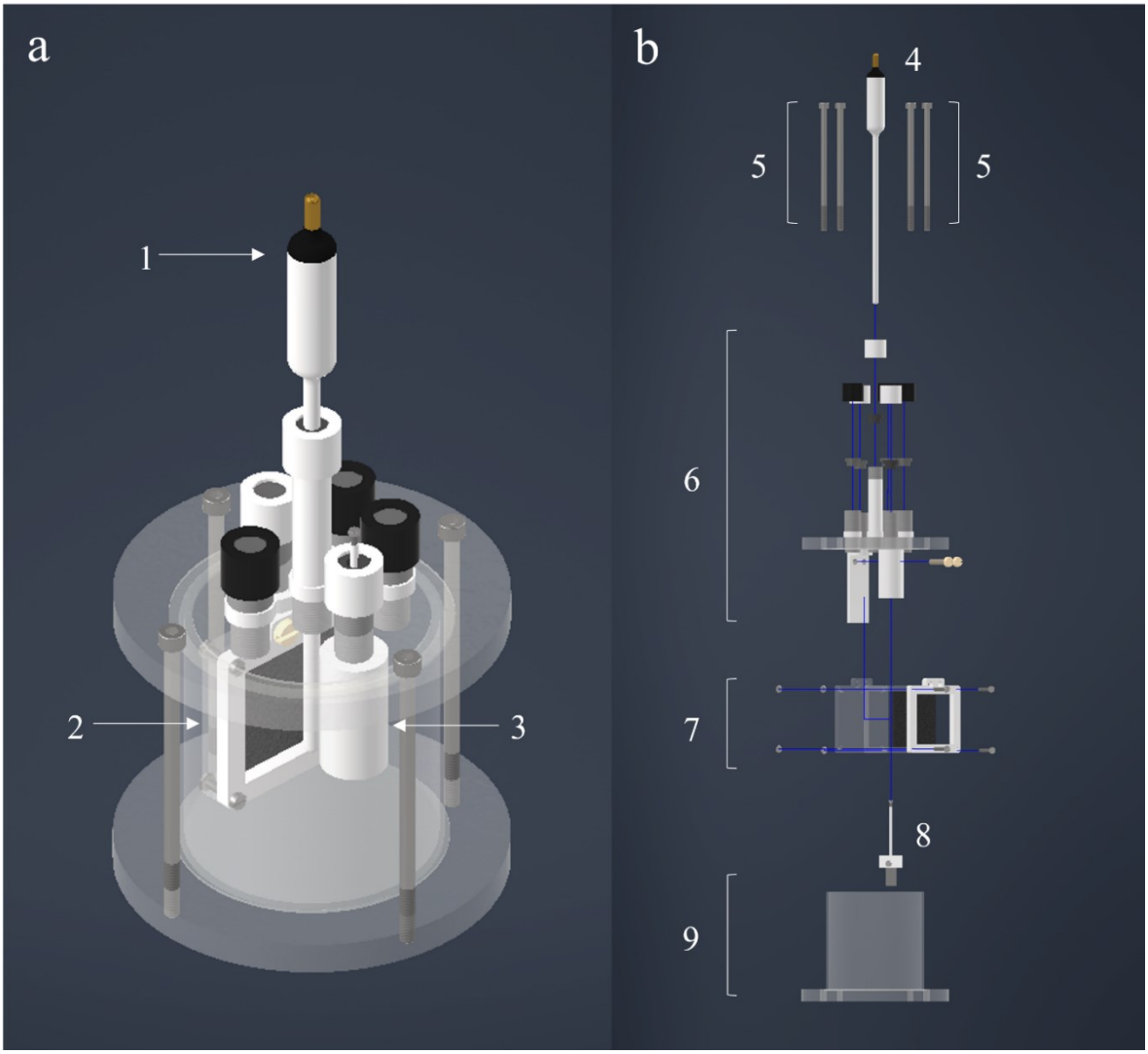

Figure 8: Design of bioelectrochemical batch reactor. (a) Reactor with 1) Ag/AgCl reference electrode; 2) fixture of anode material, graphite felt with projected area of 16 cm^2; 3) fixture of cathode, platinum mesh with projected area of 1.25 cm^2. (b) Exploded graphic of bioelectrochemical cell with 4) reference electrode, 5) screws, 6) lid with holder for anode and cathode electrode including multiple ports for sampling and gas supply, 7) anode fixture, 8) cathode, 9) bottom and beaker, holding 250 ml cultivation medium (according to Knoll *et al.*, 2022).

As the working electrode, graphite felt (SIGRACELL® GFD 2.5; SGL Carbon, Wiesbaden, Germany) with a projected area of 16 cm^2 was exposed to the electrolyte by being clamped between the open front part, the custom-made seal made of polydimethylsiloxane (PDMS) and the closed back part. The back part further included a titanium wire (Ø 0.5 mm, 99.8 %; ChemPur, Karlsruhe, Germany), which was used as a current collector for the working

electrode. The four screws (M3, V4A stainless steel, Conrad Electronic, Hirschau, Germany) and nuts (M3, polypropylene, Conrad Electronic, Hirschau, Germany) at the corners of the holder were used to clamp the graphite felt onto the current collector and the PDMS seal. This made it possible to pour still liquid synthetic biofilm onto the working electrode without it leaking during solidification. Before use, the graphite felt was soaked in 2-propanol for about 30 min and then rinsed with deionised water to improve the hydrophilicity of the material. After that, the material was constantly kept either in water or in electrolyte. The counter electrode consisted of platinum gauze (99.9 %, 1024 mesh cm^{-2}; ChemPur, Karlsruhe, Germany) with a projected area of 1.25 cm^2, which was clamped into the PTFE rod. A platinum wire (Ø 0.1 mm, 99.9 %; ChemPur, Karlsruhe, Germany) was threaded through this rod, acting as a current collector. The Ag/AgCl reference electrode (SE11, Sensortechnik Meinsberg – Xylem, Waldheim, Germany) was inserted into the system through the hole drilled in one of the septa. The reactor was closed with four M5 screws inserted from the top and screwed into the threads cut in the bottom part. A stirring bar (not shown) was used for mixing of the cultivation media during experiments (topolino, IKA-Werke, Staufen im Breisgau, Germany).

2.3.3.2 Bioelectrochemical system for hydrogel detachment

A three-electrode flow cell reactor that was described before (Hackbarth *et al.*, 2020) was used to study the detachment of the synthetic biofilm. This reactor consisted of a polyetheretherketon (PEEK) body and a transparent polycarbonate top (Figure 9). A metal top part kept the polycarbonate window in place by being fixated with 12 M5 x 35 screws from the top and washers and nuts from the bottom (Figure 9, C). The working electrode with a projected surface area of 20 cm^2 (10 x 2 cm) was located to the bottom of this flow cell. As material either graphite felt (SIGRACELL® GFD 2.5; SGL Carbon, Wiesbaden, Germany) or a graphite plate (MR40, Müller & Rössner, Niederkassel, Germany) was used. The counter electrode holder made from PEEK was fixated using M2 x 5 screws above the working electrode at the top of the flow channel and the electrode consisted of six iridium-tantalum coated titanium plates (Platinode® MMO Anode 177, Umicore, Hanau, Germany) with an active area of 20 cm^2 as well. Both electrodes were connected via titanium screws. The reference electrode (SE23I, Sensortechnik Meinsberg – Xylem, Waldheim, Germany) was installed at the inlet of the flow cell and viton® tubes (Roth, Karlsruhe, Germany) were

connected as peripheral elements to allow media input via syringe. The detachment experiment performed in this reactor system was conducted at room temperature. A pump for mixing the medium was deliberately omitted in order to avoid convection and to be able to directly attribute the detachment process to the applied current.

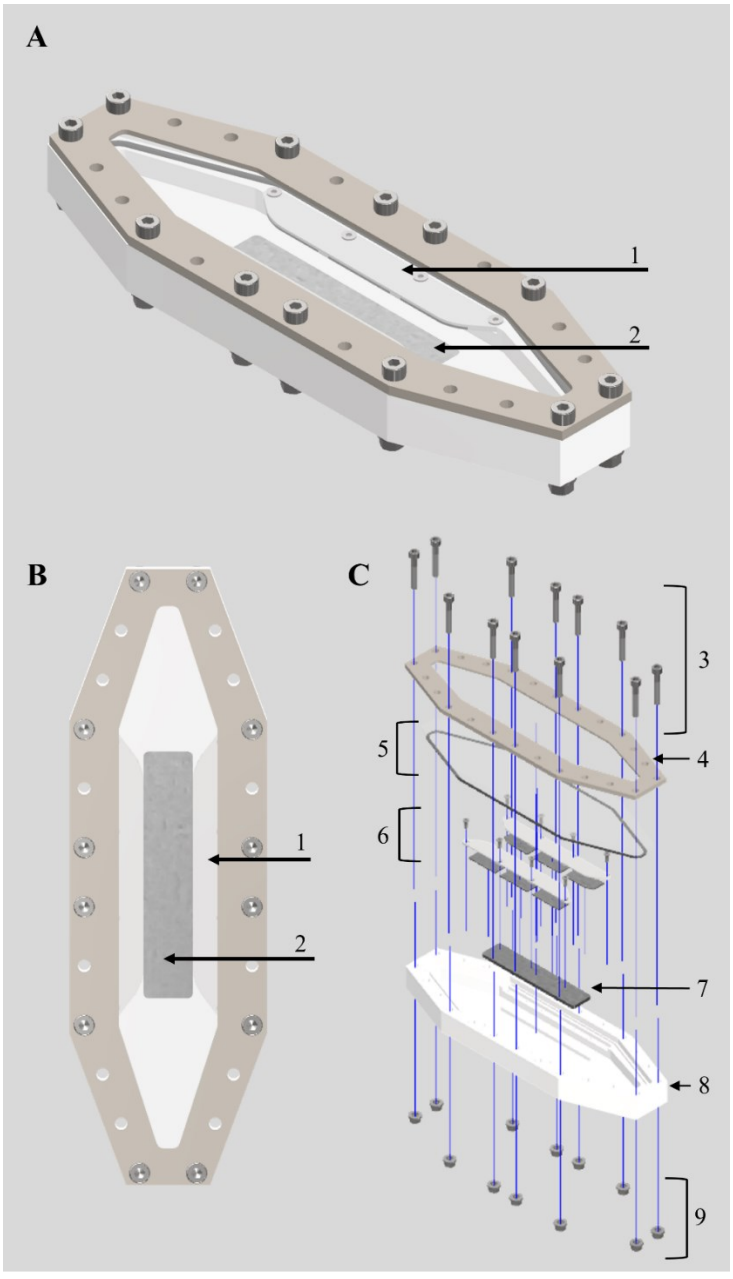

Figure 9: Design of bioelectrochemical flow reactor for continuous experiments. Side (A) and top (B) view of flow cell with 1) counter electrode and 2) working electrode. Exploded view (C) of flow cell with 3) screws; 4) metal top for fixation of polycarbonate window; 5) polycarbonate window with O-ring; 6) counter electrode consisting of 6 separate titanium coated electrodes fitted into PEEK holder that is screwed into bottom part and an active area of 20 cm^2; 7: graphite working electrode with 20 cm^2 projected area; 8) PEEK bottom; 9) washers and nuts for closing the flow cell (according to Hackbarth *et al.*, 2020).

2.3.4 **Conductivity measurements**

Abiotic conductivity measurements were carried out to analyze the electrochemical properties of the modified hydrogels. Tested hydrogels included the control with 0 % agarose, the 1.8 % agarose hydrogel as well as the hydrogels spiked with riboflavin and with riboflavin functionalized CNFs. All hydrogels were tested in a custom-made conductivity measurement cell (Figure 10) which consisted of two copper electrodes with a surface area of 2.01 x 10^{-4} m^2 and a thickness of 3.26 x 10^{-2} m. Two copper wires were welded on top of these electrodes to connect them to a multimeter (UT 131D, Conrad Electronics, Hirschau, Germany). The electrodes were put in a standardized macro cuvette (VWR, Darmstadt, Germany) with a distance of 3.78 x 10^{-3} m between them. 760 µL of the hydrogels as well as the control were pipetted between these electrodes before the resistance was measured using the multimeter. Based on the resistance (R), the surface area (A) and the distance between the electrodes (l) the resistivity (ρ) was calculated (Equation 6).

$$\rho = R \times \frac{A}{l} \tag{6}$$

The reciprocal of this resistivity is the conductivity σ (Equation 7).

$$\sigma = \frac{1}{\rho} \tag{7}$$

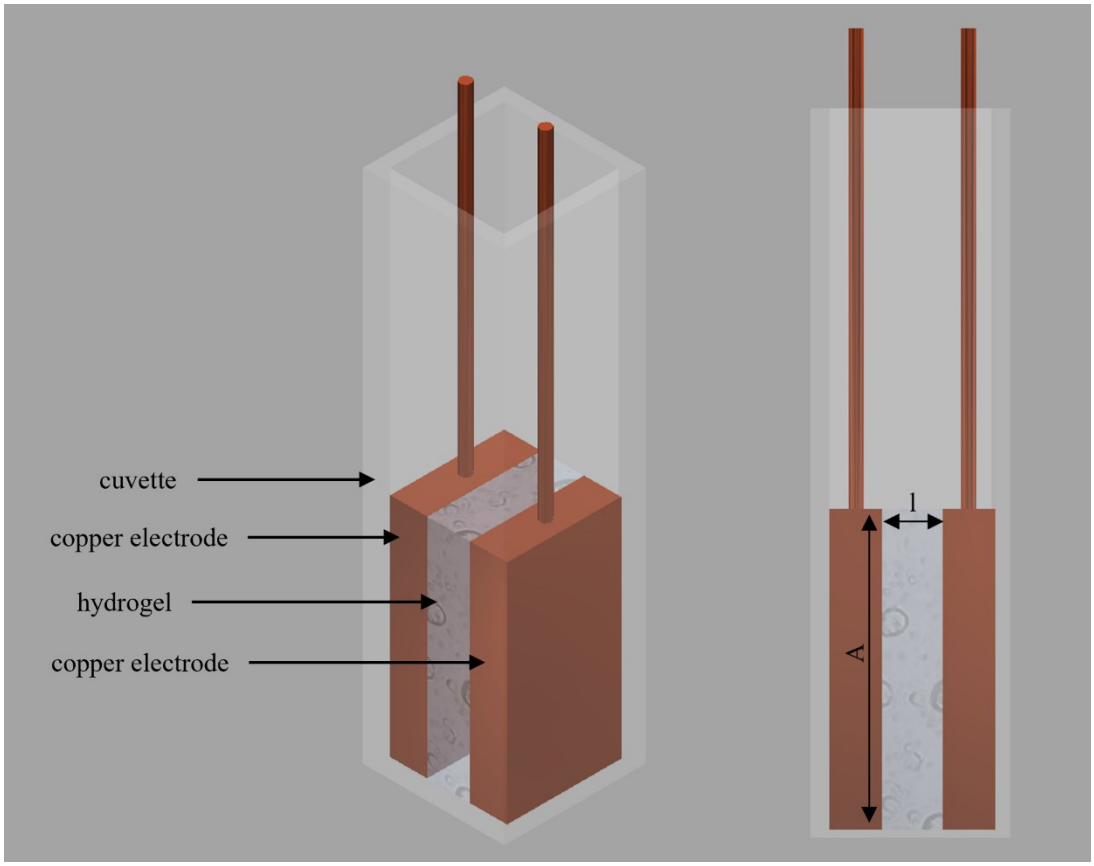

Figure 10: Conductivity measurement cell. Two copper electrodes with a surface area (A) of 2.01 x 10^{-4} m^2 and a thickness of 3.26 x 10^{-2} m were put into a standardized macro cuvette with a distance (l) of 3.78 x 10^{-3} m between them. 760 µL of hydrogel was pipetted between these electrodes and copper wires were welded to the top to connect the electrodes to a multimeter to measure the resistance of the hydrogels. This resistance can then be used to calculate the conductivity (see Equation 5 and 6).

3 RESULTS

The development of hybrid biomaterials is a major part in the research field of synthetic biology in which biological systems are programmed to perform user-defined functions. Hybrid living materials combine synthetic components and living cells, which opens up the possibility of introducing new properties and capabilities for these biomaterials (Tang *et al.*, 2021). The combination of the abiotic agarose hydrogel and the living exoelectrogenic organisms means that the synthetic biofilm established in this thesis similarly belongs to the group of hybrid biomaterials. The function that this artificial approach was to fulfil was to improve the overall performance in a MEC in terms of current generation. Besides, the focus was on simplifying the introduction of the biomaterial into the MEC system by spraying the synthetic biofilm.

In the first part, the synthetic biofilm was established using the model organism *S. oneidensis*. Therefore, various parameters and their effects on the performance of the synthetic biofilm, including the thickness of the hydrogel and the number of cells embedded in the hydrogel, were analyzed in terms of the production of current density. Further, an optical analysis of the migration behavior of *S. oneidensis* after embedding was performed and SEM analysis was used to gain insight into the characteristics of the biomaterial.

Subsequently, the spraying of the synthetic *S. oneidensis* biofilm was realized and its performance was analyzed in comparison to naturally formed biofilms.

The third part of this thesis revolved around the improvement of the before established sprayed biofilm. By introducing changes in the abiotic characteristics of the hydrogel, the influence on current production after the addition of riboflavin, a soluble electron shuttle known for enhancing mediated electron transfer, and riboflavin-functionalized CNFs was studied. In addition, *G. sulfurreducens* was implemented to investigate the performance of a mixed species, synthetic biofilm in terms of current production and the optimization of the hybrid biomaterial in general.

Further, the application of this hybrid biomaterial was realized by the implementation in a coupled MEC-biogas system. Thereby, the performance was compared to a naturally formed biofilm to highlight the differences between natural and synthetic approach.

Finally, the synthetic biofilm was deliberately detached from the electrode material to demonstrate the possibility of harvesting the hybrid biomaterial. To this end, negative currents were applied, which resulted in the formation of hydrogen bubbles that led to the detachment of the biomaterial. Optical analysis using OCT and video recording visualized this detachment process.

3.1 Characterization of synthetic *S. oneidensis* biofilms

In this first part, the hybrid biomaterial was established and characterized using the model organisms *S. oneidensis*. As this organism is known to form monolayers under BES conditions (see section 1.2.3), the embedding into agarose hydrogels offers the possibility to inoculate the system with a high cell density locally fixated onto the electrode material. Therefore, *S. oneidensis* cells were embedded into liquid 1.8 % agarose hydrogels and this biomaterial was poured onto the electrode material (see section 2.1.4). The comparison between different cell densities was based on the performances of the synthetic biofilm in terms of current density. Further, optical analyses by fluorescence microscopy and SEM were conducted to gain insight into the distribution of cells within the hydrogel and the hydrogel properties including pore size.

3.1.1 Optimization of cell density and biomaterial thickness

To characterize the synthetic biofilm with embedded *S. oneidensis* cells, the effect of various cell densities and difference in biomaterial thickness was analysed regarding the current production after 24 h (Figure 11). Firstly, the number of cells per mL gel (see section 2.1.4.1) was varied from 0.79 x 10^7 to 7.98 x 10^7 cells per mL gel resulting in different cell densities. Secondly, the thickness of the synthetic biofilm was varied from 5 mm to 1.25 mm using a constant cell number of 3.98 x 10^7 and, therefore, a defined cell density for each tested gel height.

The initial tested cell number of 0.79 x 10^7 cells per mL gel resulted in a current density of 89.9 ± 5.0 mA m^{-2} (Figure 11, A). An increase to 1.99 x 10^7 cells per mL gel led to a current density of 142.0 ± 2.1 mA m^{-2} while a cell number of 3.98 x 10^7 achieved a current density of 167.6 ± 16.7 mA m^{-2}. Further increase to cell numbers of 5.98 x 10^7 and 7.98 x 10^7 resulted in current densities of 243.0 ± 24.2 mA m^{-2} and 245.5 ± 3.8 mA m^{-2}, respectively. Between the two highest tested cell numbers, no significant difference ($p > 0.1$) could be found (Table S2), therefore, the cell number was not increased further. For the cell numbers of 5.98 x 10^7 and 7.98 x 10^7, the pre-cultivation had to be scaled up to about 3 L to obtain the required cell density of the cell suspension after harvesting. Accordingly, a constant cell number of 3.98 x 10^7 cells per mL of gel was used for the further experiments, as this allows pre-cultivation on a 1 L scale, which reduced the preparation time enormously.

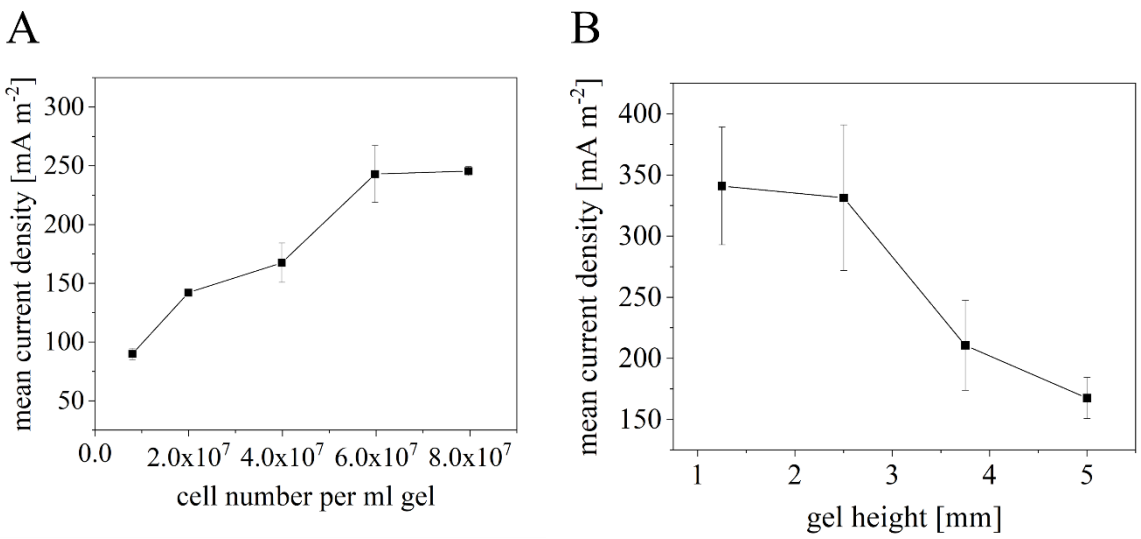

Figure 11: MEC Performance of the synthetic biofilm regarding various cell densities and biomaterial heights. After embedding *S. oneidensis* in the liquid hydrogel, the biomaterial was poured onto the graphite felt, where the synthetic biofilm solidified. A) To analyze the effects of different cell densities, cell number per mL gel was varied and mean current density after 24 h was compared. An increase in cell number above 5.98 x 10^7 led to an improved current density of 243.0 mA m^{-2} in comparison to 89.9 mA m^{-2} at a cell number of 0.79 x 10^7 per mL gel. A further increase in cell number showed no significant effect (Table S2). B) Current density increased with the reduction of the gel height from 167.6 to 341.1 mA m^{-2} for 5 mm and 1.25 mm thickness, respectively. No significant difference between a 2.5 mm and a 1.25 mm thick synthetic biofilm could be measured (Table S3). The cell density of all tested synthetic biofilm was kept at 3.98 x 10^7 cells per mL gel (modified from Knoll *et al.*, 2022).

Therefore, the reduction of the synthetic biofilm thickness was performed with a cell density of 3.98 x 10^7 cells per mL gel. To obtain different thicknesses, the prepared volume of the hydrogel was altered accordingly. Therefore, a 5 mm gel height refers to a total gel volume

of 8 mL, while 3.75 mm and 2.5 mm refers to a volume of 6 mL and 4 mL, respectively. For a gel height of 1.25 mm the final volume was kept at 2 mL of synthetic biofilm. For the reduction of synthetic biofilm thickness from 5 mm with a current density of 167.6 ± 16.7 mA m^{-2} to 3.75 mm with a current density of 210.7 ± 36.8 mA m^{-2} no significant difference ($p > 0.1$) was detected between both gel heights (Table S3 and Figure 11, B). A further decrease in thickness to 2.5 mm resulted in a current density of 331.4 ± 59.5 mA m^{-2}. This significant increase ($p < 0.1$) in current density in comparison to the 5 mm and 3.75 mm synthetic biofilm was found for the 1.25 mm thickness with 341.1 ± 48.3 mA m^{-2} as well. However, no significant difference between the 2.5 mm and 1.25 mm gel height could be detected (Table S3) and therefore, the gel height was kept at 2.5 mm for all following experiments.

3.1.2 **Migration behavior of *S. oneidensis* within the hydrogel**

The embedding of microorganisms within hydrogels could have the effect of immobilizing those cells within the polymeric matrix provided. This would limit their ability to position themselves in the best possible way in relation to the soluble electron donor and the fixed electron acceptor. Therefore, the question was addressed whether the localisation of *S. oneidensis* within the hydrogel would be permanent after the solidification of the hydrogel matrix. If migration of the organisms would be possible, the distribution in the hydrogel with regards to the positioning of the cells to the fixed electron acceptor, the graphite felt, and the soluble electron donor, lactate, in the electrolyte was supposed to be analysed as well.

To this end, an RFP-tagged *S. oneidensis* strain (Table 1) was embedded in a 5 mm thick hydrogel and poured onto the graphite felt (see section 2.1.4). The cross section between hydrogel with embedded cells and the electrode material was investigated using fluorescence microscopy (see section 2.2.1) right after the synthetic biofilm hardened (0 h), after 24 h and 48 h MEC operation. After solidification of the synthetic biofilm on top of the graphite felt at 0 h, the evenly distributed cells marked in red (Figure 12) formed a clear delineation between the hydrogel and the electrode material. Graphite fibers could be shown to penetrate the biomaterial, however, no cells appeared to be located on these fibers. After 24 h, no clear delineation was visible between biomaterial and electrode. Single cells could be found on the graphite fibers, however, cells not attached to the electrode material were detected as well.

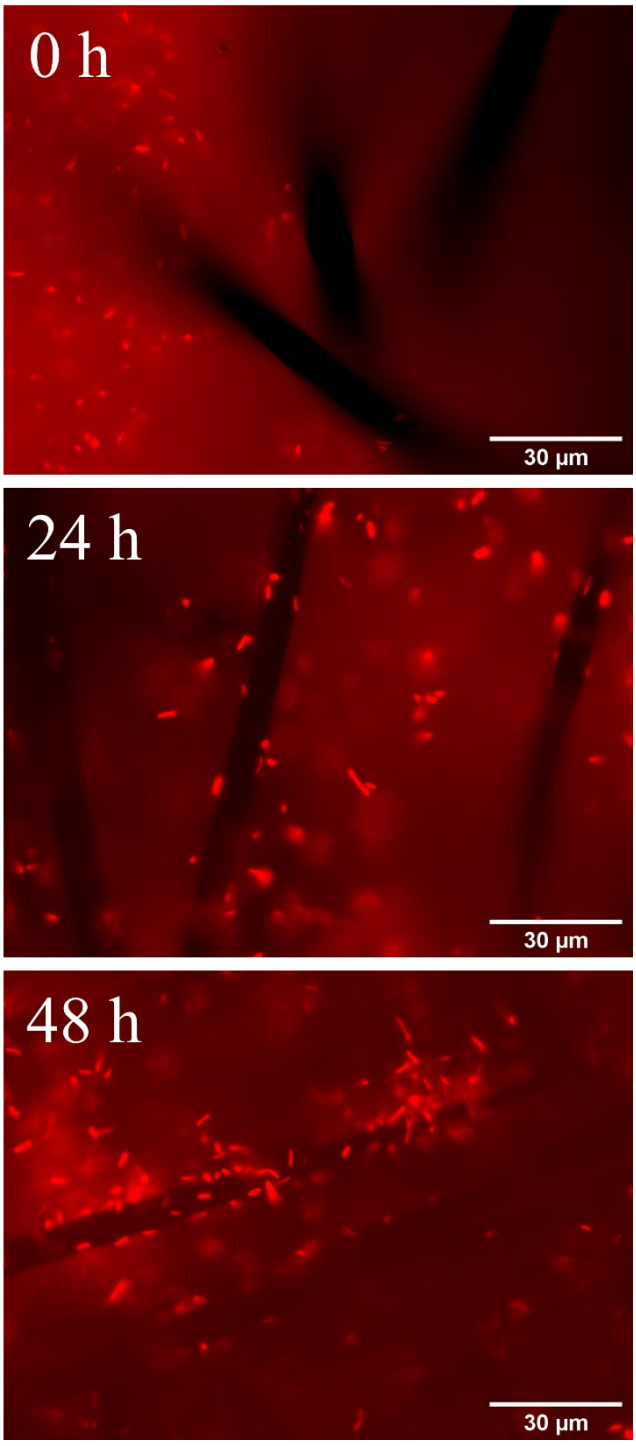

Figure 12: Fluorescence microscopic analysis of the migration behavior of RFP-tagged *S. oneidensis* cells embedded in a poured agarose hydrogel after 0 h, 24 h and 48 h MEC operation. At 0 h, the synthetic biofilm with evenly distributed cells (red) formed a clear delineation to the graphite fibers (black). After 24 h and 48 h, the cell distribution was concentrated on the graphite fibers on which the cells appeared to have accumulated. 630-fold magnification (modified from Knoll *et al.*, 2022).

After 48 h, even more cells appeared to be located on the graphite fibers and a denser colonization of electrode material was observed in comparison to 24 h. The number of individual cells not attached to graphite fibers appeared less than 24 h prior. Thus, it seemed that the cells could migrate within the poured biomaterial to the individual graphite fibres. The embedded cells were thus not locally fixed by the hydrogel and could migrate through the entire hydrogel matrix. This apparently allowed *S. oneidensis* to position itself between the stationary electron acceptor and the soluble electron donor dissolved in the cultivation medium, which should ensure the organism's proliferation.

3.1.3 **Optical analysis of synthetic biofilm using SEM**

The agarose hydrogel was used as a synthetic 3D scaffold in which the exoelectrogenic organisms could proliferate. Therefore, the material properties, including the pore size and the nature of the hydrogel matrix, were of interest and SEM analysis was performed for visualisation (see section 2.2.2). A 3D network with pores of various sizes was found when inspecting the hydrogel by SEM (Figure 13, A). The size of individual pores was measured during the analysis and the pores ranged from 10 to 40 µm in diameter. Further, the agarose fibers were clearly visible and the network consisted of thin, string-like filaments as well as thicker filaments that spanned over a larger area. When zooming in on one of the larger fibers (Figure 13, B) single cells (red arrow) were found to be attached to the agarose filaments. The size of the single cells was measured during SEM analysis as well and were found to be about 1 to 2.5 µm in length and about 0.5 µm in width.

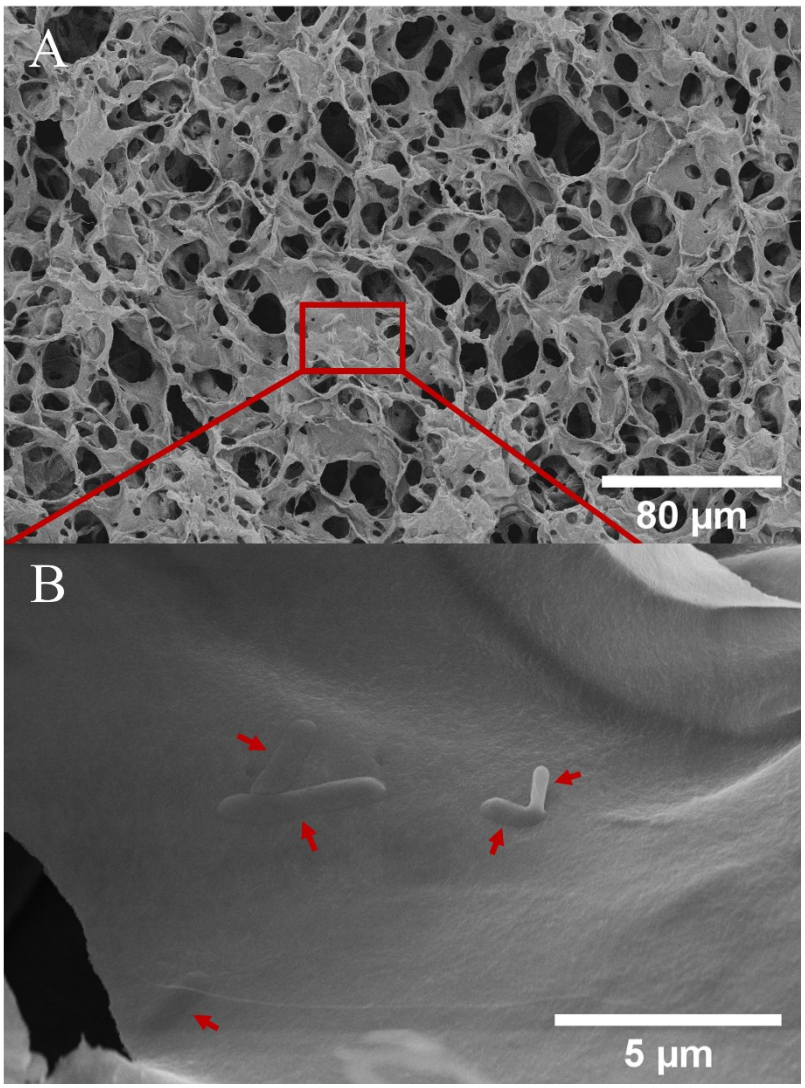

Figure 13: SEM analysis of a poured agarose hydrogel with embedded *S. oneidensis* cells. A) The 3D structure of the hydrogel was clearly visible with pore sizes ranging from 10 to 40 µm. B) Cells attached to the agarose fibers are marked (red arrow) and range in length of about 1-2.5 µm and width of about 0.5 µm (modified from Knoll *et al.*, 2022).

3.2 Introduction of sprayability aspect to synthetic biofilms

In the first step, the hybrid biomaterial consisting of an agarose hydrogel and *S. oneidensis* cells was successfully established and characterized. Thus, the biomaterial was defined in terms of optimal cell density with a thickness of 2.5 mm and a cell number of 5.98 x 10^7 cells per mL gel. In addition, the migration behaviour of *S. oneidensis* and the material properties of the 3D matrix of the agarose, was visualized using SEM analysis. The next part of this thesis revolved around the sprayability of the synthetic biofilm. By introducing the possibility

to spray this biomaterial on any kind of surface, a simple implementation and thus inoculation of reactor systems with ready-to-use biofilms should be realised. In contrast to the biomaterial established here, natural biofilms in these reactor systems are usually formed after planktonic inoculation of the cell suspension directly into the cultivation medium. Once settled on the electrode material, the cells begin to proliferate the surface, forming the 3D network known as the extracellular matrix, which is characteristic of each organism and the corresponding biofilm formed. In contrast, the synthetic approach studied in this thesis offered the possibility to inoculate the BES system with a ready-to-use biofilm embedded in a defined 3D network of agarose fibers.

Therefore, the start-up performance of synthetic versus naturally formed biofilms was compared in terms of the current density in and beyond the start-up phase (the first 24 h). For this, the biomaterial was sprayed using a spray applicator (Figure 7) consisting of laboratory standard equipment that is scalable and sterilizable. Additionally, a comparison between the inoculation by pouring and spraying of the synthetic biofilm was additionally carried out. As the spraying procedure could be very stressful for the cells due to shear forces and rapid acceleration, this part of the thesis addressed the possible negative effects on current production. To see what role the hydrogel matrix and the embedding of the organisms might play in this inoculation technique, a negative control with 0% agarose content was performed as well.

3.2.1 **Performance of naturally formed versus synthetic biofilms**

The sprayed, synthetic biofilm was compared to naturally formed biofilms in terms of current density in the first 24 h after inoculation of the BES reactor. The naturally formed biofilm was obtained by planktonic inoculation of a cell suspension with the same cell number that was embedded into the agarose hydrogel into the electrolyte of the system. The planktonic control started to produce current after about 3 h, while for the synthetic biofilm a current density of around 200 mA m^{-2} could already be monitored at that time point (Figure 14, A). As time progressed, both the synthetic biofilm and the planktonic control showed an almost linear increase in current density between 6 and 24 h. The maximal current density was monitored after 24 h with 500 mA m^{-2} for the synthetic biofilm and 300 mA m^{-2} of the naturally formed biofilm.

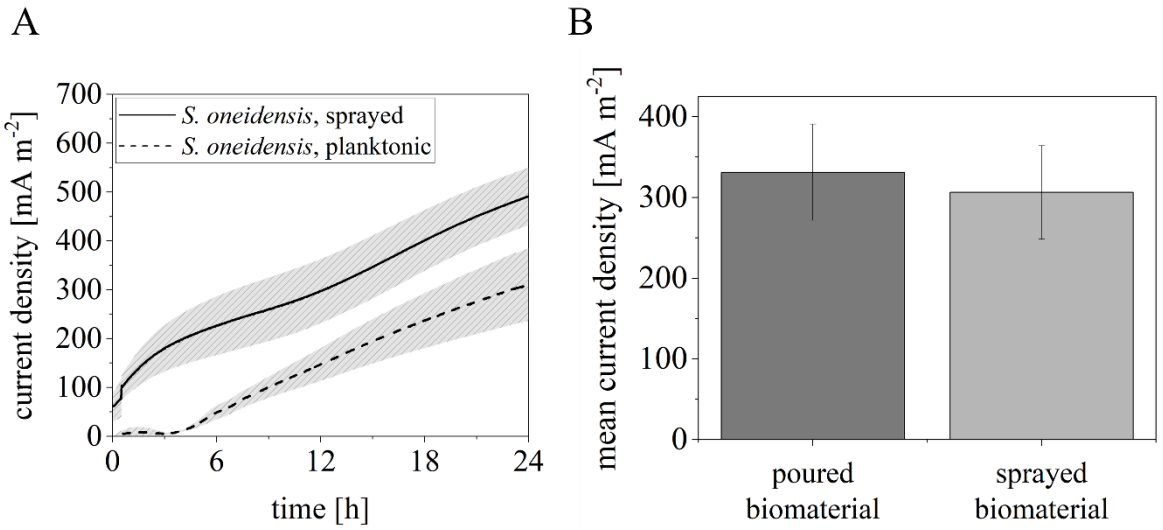

Figure 14: Performance of naturally formed *S. oneidensis* biofilm compared to a sprayed or poured synthetic biofilm in the MEC. A) Current density of sprayed, synthetic biofilm (–) and planktonic inoculated, naturally formed biofilm (- -). The latter biofilm showed current production after 3 h, while the synthetic biofilm was already producing around 200 mA m^{-2} at this time point. Between 6 h and 24 h both biofilms resulted in an almost linear increase in current density with the maximum current density after 24 h with 500 mA m^{-2} and 300 mA m^{-2} for the sprayed and the planktonic inoculation technique, respectively. B) Mean density of poured with 331.4 ± 59.5 mA m^{-2} and sprayed inoculation with 306.3 ± 58.0 mA m^{-2} of the synthetic biofilm were compared. No significant difference ($p > 0.1$) was found between both inoculation strategies (modified from Knoll *et al.*, 2022).

Further, the performance of poured and sprayed synthetic biofilm was analysed to gain insight into the potential negative side effects the spraying procedure could have on the performance of the biomaterial. While the poured biofilm resulted in a mean current density after 24 h of 331.4 ± 59.5 mA m^{-2}, the sprayed biofilm supported a mean current density of 306.3 ± 58.0 mA m^{-2} (Figure 14, B). However, no significant difference ($p > 0.1$) between both inoculation strategies could be shown (Table S4). Thus, it was possible to apply the synthetic biofilm via spraying without any deterioration in performance in comparison to pouring. No negative side effect due to the harsh spraying conditions could be found on *S. oneidensis* embedded in an 1.8 % agarose hydrogel. This allowed for the inoculation of the synthetic biofilm without the need of a special electrode material mount that was necessary for pouring in order to let the liquid biofilm solidify without leakage. To conclude, spraying could be established as the preferred inoculation strategy as it allows flexible introduction of the biomaterial into different reactor configurations without special design requirements. Further, the mean current density of the naturally formed biofilm reached a value of 145.3 ± 23.9 mA m^{-2} after 24 hours (Figure 15). Accordingly, the synthetic biofilm

resulted in a 2.1-fold and 2.3-fold increase in mean current density for spray and pour inoculation, respectively, compared to planktonic inoculation. Thereby, it could be shown that not only the start-up of the MEC system was facilitated by sprayable inoculation of the hybrid biomaterial, but that this biomaterial at the same time provided an overall improvement in performance compared to natural *S. oneidensis* biofilms.

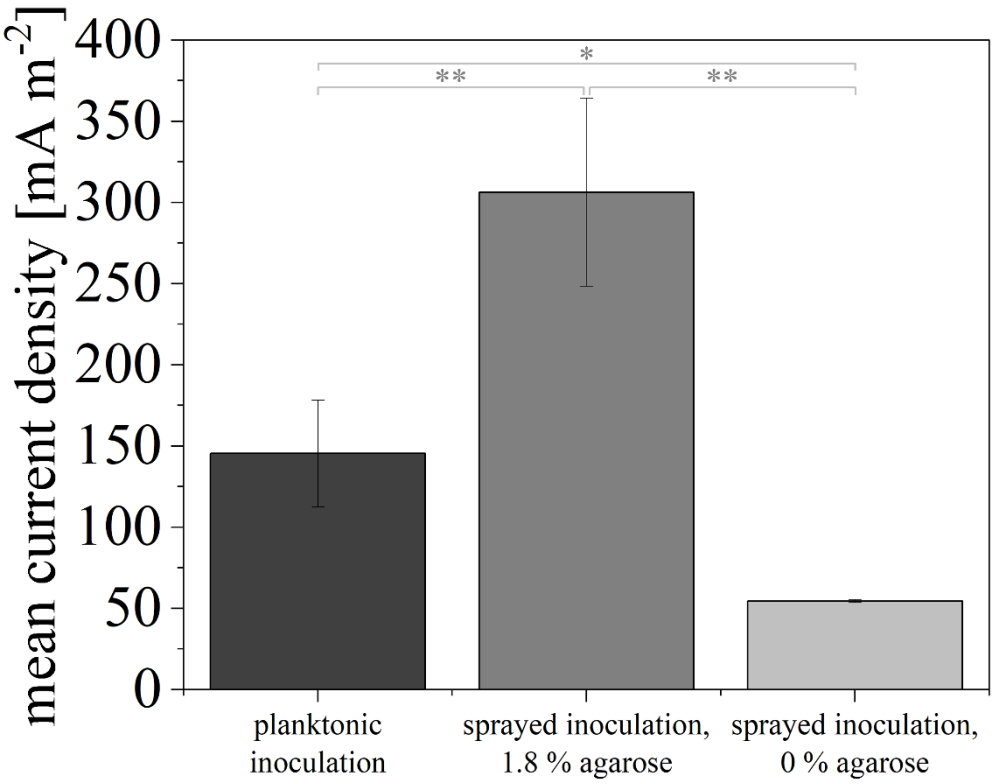

Figure 15: Effects of agarose addition during spray inoculation on current output in the MEC. *S. oneidensis* cells were sprayed without the addition of agarose (0 % agarose) and the mean current density after 24 h was compared to spray inoculation with 1.8 % agarose addition and planktonic inoculation. Spraying without agarose addition resulted in significantly lower mean current densities of 54.4 ± 1.0 mA m^{-2} compared to spraying with 1.8 % agarose at 306.3 ± 58.0 mA m^{-2} and planktonic inoculation at 145.3 ± 23.9 mA m^{-2}. Thus, the addition of agarose appeared to be necessary to protect the cells from the harsh conditions during spray inoculation (according to Knoll *et al.*, 2022).

Next, the question should be addressed whether *S. oneidensis* sprayed without an agarose matrix could lead to similar performance and whether the use of agarose as a 3D scaffold was indeed necessary. Therefore, a negative control with 0 % agarose and the same number of cells as for the synthetic hybrid biomaterial was sprayed on the electrode material in the

next step. The mean current density after 24 h of this 0 % agarose approach was significantly lower compared to the sprayed biofilm with 1.8 % agarose, with 54.4 ± 1.0 mA m^{-2} and 306.3 ± 58.0 mA m^{-2}, respectively. Further, the inoculation by spraying with 0 % agarose produced a significantly lower mean current density than planktonic inoculation with 145.3 ± 23.9 mA m^{-2}. Accordingly, spraying *S. oneidensis* cells without agarose addition significantly decreased performance compared to planktonic and spray inoculation with 1.8 % agarose addition. This suggests that the scaffold of the agarose hydrogel not only did not hinder the performance of *S. oneidensis*, but that these agarose fibres rather protected the cells from the harsh spray conditions.

3.2.2 **Performance of synthetic biofilms after start-up phase**

Up to this point, the performance of the hybrid biomaterial was only investigated within the first 24 h. During this start-up phase, it could be shown that the sprayed, synthetic biofilm resulted in a 2.1-fold increase in mean current density in comparison to the naturally formed biofilm (see section 3.2.1). However, the question was whether this increase in performance would be stable after this initial phase and whether the hybrid biomaterial would lead to increased current output over a longer period of time. Therefore, for each inoculation strategy, a triplicate was studied in terms of mean current density at 24 h intervals over a total period of 96 h. To highlight the improvement due to spray inoculation, the total values of the mean current density for each experiment were normalised to the value of the naturally formed biofilm after 24 h (see section 2.2.4).

The spray inoculation resulted in an improvement in comparison to the planktonic inoculation after 24 h of about 1.69 ± 0.44 (Figure 16). After 48 h, 72 h and 96 h this value increases for the spray inoculation to 1.98 ± 0.37, 2.26 ± 0.49 and 2.36 ± 0.61, respectively, while the planktonic inoculation resulted in an improvement factor of 1.21 ± 0.03 for 48 h, 1.28 ± 0.12 for 72 h and 1.46 ± 0.05 for 96 h. It is noticeable that the standard deviation for spray inoculation is substantially higher than for planktonic inoculation. This could be due to the fact that spraying the synthetic biofilm requires a more manual approach, which leads to higher deviations between the individual replicates. Nonetheless, the improvement factor of the sprayed, synthetic biofilm was higher than that of the naturally formed biofilm over 96 h. After 72 h, this improvement was still significant (Table S3). However, after 96 h, no

significant differences in the improvement factor between synthetic and naturally formed biofilm could be observed. In conclusion, the hybrid biomaterial offered a performance advantage compared to natural *S. oneidensis* biofilms, with the current output after 96 hours of synthetic and naturally formed biofilm appearing to equalize. In addition, the hourly increase was calculated for natural and synthetic approach (see section 2.2.4). For planktonic inoculation, the calculated gradient was 0.0061 h^{-1} and for the sprayed inoculation 0.0095 h^{-1}. Thus, after 96 h, the synthetic biomaterial resulted in a 1.5-fold steeper hourly incline in current density compared to the natural system.

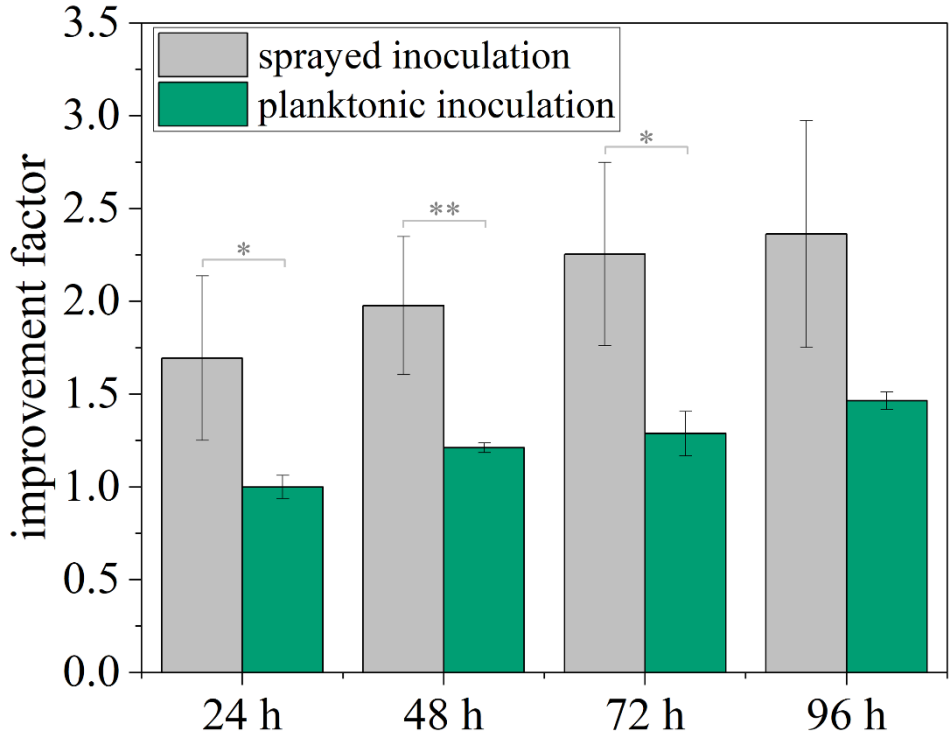

Figure 16: Comparison of performance of synthetic versus naturally formed *S. oneidensis* biofilm after initial start-up phase in the MEC. To calculate the here given improvement factor, the mean current density after each time point was normalized to the value of the naturally formed biofilm (planktonic inoculation) after 24 h. The synthetic biofilm (sprayed inoculation) led to an improvement factor of 1.69 ± 0.44 for 24 h, 1.98 ± 0.37 for 48 h, 2.26 ± 0.49 for 72 h and 2.36 ± 0.61 for 96 h. Meanwhile, the planktonic inoculation technique resulted in an improvement factor of 1.21 ± 0.03 for 48 h, 1.28 ± 0.12 for 72 h and 1.46 ± 0.05 for 96 h. To conclude, there was a performance advantage of the hybrid biomaterial compared to natural *S. oneidensis* biofilms, where the current output seemed to equalize after 96 hours (modified from Knoll *et al.*, 2022).

3.3 Performance improvement of sprayed biofilms

After establishing the hybrid biomaterial and the comparison between synthetic and naturally formed biofilm, the question arose whether the 3D scaffold provided by the agarose could be optimized in a way that would boost current output even further. The matrix in which the organisms are embedded is essentially the substitute for the extracellular matrix built in natural biofilms. It is known in literature (Malvankar *et al.*, 2012; Malvankar and Lovley, 2012), that this scaffold is directly linked to the current output and that factors such as conductivity of these supporting structures could improve the performance of exoelectrogenic organisms (see section 1.2.3). In this context, the aim was to change the abiotic characteristics of the hydrogels itself to obtain material properties that would subsequently lead to an improvement in current production in the MEC system. Two enhancing additives were chosen for this: first, riboflavin, a well-studied soluble electron shuttle, and second, CNFs functionalised with riboflavin to increase hydrophilicity of these fibers. Further, the addition of another exoelectrogenic organism was studied to gain insight into the performance of a mixed species biomaterial. The organism selected was *G. sulfurreducens*, as this exoelectrogenic organism is associated with excellent performance in MEC systems (see section 1.2). In the following, current density of these engineered biomaterials spiked with either riboflavin, CNFs or *G. sulfurreducens* was compared to the synthetic biofilm without any additives.

3.3.1 Conductivity of abiotic hydrogels

To improve the performance of the synthetic biofilm even further, two additives were selected to be introduced into the hydrogel fibers alongside *S. oneidensis*. Before the effects on current output were investigated in the BES batch reactor, the abiotic hydrogels were tested regarding their conductivity. For this, a custom-made conductivity cell was used to measure the resistance from which the conductivity could be calculated (see section 2.3.4). The 1.8 % agarose solution with riboflavin, with CNFs and without any additives as well as the 0 % agarose solution were tested in terms of their abiotic conductivity. Since CNFs have to be functionalised with riboflavin to produce hydrophilicity, it was not possible to produce a hydrogel with only CNFs, so no conductivity can be given at this point. The 0 % agarose solution was included to gain insight into the effects the agarose fibers have on conductivity.

As 25 % of the final hydrogel solution consisted of defined salt buffer (see section 2.1.4) an ionic conductivity for all four solutions was expected. The 0 % agarose solution resulted in a conductivity of 3.74 x 10^{-3} S m^{-1} and was significantly lower than all other tested hydrogels. The 1.8 % agarose solution showed a conductivity of 4.91 x 10^{-3} S m^{-1} without any additives and 4.95 x 10^{-3} S m^{-1} with the addition of riboflavin. There was no significant difference found between these two hydrogels (Table S5). With a conductivity of 6.97 x 10^{-3} S m^{-1}, the 1.8 % agarose solution with CNFs was significantly higher than all the other studied hydrogels. In the next part of this thesis, each hydrogel was investigated in terms of current output in the MEC system.

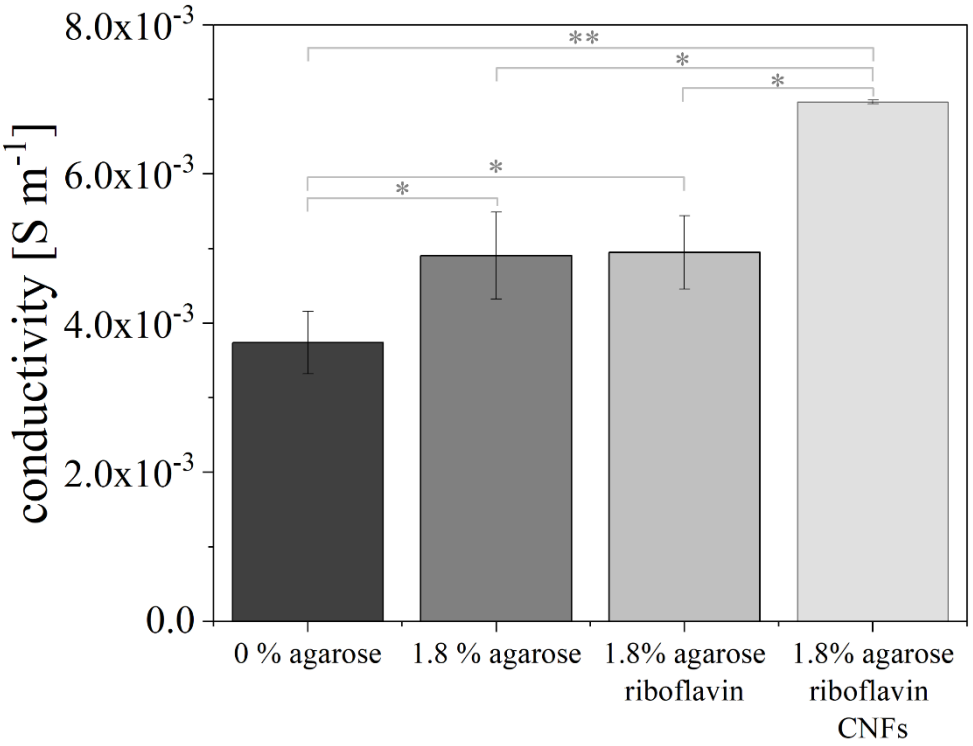

Figure 17: Conductivity of abiotic hydrogels with different additives. With a conductivity of 3.74 x 10^{-3} S m^{-1}, the 0 % agarose solution resulted in a significantly lower conductivity than the other tested hydrogels. The conductivity of 4.91 x 10^{-3} S m^{-1} and 4.95 x 10^{-3} S m^{-1} for the 1.8 % agarose solution without and with riboflavin addition, respectively, showed no significant effect on the conductivity with respect to the addition of the electrode shuttle (Table S5). With a conductivity of 6.97 x 10^{-3} S m^{-1} the hydrogel spiked with CNFs resulted in a significantly higher conductivity compared to the other hydrogels (according to Knoll *et al.*, 2022).

3.3.2 **Enhancing current production of synthetic *S. oneidensis* biofilm**

The analysis of the abiotic conductivity of the hydrogels spiked with riboflavin and CNFs showed that the hydrogel with added CNFs resulted in the most conductive scaffold for *S. oneidensis*. Accordingly, three different biomaterials were fabricated and the performances of the synthetic biofilm with riboflavin and CNFs was compared to the one without additives as well as to naturally formed biofilms. The mean current density after 24 h was once again selected as reference value.

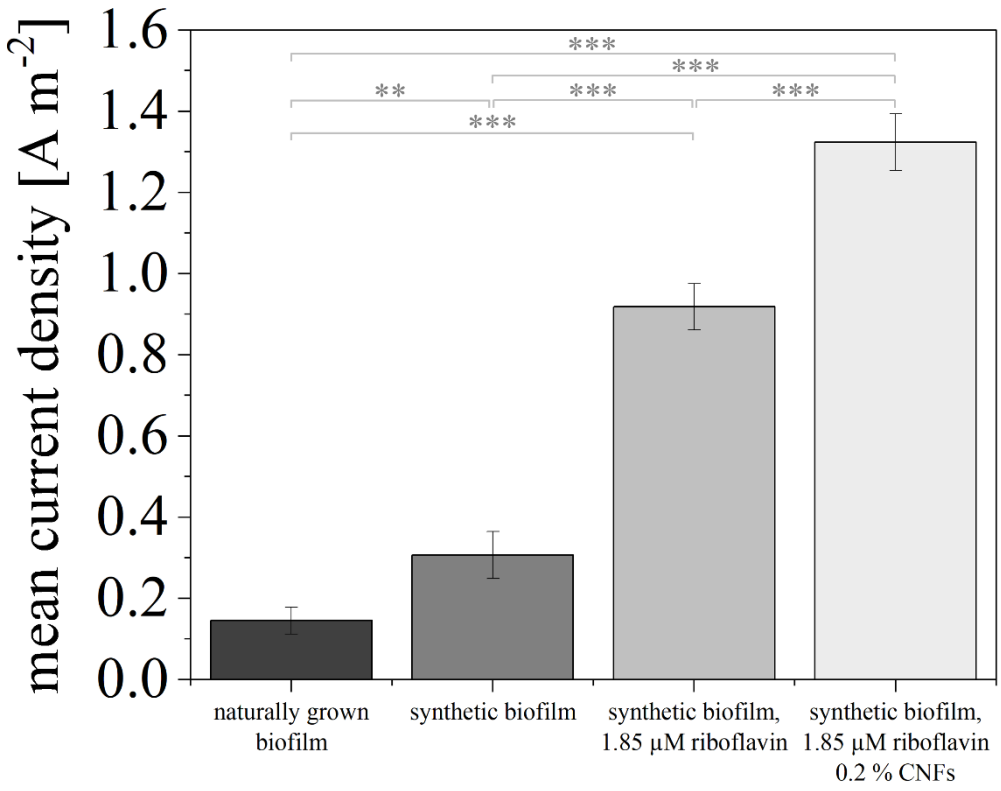

Figure 18: Effects of hydrogel additives on current output of synthetic *S. oneidensis* biofilms in comparison to naturally grown biofilms. Mean current densities after 24 h were compared for naturally grown biofilms and three different hybrid biomaterials. The naturally grown biofilm and the synthetic biofilm without additives resulted in a mean current density of 145.3 ± 23.9 mA m^{-2} and 306.3 ± 58.0 mA m^{-2}, respectively. The addition of riboflavin led to a current density of 918.4 ± 57.1 mA m^{-2}, while the further addition of CNFs resulted in a current density of 1324.0 ± 69.5 mA m^{-2}. The synthetic biofilm spiked with CNFs resulted in a significant improvement of 4.3-fold compared to the synthetic biofilm without additives and 9.1-fold compared to the naturally grown biofilm (modified from Knoll *et al.*, 2022).

As mentioned before, the naturally grown biofilm and the synthetic biofilm without additives resulted in a mean current density of 145.3 ± 23.9 mA m^{-2} and 306.3 ± 58.0 mA m^{-2}, respectively. The synthetic biofilm consisting of agarose hydrogel, *S. oneidensis* cells and riboflavin led to a current density of 918.4 ± 57.1 mA m^{-2}, which was significantly higher than the performance of both synthetic biofilm without additives and naturally formed biofilm. Further, the synthetic biofilm formed from riboflavin functionalized CNFs, cells and agarose hydrogel resulted in a mean current density after 24 h of 1324.0 ± 69.5 mA m^{-2}. Again, this improvement in current density was significant in comparison to the three other tested biofilms (Table S4). Conclusively, the addition of riboflavin and CNFs improved the performance of the synthetic biofilm by 4.3-fold. Overall, this meant a 9.1-fold improvement when the riboflavin and CNFs enriched synthetic biofilm was compared to the naturally formed biofilm. Thus, the hydrogel scaffold of agarose fibers, riboflavin and CNFs, which abiotically exhibited the highest conductivity, was found to be the optimized hybrid biomaterial with the highest current density. In other words, the hybrid biomaterial established and investigated in this work not only improved the start-up in terms of inoculation procedure and current output in the first 72 h compared to naturally formed biofilms. By adding reinforcing supplements such as riboflavin and CNFs, the material properties were additionally modified in such a way that the function defined by the user - in this case the optimisation of current output - was accomplished in a significantly more effective manner.

3.3.3 **Performance of sprayed, mixed species biofilms**

The addition of abiotic additives, more specifically riboflavin and CNFs, resulted in a 9.1-fold increase in current density compared to the biofilm naturally formed by *S. oneidensis*. The next step was to determine whether the performance of *S. oneidensis* in this hybrid biomaterial could be further enhanced by the addition of another exoelectrogenic organism. The selected organism, *G. sulfurreducens*, is widely utilised in BES technology and its performance in terms of current density far exceeds that of *S. oneidensis* (see section 1.2). Thus, *G. sulfurreducens* cells were embedded together with *S. oneidensis* cells in an overall ratio of 1:10 in terms of optical density (see section 2.1.4). As *G. sulfurreducens* is a

strict anaerobic bacterium that can only tolerate a minimum of oxygen, the spraying of this organism presented a further challenge.

To overcome this problem, the hybrid biomaterial consisting of *S. oneidensis* and *G. sulfurreducens* was first tested regarding its oxygen sensitivity in two possible ways. First, a gas line was built into an anaerobic chamber, in which the oxygen content was always kept below 0.005 %, and the spraying was performed in this anoxic atmosphere. Second, a constant stream of argon was directed onto the spray mist while the spraying was performed (argon atmosphere). In a second step, the performance in terms of mean current density after 72 h of this hybrid biomaterial was compared to a naturally grown biofilm from *S. oneidensis* and *G. sulfurreducens* and the effects of spraying on the mixed species biomaterial were investigated by an additional pour inoculation. Further, riboflavin-functionalized CNFs were added to the biomaterial as these supplements led to the highest performance increase for the synthetic *S. oneidensis* biofilm. Additionally, the effects of additional acetate as electron donor on the performance were investigated in a one-shot experiment (no triplicate due to technical data loss). In a last step, the performance of the start-up period (first 24 h) of the synthetic *S. oneidensis* and *G. sulfurreducens* biofilm was compared to the other tested biomaterials from section 3.3.2.

3.3.3.1 Adaption of the spraying technique for *G. sulfurreducens*

G. sulfurreducens was long believed to be a strict anaerobic organism until it was found that the bacterium could not only tolerate oxygen but further use it as a terminal electron acceptor (Lin *et al.*, 2004). However, the study also demonstrated that an oxygen content above 5 % has significantly negative effects on cell growth of *G. sulfurreducens*. Therefore, the exclusion of oxygen during the spraying was essential. For this, two different atmospheres for spraying were tested regarding to the produced mean current density after 72 h (argon versus anoxic atmosphere).

The spraying of *G. sulfurreducens* and *S. oneidensis* embedded in a 1.8 % agarose hydrogel resulted in a mean current density of 2.46 ± 0.7 A m^{-2} after spraying in the argon atmosphere and 1.79 ± 0.3 A m^{-2} after spraying in the anoxic atmosphere (Figure 19, A). No difference could be found between both atmospheres. Since spraying using a constant flow of argon

offered a more flexible approach, all hybrid biomaterials consisting of *G. sulfurreducens* and *S. oneidensis* were sprayed in the argon atmosphere in the subsequent experiments.

In the next step, the performance of the synthetic, mixed species biofilm was compared to the performances of a naturally formed biofilm of *G. sulfurreducens* and *S. oneidensis*. For this, the same number of cells was inoculated planktonically into the electrolyte of the BES and the mean current density after 72 h was compared. The naturally formed biofilm resulted in a mean current density of around 3.97 ± 0.5 A m^{-2}. In addition, the effect of spraying itself was again tested by comparing the current density of spray and pour inoculation, as a negative effect on the pili of *G. sulfurreducens* in particular was conceivable. The poured mixed species biomaterial achieved a mean current density of 1.83 ± 0.1 A m^{-2} and, again, no difference between both inoculation approaches was found. Therefore, the spraying process itself did not appear to negatively influence the performance of the mixed species biomaterial in terms of current output. However, a difference between planktonic inoculation for the naturally formed biofilm and the spray as well as the pour inoculation for the synthetic biofilm was observed. Hence, the conclusion was drawn that the naturally biofilm consisting of *S. oneidensis* and *G. sulfurreducens* outperformed the synthetic mixed species biofilm in terms of mean current density after 72 h. In a next step, riboflavin-functionalized CNFs were added to the biomaterial as this supplement led to significant increase in performance for the synthetic *S. oneidensis* biofilm. The mean current density for the mixed species biomaterial complemented with CNFs was measured with 1.64 ± 0.4 A m^{-2} and no increase compared to the synthetic biofilm without CNFs could be found. In a last step, acetate was complemented as second electron donor to the media. While *S. oneidensis* is able to utilize lactate as electron donor and produces acetate in doing so, *G. sulfurreducens* can only metabolize acetate. Therefore, the acetate production of *S. oneidensis* is necessary for *G. sulfurreducens* to be able to proliferate in the synthetic biomaterial. By the addition of 20 mM acetate in this singlicate experiment the dependency of *G. sulfurreducens* on *S. oneidensis* was therefore eliminated to investigate the effect this addition could have on current production. This approach resulted in a mean current density of 1.14 A m^{-2} which is lower in comparison to all other experiment.

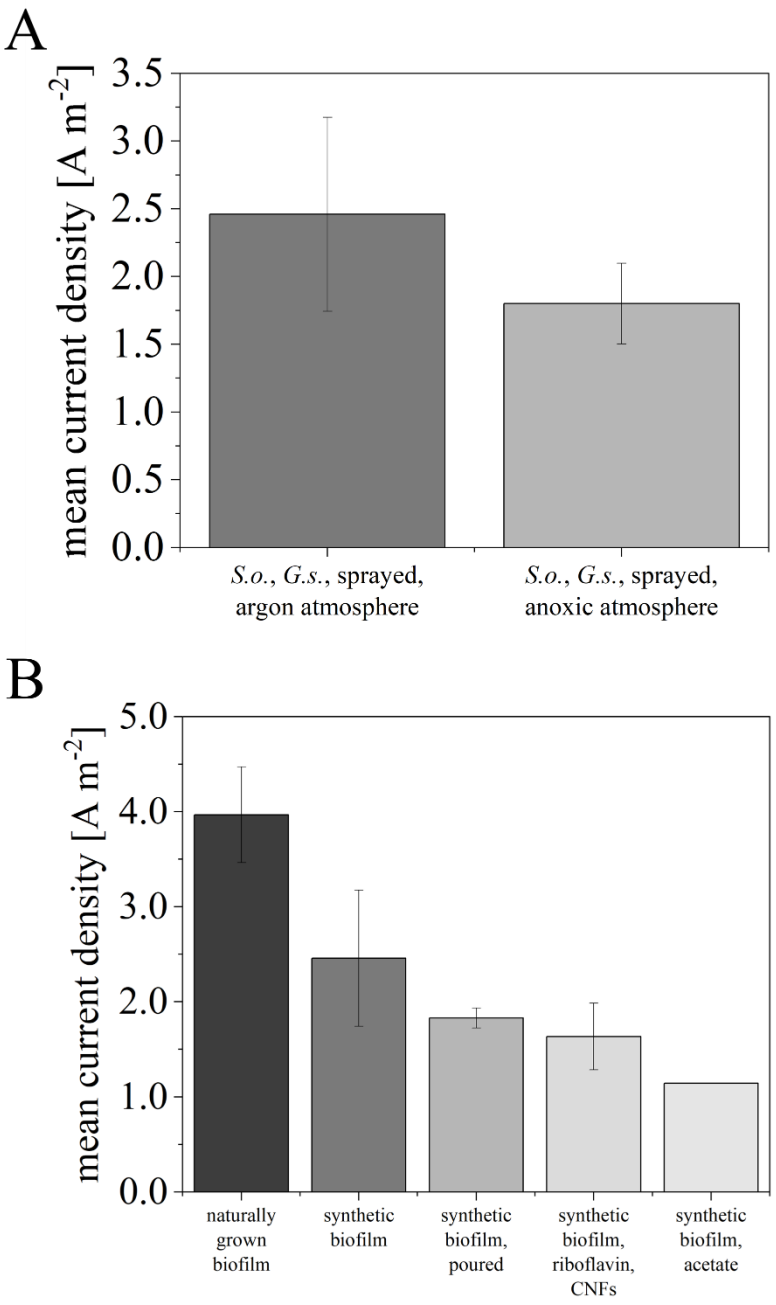

Figure 19: Performance of mixed species biomaterial in terms of mean current density after 72 h. A) The hybrid biomaterial with embedded *G. sulfurreducens* and *S. oneidensis* was sprayed under a constant stream of argon (argon atmosphere) and in an anaerobic chamber with an oxygen content < 0.005 % (anoxic atmosphere). Current density was measured at 2.46 ± 0.7 A m^{-2} after spraying in the argon atmosphere and 1.79 ± 0.3 A m^{-2} after spraying in the anoxic atmosphere. B) Current density of a naturally grown biofilm (3.97 ± 0.5 A m^{-2}, n = 2), the synthetic mixed species biofilm with spray (2.46 ± 0.7 A m^{-2}, n = 3) and pour (1.83 ± 0.1 A m^{-2}, n = 2) inoculation as well as after the addition of riboflavin functionalized CNFs (1.64 ± 0.4 A m^{-2}, n = 3) and the supplementation of additional electron donor in the form of acetate (1.14 A m^{-2}, n = 1) was compared. The number of experiments (n) performed is given for each approach. For experiment with n = 2, namely poured, sprayed in anoxic atmosphere and naturally grown biofilms, the error bars represent the deviation of the duplicates from the mean value, for n = 3 standard deviation was calculated according to Equation 5.

In conclusion, the naturally grown biofilm resulted in a higher current density than the biomaterial after spray as well as pour inoculation. The natural system appeared to surpass all synthetic approaches investigated in this part of the thesis. Nevertheless, it could be shown that the harsh conditions during spraying did not hinder the performance of this biomaterial itself (pour versus spray). Additionally, the comparison between spraying in the argon or the anoxic atmosphere confirmed the possibility of spraying oxygen sensitive organisms.

3.3.3.2 Overview of current output in the start-up phase of different biomaterials

After establishing the sprayed, mixed species biomaterial, the performance was compared with that of the synthetic *S. oneidensis* biofilm. The aim of this part of the thesis was to investigate the effects of different additives on the hybrid biomaterial and thus optimise the function of the material for application purposes. Therefore, the mean current density in the initial start-up phase was calculated for the mixed species biomaterial as well and compared with the current output of the assessed *S. oneidensis* biofilms from section 3.3.2 (Figure 20). After 24 h, the mean current density of the mixed species biomaterial was 1.50 ± 0.4 A m^{-2} instead of 2.46 ± 0.7 A m^{-2} after 72 h. Relative to the naturally formed *S. oneidensis* biofilm with a mean current density of 0.15 ± 0.03 A m^{-2}, the addition of *G. sulfurreducens* as a supplement thus led to a significant increase in current output of about 10-fold. As mentioned above, the mean current density of the synthetic *S. oneidensis* biofilm was determined to be 0.31 ± 0.06 A m^{-2}, so that a 4.8-fold increase in current output could be achieved by adding *G. sulfurreducens* to this biomaterial. However, the current production of the natural biofilm formed by *S. oneidensis* and *G. sulfurreducens* exceeded that of the synthetic biofilm by a factor of 1.6. A comparison between the synthetic biofilm supplemented with CNFs, which yielded a mean current density of 1.32 ± 0.07 A m^{-2}, and the synthetic biofilm supplemented with *G. sulfurreducens* revealed no significant difference between the two biomaterials.

In conclusion, the performance of naturally formed biofilms of *S. oneidensis* was significantly improved by embedding this organism in the agarose hydrogel matrix. Not only could a spray inoculation be established for flexible application, but the performance of this synthetic biofilm also exceeded that of the natural system. After investigating three possible supplements, more specifically riboflavin, riboflavin-functionalised CNFs and another exoelectrogenic organism *G. sulfurreducens*, it was shown that current production in the

initial start-up phase in the MEC system could be improved by up to 10-fold. In particular, the addition of CNFs or *G. sulfurreducens* was proved to be essential for the increase in performance. Thus, the hybrid biomaterial was characterised and optimised with regard to current generation. Subsequently, the effects of this hybrid material were to be investigated in an application scenario (see section 3.4).

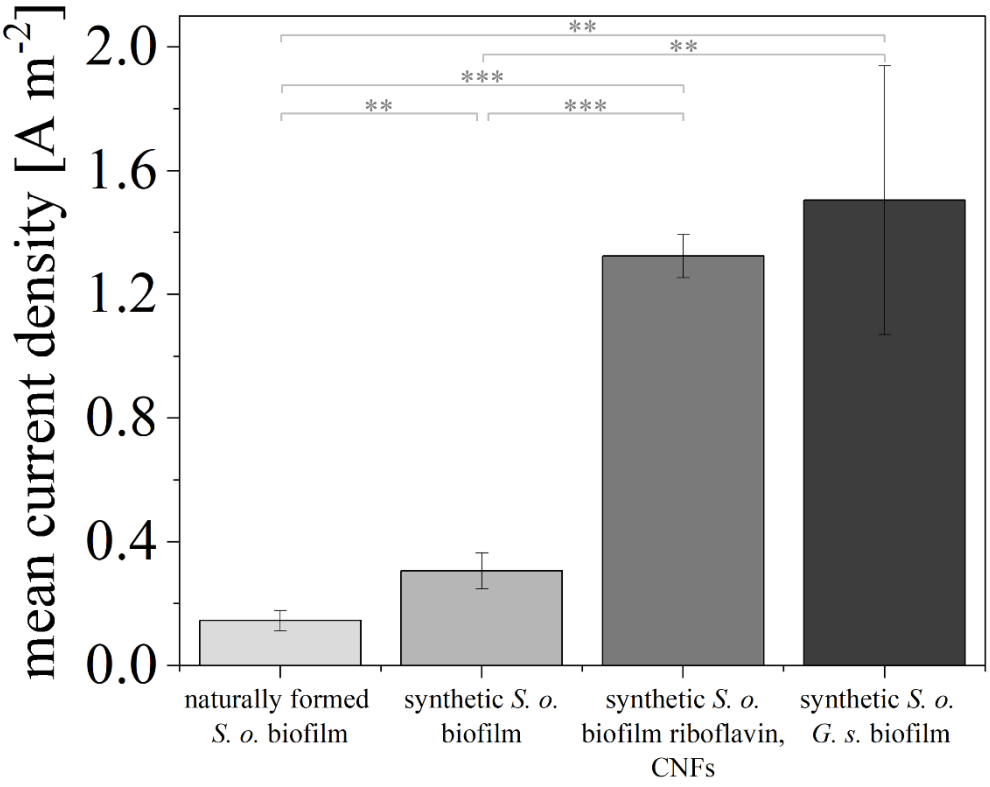

Figure 20: Effects of the addition of CNFs and *G. sulfurreducens* on current output of synthetic *S. oneidensis* biofilms in comparison to naturally grown biofilms. Mean current density after 24 h were compared. The naturally grown biofilm and the synthetic biofilm without additives resulted in a mean current density of 0.15 ± 0.03 A m^{-2} and 0.31 ± 0.06 A m^{-2}, respectively. The addition of riboflavin and CNFs led to a current density of 1.32 ± 0.07 A m^{-2}, while the addition of *G. sulfurreducens* resulted in a current density of 1.50 ± 0.4 A m^{-2}. No significant difference was found between the synthetic biofilm with CNFs and the one with *G. sulfurreducens*. Consequently, an improvement in current density of up to 10-fold in comparison to naturally formed *S. oneidensis* biofilms was achieved with these additives.

3.4 Application of sprayed biofilm – electrical anaerobic digestion

The in this thesis established biomaterial was in the next step analysed in an application example. As example, a coupled MEC-biogas system was selected. Biogas plants in which waste streams can be utilized by microorganisms to form biogas are already widely applied. However, the biogas production is rather sensitive to an accumulation of organic acids that inhibits methanogenesis. To optimize this process, one approach is to integrate a MEC module into existing biogas plants (see section 1.3). With this, organisms growing on the anode including *S. oneidensis* and *G. sulfurreducens* can metabolize the accumulating organic acids and transfer their respiratory electrons onto the electrode to produce hydrogen on the cathodic side of the MEC. As a result, the electron flow can be directed via the applied anodic potential either towards hydrogen formation via MEC or towards biogas production. In this thesis, a coupled MEC-biogas system was set-up in the BES batch reactors (see section 2.3.3.1). A naturally formed biofilm of *S. oneidensis* and *G. sulfurreducens* was pre-cultivated for 7 days in the reactor (Figure 21, phase I) before biomass addition was started on the seventh day (Figure 21, phase II). The hybrid biomaterial consisting of agarose hydrogel, *S. oneidensis* and *G. sulfurreducens* was inoculated in a second system without pre-cultivation simultaneously with the addition of biomass. Both approaches were tested in one experiment without replicates. Seven days after the start of phase II, the total volume of cultivation media was substituted by the addition of biomass and the current density of both the natural system and the synthetic system was monitored for another 21 days (Figure 21, phase III). The BES batch reactor was kept anoxic by supplying the system with a constant stream of N_2 gas as for all other experiments (see section 2.3.3.1). However, on day 10 a disruption in gas supply due to technical malfunctions was monitored.

At the end of the pre-cultivation phase, natural biofilm formation due to the planktonic inoculation on the anode was visible to the naked eye. This biofilm resulted in a maximum current density in the pre-cultivation phase of 0.3 mA cm^{-2} around day 2 and showed a current density of 0.25 mA cm^{-2} right before the addition of biomass was started. During phase II, the biomass addition phase, the current density was found to increase to 0.4 mA cm^{-2} on the first day and appeared to stabilize at 0.28 mA cm^{-2} until day 10. Then, a rapid decrease in current density below 0.1 mA cm^{-2} could be monitored until day 14. The system inoculated with the synthetic biofilm, that was started on day 7, increased in current density rapidly in

the first two days to a maximum current density of 0.18 mA cm^{-2}. A decrease in current density was found on day 10 as for the natural system to a minimum of 0.05 mA cm^{-2}. On day 14, the addition of biomass was stopped and both systems were kept in batch mode. In this phase, both systems increased in current density after day 17. The system with a naturally formed biofilm increased to a maximum current density of 0.25 mA cm^{-2} in this phase. A drop in current density was found on day 30, after which the current density appeared to stabilize at 0.15 mA cm^{-2}. Meanwhile, the synthetic system exhibited a maximum current density of 0.4 mA cm^{-2} on day 25 in this phase. However, the current density measured for the synthetic approach decreased rapidly after day 30 to below 0.05 mA cm^{-2}.

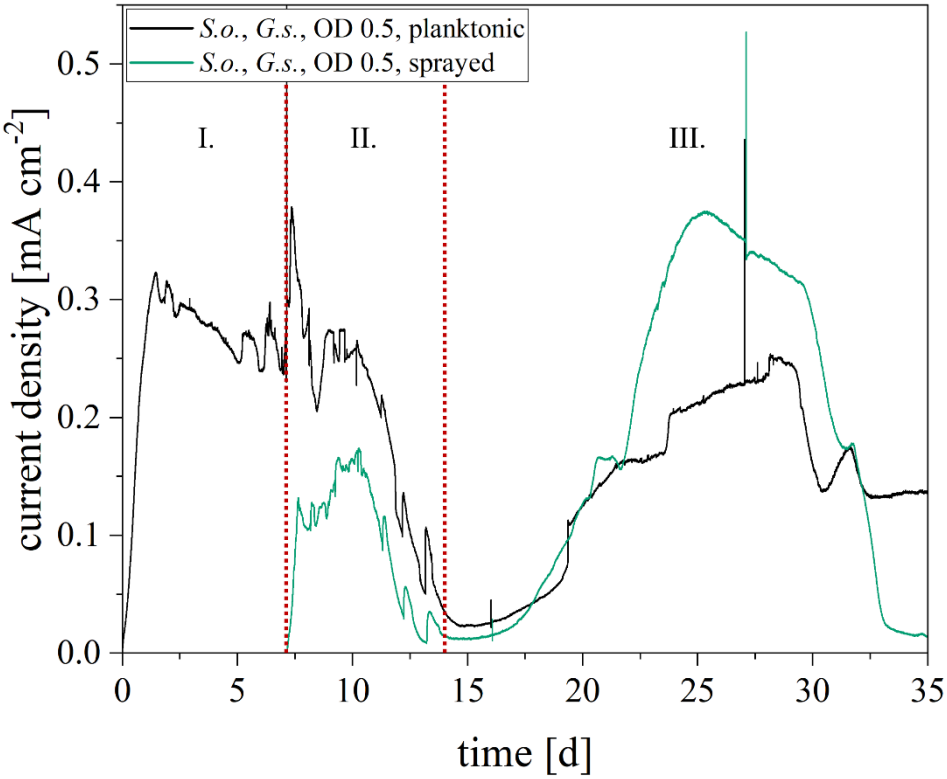

Figure 21: Current density of naturally grown biofilm (planktonic) and synthetic biofilm (sprayed) in coupled MEC-biogas system. For each approach, one system (n = 1) was started. Phase I) Pre-cultivation phase in the natural system. *S. oneidensis* and *G. sulfurreducens* were inoculated planktonically and a natural biofilm was formed for 7 days. The maximum current density was 0.3 mA cm^{-2} in this phase. Phase II) Daily addition of biomass. The synthetic system was started by spray inoculation of *S. oneidensis* and *G. sulfurreducens* embedded in agarose and biomass was added to both systems for 7 days. The natural system showed first an increase in current density to around 0.4 mA cm^{-2}, while the synthetic system increased to around 0.15 mA cm^{-2}. At day 10 a decrease in current density below 0.1 mA cm^{-2} was found for both systems. Phase III) Batch mode. The daily addition of biomass was stopped and both systems were operated at batch mode. Both systems resulted in an increase in current density after day 17 to 0.4 mA cm^{-2} and 0.25 mA cm^{-2} for the synthetic and natural system, respectively. At day 30 a drop in current density to 0.15 mA cm^{-2} for the natural system and 0.05 mA cm^{-2} for the synthetic system could be monitored. At day 35 both systems were stopped.

The systems were stopped after 35 days and the electrodes of both systems were stored for subsequent metagenomic analysis to gain insight into the microbiome colonizing the anode and contributing to the current production. However, the downstream processing of this analysis was still on-going and for now the yielded current densities were used for a comparison of the performance of natural versus synthetic system. Noticeably, the system in which a pre-cultivation phase was carried out to obtain a natural biofilm had a higher maximum current density right after the addition of biomass (phase II), but was surpassed by the system with synthetic biofilm in phase III.

3.5 Induced hydrogel detachment via hydrogen evolution

In the last part of this thesis, the established hybrid biomaterial was tested in terms of the detachment and the corresponding harvesting of the biofilm in a MEC system. This process is of interest because organisms used in BES can not only metabolize organic acids, as has been mentioned for *S. oneidensis* or *G. sulfurreducens*, but also produce industrially relevant products on an intercellular level. As the synthetic biofilm established in this thesis offers the possibility to embed such organisms as well, the harvesting of the hybrid biomaterial was to be investigated. Further, it could be demonstrated that the thickness of a biofilm could also be limiting due to diffusion limitations of the energy source, in this case organic acids. In *G. sulfurreducens* biofilm, no acetate could be detected below a depth of 100 µm (Renslow *et al.*, 2013). Therefore, targeted detachment of parts of the biofilm could increase acetate penetration and increase overall current performance.

To investigate this effect on the hydrogel, a BES flow cell (see section 2.3.3.2) was used for optical visualization of the detachment process. The applied current was ranged from -0.5 mA cm^{-2} to -5 mA cm^{-2} and decrease in 0.5 mA cm^{-2} steps. Further, two different electrode materials were tested, including the graphite felt used in the BES batch reactor and a graphite plate. The first one was selected to demonstrate the effects on the same material that was used for characterization of the biomaterial. The second one was chosen for the visualization using OCT as a flat surface of the electrode material is needed as reference surface for this technique (see section 2.2.3). A time lapse video for both materials was

created (see section 6.4) and from this time lapse, specific time points were chosen to be included in this section and are displayed below (Figure 22, Figure 23 and Figure 24).

3.5.1 **Detachment of biomaterial from graphite felt**

First, the detachment of the biomaterial was investigated after spraying on graphite felt. As this material is constructed of a 3D network of graphite fibers, OCT analysis was not possible. Therefore, only video analysis was evaluated and the picture at an applied current of -1 mA cm^{-2} and of -5 mA cm^{-2} of the detachment process are displayed (Figure 22).

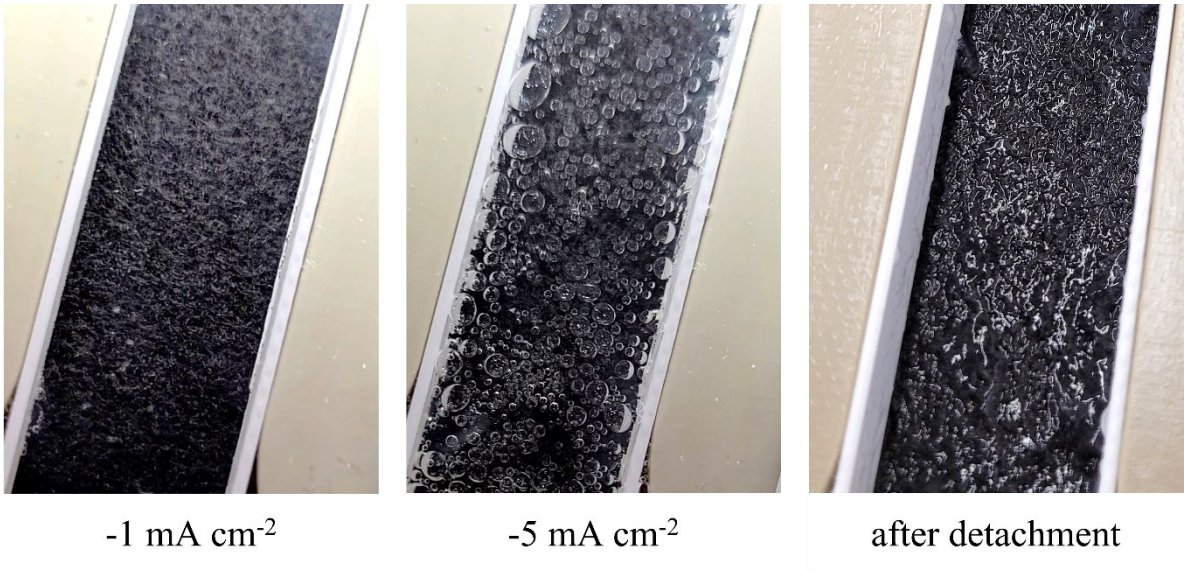

Figure 22: Induced hydrogel detachment from graphite felt. Negative currents ranging from -0.5 to -5 mA cm^{-2} were applied to the system and the H_2 formation was monitored using video imaging. Miniature bubbles passing through the hydrogel and collecting at the top of the flow cell could be observed at less negative currents (-1 mA cm^{-2}). With a decrease in current, the H_2 bubbles increased in size and number until the top of the flow cell was completely covered with bubbles (-5 mA cm^{-2}). After the detachment process, the lid and cultivation media were removed from the system and the bare hydrogel was observed. Various channels formed by the passing H_2 bubbles were found and larger parts of the hydrogel appeared to have been detached completely.

After -1 mA cm^{-2} was applied to the system for 1 min, miniature bubbles in the biofilm matrix could be observed (Figure 22, left). These bubbles passed through the hydrogel and collected at the top of the flow cell. Further, the H_2 bubbles increased in size and number with each decrease in applied current until the top part of the flow cell reactor was filled with H_2 bubbles as seen after 1 min application of a current of -5 mA cm^{-2} (Figure 22, middle). The highest increase in H_2 formation was observed between -2 and -2.5 mA cm^{-2} (see section 6.4) After the detachment, the top part of the flow cell was dismounted and the hydrogel on the graphite

felt was observed without the polycarbonate lid and cultivation media (Figure 22, right). It was clearly visible that the formation of H_2 bubbles disrupted the hydrogel structure and that channels formed by these bubbles significantly changed the smooth surface of the hydrogel that could be observed before the application of negative current to the system. Larger parts of the hydrogel were even completely detached and the hydrogel appeared to be more structured in comparison to the beginning.

3.5.2 **Detachment of biomaterial from graphite plate**

To visualize the detachment process of the agarose hydrogel more precisely, OCT analysis was performed during the detachment of a hydrogel sprayed onto a graphite plate. A 2D scan (B-scan) was initially carried out to verify that visualisation of the hydrogel using OCT is indeed possible. A 2.2 mm high and 6 mm long section was examined (Figure 23) in which the electrode surface (arrow 3), the hydrogel (arrow 1) with its surface (arrow 4) and bubbles from the spraying of this hydrogel (arrow 2) were visualized.

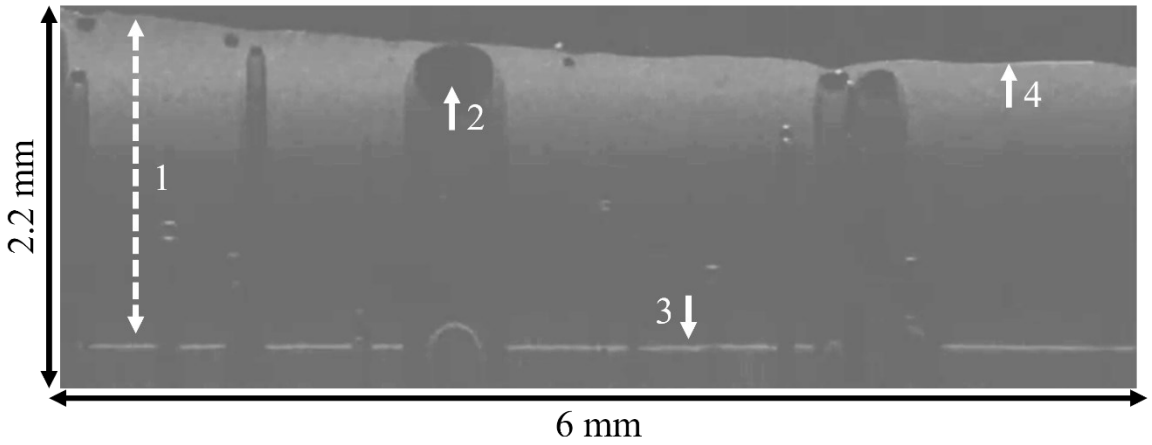

Figure 23: 2D view of the hydrogel on a graphite plate using OCT imaging. A 2.2 mm high and 6 mm long section was examined, in which the electrode surface (arrow 3), the hydrogel (arrow 1) with its surface (arrow 4) and bubbles from spraying on this hydrogel (arrow 2) were visualized. The graphite plate was visible as a clear white line, however, after covering the material with hydrogel, gaps and bends in this line were present, which corresponded with the bubbles observed in the hydrogel. These bubbles interfered with the OCT light beam resulting in these gaps and bends. Similar, only the upper part of the hydrogel showed a white opacity, presumably, as the light beam was scattered by the particles in the upper part of the gel and, therefore, hindering the light beam from penetrating to the lower part of the hydrogel.

Without hydrogel, the electrode surface was visible as a continuous white line, however, after covering of the electrode with the hydrogel, gaps and bends in this line were present. These gaps and bends corresponded to the bubbles found in the upper part of the hydrogel. Thus, these bubbles scattered the OCT light beam, resulting in the changes observed for the electrode material. It was found that this interference of the light beam also affected the visualisation of the hydrogel, as only the upper part of the hydrogel showed white opacity. Presumably, the particles in the top layer interfered with the light beam in such a manner that the light beam could not penetrate to the lower part of the hydrogel. The changes in this 2D view of the hydrogel on the graphite plate was monitored during the detachment process (Figure 24).

As with the detachment of the hydrogel from the graphite fleece, a time-lapse video was recorded for the detachment from the graphite plate. Sections of this at an applied current of -1, -2, -3, -4 and -5 mA cm^{-2} were selected to show the detachment process using 2D scans (Figure 24, A). As previously noted, H_2 bubble development began to be clearly visible at currents starting at -2 and -2.5 mA cm^{-2}. This was particularly noticeable in the 2D scan as it was possible to observe the bubbles within the hydrogel (white arrows) moving further upwards. In addition, the previously recognizable clear surface of the hydrogel is no longer visible in the 2.2 mm high section. This indicated that the H_2 development caused the hydrogel as a whole to be detached from the electrode surface. This effect continued to increase as the applied current was decreased. Small bubbles (especially evident in the time-lapse video) formed at the electrode surface were visualized by OCT and could be observed rising in newly formed channels. In addition, the formation of large bubbles directly at the electrode, as seen in the 2D scan at -4 mA cm^{-2}, could be visualized due to the extreme curvature of the electrode surface. Here, it appeared as if the H_2 formed accumulated under the hydrogel to form large bubbles before it could escape via an emerging channel. This became even more evident in the time lapse video.

OCT was further used to obtain a 3D scan of a 10.6 mm^3 (2.2 x 2.2 x 2.2 mm^3) section before and after the detachment process (Figure 24, B). Before the detachment, the 3D view of the hydrogel showed the rather smooth surface of the gel with bubble channels as seen in the 2D scan. Again, a white opacity in the upper part of the hydrogel as well as gaps and bends in the white line visualizing the electrode surface were observed due to interference. In

comparison, the 3D scan after detachment showed that the hydrogel surface was displaced from the scanned 10.6 mm^3 section. The upper part exhibiting the white opacity was also absent in this scan, indicating that this part of the hydrogel had been moved upwards, as seen in the 2D scan, and was no longer in the focal plane of the OCT light beam. In addition, the electrode surface on the right side showed a strong curvature, indicating the formation of an H_2 bubble trapped under the hydrogel. Hence, in both the 2D and 3D scans, detachment of the hydrogel from the graphite plate could be visualized, which was completely different from the detachment observed on the graphite felt. While the application of negative current to the graphite felt resulted in partial detachment of hydrogel pieces, the gel as a whole was detached when H_2 formation was induced on the graphite plate.

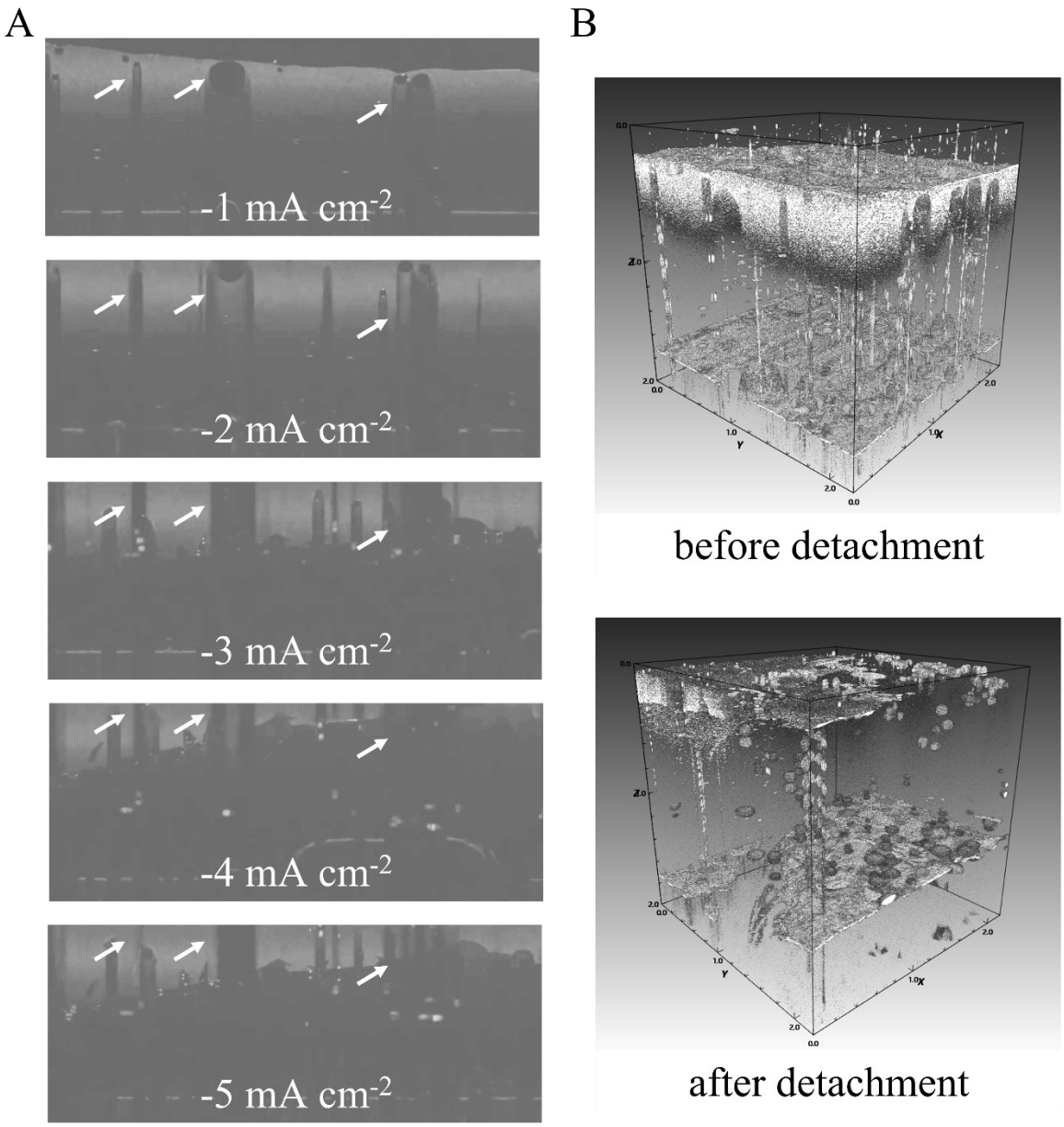

Figure 24: Hydrogel detachment from graphite plate. A) 2D view during application of -1 to -5 mA cm^{-2}. Bubbles (white arrows) were highlighted to demonstrate the effects the H_2 formation had on the hydrogel. With a decrease in negative current, the hydrogel including the top layer with white opacity and the already exciting bubble channels were shown to be lifted upwards. Small bubbles could be visualized to rise from the electrode surface and escaping through newly formed channels. Formation of large H_2 bubbles directly at the electrode surface could be found due to the extreme curvature of the electrode surface as seen for an applied current of -4 mA cm^{-2}. B) 3D view of hydrogel before and after detachment. Before the detachment, a 3D view of the hydrogel showed the rather smooth surface of the hydrogel with bubble channels as seen in the 2D scan. After detachment, the upper part showing the white opacity and the surface of the hydrogel were no longer found in this scan, indicating that the hydrogel has been lifted upwards and was no longer in the focal plane of the OCT light beam. The electrode surface showed a major curvature on the right side, indicating the formation of a H_2 bubble that was trapped under the hydrogel.

4 DISCUSSION

The increasing severity of climate change is a clear indication for the urgency of replacing production processes that are harmful to the environment in the interests of sustainability. This particularly includes the production of electricity. While the worldwide energy demand in the last 40 years already increased significantly (see section 1), forecasts showed that this demand can only be expected to grow even further to up to 11 % by 2030 (Kemmler *et al.*, 2021). At the same time, the share of renewable energy production based on the use of hydro, wind, solar, geothermal, biofuels and waste streams was only 26.8% in total in 2019, while the majority of electricity was generated by burning coal at 36.7% (International Energy Agency, 2019). This underlines humanity's continued reliance on fossil fuel-based production processes, which urgently need to be replaced by sustainable technologies as part of the energy transition required to reduce the sector's environmental footprint. In particular, more extensive utilization of biofuels and waste streams as resources could be key, as both accounted for only 2.4% of total electricity generation in 2019 (Figure 25, International Energy Agency, 2019).

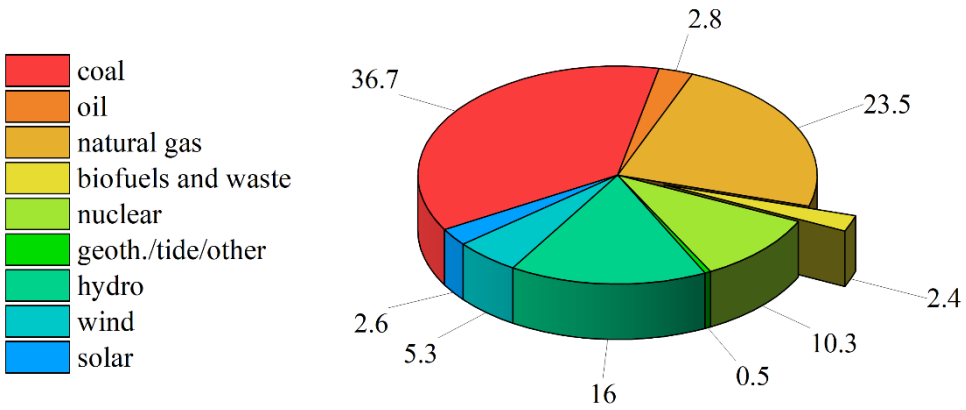

Figure 25: Share of sources for electricity production worldwide in 2019. The major share was electricity production by coal combustion with 36.7 %, followed by usage of natural gas with 23.5 %. Renewable energy generation including hydro, wind, solar, biofuels and waste as well as geothermal made up only 26.8 % in total. In particular, 2.4 % of energy originated from biofuel and waste stream, in which BES technology would also be categorized. The potential increase in this percentage offers the opportunity to reduce the negative environmental impact of petrochemical-based energy production (according to International Energy Agency, 2019).

The BES technology enables previously unexploited usage of biological waste streams by transferring chemical into electrical energy utilizing microorganisms as biocatalysts for this conversion. To this end, the microorganisms colonize the BES electrode in the form of a biofilm to facilitate the transport of their respiratory electrons on this electrode. One of the major bottlenecks of BES technology is this biofilm-electrode interaction, as it is not as efficient as would be required to achieve sufficient space-time yields for industrial application. To improve this interaction, synthetic biology can be used to develop hybrid biomaterials that surpass the performance of natural systems in these BES applications. In this thesis, such a hybrid biomaterial was built by embedding the exoelectrogenic organism *S. oneidensis* in an agarose hydrogel.

Hydrogels have been used in medicine and basic science as artificial substitute for the EPS matrix that is naturally self-produced by the organisms in a biofilm (see section 1.4). In this thesis, an agarose hydrogel was chosen to serve this purpose for the fabrication of an electroactive biomaterial which was applied in a BES for current generation. Agarose is a relatively inexpensive polymer that consists of repeating units of β-1,3 linked D-galactose and α-1,4 linked 3,6-androhydro-L-galactopyranose (Araki, 1956) and dissolves in water when heated above its melting point. Upon cooling, rigid hydrogen bonds between the individual agarose chains form a porous, thermally reversible hydrogel whose pore sizes depend on the concentration (Serwer and Hayes, 1986; Armisén, 1991). The formation of microchannels enables the supply of nutrients to the microorganisms embedded in them, the removal of metabolic end products and thus also the growth of the organisms within the gel (Strathmann *et al.*, 2001). Therefore, besides its best known application in the electrophoretic separation of nucleic acids and proteins (Johansson, 1972), agarose hydrogels have been implemented as EPS substitutes for drug delivery (Wang and Wu, 1997; Khodadadi Yazdi *et al.*, 2020), tissue engineering (Zarrintaj *et al.*, 2018) but also model for bacterial biofilms (Strathmann *et al.*, 2001; Sahle-Demessie and Tadesse, 2011). Compared to other hydrogels, agarose offers the advantage that the gelation process is determined exclusively on the basis of temperature. Spraying an agarose hydrogel as it begins to solidify due to cooling is therefore particularly convenient, as no further complexing agents need to be taken into account, thus considerably simplifying the process. As the aim of this thesis was to develop a sprayable biomaterial, agarose was chosen as a suitable candidate. In addition, to reduce

the heat damage described for bacterial cells during encapsulation in an agarose scaffold (Strathmann *et al.*, 2000), low-melt agarose with a gelling temperature ≤ 28 °C was chosen. The following chapters 4.1, 4.2 and 4.3 revolve around the major finding of Knoll *et al.* (2022), in which the sprayable hybrid biomaterial was first characterized.

4.1 Characterization of novel hybrid biomaterial

4.1.1 Influence of cell density and biomaterial thickness on current output

For an optimal performance, each cell in the biomaterial should contribute to the current production and is connected to the electrode surface for optimal EET. In theory, therefore, there should be a direct correlation between the increase in the number of cells and the increase in the current output if there is unhindered access to the electrode as an electron acceptor. In this thesis, this applied for the studied biomaterial when the cell number was increased from 0.79×10^7 to 5.98×10^7. However, an increase in cell number above 5.98×10^7 showed no significant improvement in current density and a plateau in current production was reached. At this point, no increase in biomaterial efficiency through the addition of more individual cells appeared to be achievable. This could be due to diffusion limitations as they occur in natural biofilms. It has been reported that microniches due to limiting nutrient diffusions are created in biofilm structures and that these result in a heterogeneous growth of the organism within the biofilm matrix (Wentland *et al.*, 1996; Xu *et al.*, 1998; Nagar and Schwarz, 2015). It is possible that the high cell density led to the exhaustion of these niches due to nutrient starvation. As a result, not all cells could be adequately supplied with the soluble electron donor lactate, which would slow down the overall respiratory rate and consequently the EET rate of the organisms.

Another factor that limits current production, is the inhibition of current-producing cells due to proton accumulation. Torres *et al.* (2008) stated that ‘for every electron (negative charge) flowing out of the biofilm and into the anode, an ion must migrate out (cation) or in (anion)’. This proton migration is influenced by diffusion, resulting in the formation of a proton gradient throughout the biofilm. The spatial heterogeneity caused by this within a 50 µm thick, anodic biofilm was demonstrated in a study using a pH-sensitive fluoroprobe, which

reported a tenfold difference in pH with pH 7 at the biofilm-electrolyte interface and pH 6 at the biofilm-electrode interface (Franks *et al.*, 2009). As proton accumulation inhibits microbial activity, this proton gradient was reported to limit the current output of MES (Logan *et al.*, 2006; Rozendal *et al.*, 2006a; Torres *et al.*, 2008; Franks *et al.*, 2009). Accordingly, more cells would lead to an amplified accumulation of protons, which in turn would increase the inhibition caused by this accumulation. It is possible that above a cell density of 5.98 x 10^7, the resulting proton gradient is limiting due to the restricted diffusion of protons throughout the hydrogel matrix, which would explain the observed current plateau.

It is also conceivable that the efficiency of electron transfer for the individual cell is hindered by limited access to the electrode as an electron acceptor. Above a certain cell density in the natural as well as in the synthetic biofilm, the electrons can no longer be transferred efficiently via short-range DET (see section 1.2.1) to the stationary electron acceptor (graphite felt) if the biofilm structures lack conductivity, and the EET turnover rate decreases. The conductivity of the biomaterial and its effect on EET is discussed further in section 4.3.1. In conclusion, either a limited respiratory transfer rate due to diffusion limitation, a inhibition due to proton accumulation or a limited EET rate due to suboptimal cell-electrode positioning could contribute to the current plateau observed above the cell density of 5.98 x 10^7.

The next step was to reduce the height of the synthetic biofilm, and thus fix the cells even closer to the electrode, to investigate the positive effect this might have on the EET and thus on current production. Lower gel heights resulted in higher current densities when the same cell density was applied (Figure 11). Surprisingly, current production doubled from 167.6 to 341.1 mA m^{-2} when the gel thickness, and therefore the total number of cells, was reduced by a quarter from 5 mm to 1.25 mm. As mentioned above, this can be either attributed to a reduction in diffusion barrier or the optimized cell-electrode positioning for improved EET. With regard to the reduction of the diffusion barrier, Stewart established a mathematical relation of diffusion in the biofilms and postulated a proportional correlation between the penetration time and the biofilm thickness (Stewart, 2003). For natural *G. sulfurreducens* biofilms, it could be shown that acetate could not be detected below a biofilm thickness of 100 µm (Renslow *et al.*, 2010). Therefore, this was postulated as the diffusion limit for acetate in these biofilms. Consequently, in the synthetic biofilm established in this thesis, it

appears indeed plausible that reducing the gel height corresponds to reducing the diffusion barrier.

However, an increase in current density was no longer associated with a reduction in gel height below 2.5 mm. Apparently, the rate of EET had replaced mass transfer as a limiting factor at this point. Electron transfer could have been affected by the reduced gel thickness due to lower resistance within the gel as a result of shorter distances and optimized cell distribution. Although the total number of cells was halved when the biomaterial thickness was reduced from 2.5 mm to 1.25 mm, there was no difference in current density. Thus, fewer cells produced the same current output, meaning that the EET rate for each individual cell was improved at 1.25 mm compared to 2.5 mm. However, the number of cells in the thicker biofilm compensated for this lower EET rate per individual cell to produce the same current output, indicating that the balance between diffusion rate, EET rate and cell number is essential for the performance of the biomaterial. Consequently, an improved performance window for the established biomaterial in terms of cell distribution for EET and diffusion limitation was defined by varying cell density and hydrogel thickness. These variations allowed a 3.7-fold improvement in current density from 89.9 mA m^{-2} to 331.4 mA m^{-2} when cell density was increased from 0.79×10^7 to 3.98×10^7 and biomaterial thickness was reduced from 5 mm to 2.5 mm, respectively.

Further, the findings during the characterization of the biomaterial are in line with studies that report improved current densities by the use of smaller reactors. In these studies, short diffusion length and reduced resistance due to shorter distances are realized by high electrode surface to reactor volume ratios in so-called mini-MFCs (Ringeisen *et al.*, 2006; Biffinger *et al.*, 2007; Tominaka *et al.*, 2008; Hou *et al.*, 2009; Chen *et al.*, 2011). For example, a study postulated power outputs similar to the maxima known in literature of 20 mA m^{-2} using a graphite felt electrode (Ringeisen *et al.*, 2006) which refers to a total current of 1.25 mA. The agarose biomaterial in this thesis resulted in a total current of 0.49 mA without any additives and 2.12 mA when spiked with CNFs (Table S1). With both systems having a similar optimization strategy, the hybrid biomaterial could be an interesting addition to these miniature systems to further improve current production.

4.1.2 **Analysis of hydrogel structure and migration behaviour of *S. oneidensis***

Agarose as substitute for EPS matrices of bacterial biofilms was already suggested before (Strathmann *et al.*, 2001). The authors developed agarose beads with embedded cells and analyzed the physicochemical properties of the artificial EPS scaffold including the porous structure of the agarose beads. In the SEM analysis carried out in the present thesis, pores ranging in size from 10 to 80 µm were visualized (Figure 13), which is consistent with the pore size of the agarose beads described in the aforementioned report and correlates well with pores of natural biofilms (Strathmann *et al.*, 2001). Thus, the concentrated cell suspension added in this thesis had no effect on the physical properties of the agarose, leaving the channel structure unobstructed, an important factor influencing mass transfer processes in this material. This illustrates the potential for integrating the hybrid biomaterial into existing industrial biofilm processes, as the physical accessibility of the synthetic biofilm is comparable to that of natural biofilms.

In the next step, the possible migration of *S. oneidensis* after embedding in the hydrogel was investigated. The RFP-tagged strain was shown to migrate or even proliferate over a time course of at least 48 h towards the stationary electron acceptor (Figure 12). Thus, although the cells were initially synthetically dispersed, the agarose scaffold still allowed for self-positioning of *S. oneidensis* within the hydrogel fibers. This is essential for an optimized positioning between soluble electron donor and stationary electron acceptor. These two form a gradient throughout the hydrogel, with electron donor influenced by diffusion from the electrolyte into the hydrogel and electron acceptor limited due to EET efficiencies and limited electroactive surface area. The proven ability to migrate within the hydrogel matrix allowed the optimal self-positioning of the cells within these gradients, similar as it is demonstrated in natural biofilms. This again underlines the comparability of the here fabricated biomaterial with natural systems.

4.2 Spraying of synthetic biofilm as novel inoculation strategy

4.2.1 Performance of sprayed biomaterial versus natural biofilm

In this part, the ability of the synthetic biofilm to be sprayed and the corresponding performance in terms of current output in comparison to the natural biofilm is discussed according to Knoll *et al.* (2022). The spraying of the biomaterial was the central aspect of this thesis, as it enabled a flexible form of application. This should subsequently form the basis for the application on a laboratory scale (see section 4.5) as well as a later upscaled, industrial application. Natural biofilms form from free-living planktonic cells that first settle on the surface. The attached microbes then start proliferating and producing the EPS matrix and mature into a productive biofilm (Sauer *et al.*, 2002; Sauer *et al.*, 2022). Such a natural biofilm is produced by *S. oneidensis* on the anode electrode and its performance was compared with the sprayed biomaterial, which provides the 3D scaffold for proliferation in the form of the agarose hydrogel. While the natural biofilm showed no current production in the first 3 h, the synthetic biofilm resulted in a current density of 200 mA m^{-2} (Figure 14). Further, the current density after 24 h for the sprayed biomaterial was found to be 2.1-fold increase compared to the natural biofilm.

Therefore, the spatial fixation and the provision of the agarose scaffold resulted in an improved performance of *S. oneidensis* in terms of current density. This was particularly apparent in the first 3 h after inoculation. After planktonic inoculation, the cells were suspended in the electrolyte in an evenly distributed manner. This also meant that statistically only a small number of cells were in direct contact with the electron acceptor, the graphite felt, which limited current production, especially in the initial phase, as the cells had to attach first. In comparison, the spray inoculation resulted in a forced spatial proximity of the cells to the electron acceptor which appeared to result in a significant increase in current production.

Besides the forced direct interaction of cells and electrode in the biomaterial, another factor could be involved in the improved performance of *S. oneidensis* after embedding the 3D matrix of the agarose hydrogel. After entrapping *S. oneidensis* in biofilm mimicking scaffolds, the organism was reported to exhibit reduced production of EPS components

(Zhang *et al.*, 2014). Another study then demonstrated that *S. oneidensis* resulted in an improved current production after the depletion of the EPS matrix (Xiao *et al.*, 2017). The authors demonstrated that although the EPS also contains redox-active species and is therefore involved in the EET, it was suggested that the interaction of the *c*-type cytochromes with the electrode is more efficient after EPS depletion. Accordingly, by providing agarose as an EPS substitute, a more suitable matrix may have been created compared to the self-produced one, allowing more efficient interaction of the *c*-type cytochromes with the EPS and likewise the electrode. This is particularly conceivable in the early stages of operation after inoculation, as this is when an EPS structure needs to be produced in the natural system. During this initial growth phase, *S. oneidensis* was reported to achieve full surface coverage only after about 20 h, with the first three-dimensional structures observed after 12 h (Thormann *et al.*, 2004). Thus, in addition to the spatial fixation of cells in close proximity to the electrode, the provision of the artificial matrix could support EET processes compared to the natural system, which is still in the early stages of EPS matrix development.

Although agarose as a polymer is described as non-conductive (Trivedi *et al.*, 2012), ionic conductivity was found for hydrogels prepared from an ion-buffered solution and agarose polymers (Pomfret *et al.*, 2013) as done in this thesis (see section 2.1.4). This ionic conductivity was associated with the formation of cross-linking networks with other electrolyte components (i.e. ions in ion-buffered solutions), which favorably affected ionic transport through the material (Yang *et al.*, 2011). Due to the rapid charge-discharge rate of ionic species, the use of agarose hydrogels as supercapacitors has even been proposed (Moon *et al.*, 2015). In the context of anodic MES, as stated in section 4.1.1, proton transport within the biofilm has been reported to limit current output (Logan *et al.*, 2006; Rozendal *et al.*, 2006a; Torres *et al.*, 2008; Franks *et al.*, 2009). Consequently, enhanced ionic transport through the agarose matrix as an electrolyte may be another factor contributing to the improved current production compared to the natural system.

4.2.2 **Influence of spraying technique on *S. oneidensis***

As described in Knoll *et al.* (2022), the spraying of the established biomaterial was the first report of spray application for synthetic, exoelectrogenic biofilms. For this, the spray applicator was used to facilitate the generation of the spray mist of the biomaterial (see

section 2.1.4.3 and Figure 7). As this spray mist was created when the liquid biomaterial met the gas flow in the Y-tube connector, the embedded organisms were subjected to a sudden acceleration. Although no negative effects of massive accelerations above 20 gigapascals on *Bacillus subtilis* spores were found (Horneck, 2001), the effects of this spraying procedure on the performance, i.e. current output, of exoelectrogenic bacteria should be investigated, as no studies on this can be found in the literature. For this purpose, the achieved current density of the poured biomaterial (no acceleration) was compared with that of the sprayed biomaterial (acceleration < 50 kilopascals, see section 2.1.4.3). No significant difference was found. Thus, no negative impact of spraying was found in the presence of the hydrogel scaffold.

However, in the absence of the hydrogel, as in the control experiment with 0 % agarose, the current density achieved was lower than for the planktonic control and the sprayed hydrogel (Figure 15). Shear stress is defined to be linked to the velocity of the surrounding fluid as it is caused by the flow of a fluid across a surface. The sudden acceleration of the cells during the spray process and their impact on the electrode surface equals therefore an exposure of the cells to shear stress. In this context, biofilms have been described to behave like viscoelastic fluids exhibiting both irreversible deformation and reversible elastic response (Klapper *et al.*, 2002). Negative effects on overall biofilm fitness were reported when the biofilm was exposed to shear stress during development, indicating that the performance of a biofilm is dependent on its stress history (Jones and Buie, 2019). In contrast, agarose fibers were described to be stiff enough to exhibit scalar elasticity (Fujii *et al.*, 2000). As a result, the agarose fibres appeared to have increased the mechanical stress tolerance of the embedded cells, resulting in improved current output compared to cells sprayed without a protective matrix.

4.2.3 **Performance of synthetic biofilm after start-up phase**

The provision of the synthetic scaffold in the form of the agarose hydrogel provided an improvement in performance in terms of current density during the initial start-up phase (first 24 h) of the MEC system. As discussed in section 4.2.1, this could be attributed to the spatial fixation of the cells in close proximity to the electron acceptor as well as the provided scaffold for enhanced EET processes of *S. oneidensis*. This led to the question of whether the

performance improvement would be maintained over a longer period of time. To this end, the mean current density after up to 96 h of MEC operation of a natural and a synthetic biofilm was compared (Figure 16) which showed that the improvement provided by the synthetic matrix was significant until 72 h of MEC operation. Until this time point, the biomaterial outperforms the natural system in terms of current production.

As mentioned above, the formation of a natural biofilm occurs over multiple steps, namely adhesion of the cells, proliferation on the substrate resulting in EPS formation and subsequently dispersion of single cells (Sauer *et al.*, 2002; Sauer *et al.*, 2022). Therefore, the obtained current production of naturally formed biofilms was reported to exhibit an initial lag-phase before rapid cell growth with total substrate coverage after 20 h (Thormann *et al.*, 2004) and corresponding stable current production can be achieved (McLean *et al.*, 2010). This may be due to the necessary initial adaptation of planktonic cells to facilitate EET with fixed electron acceptors and the corresponding upregulation of genes encoding the necessary proteins and production of the required components, e.g. EPS components (McLean *et al.*, 2010). In contrast, EPS production has been shown to be down-regulated in organisms embedded in synthetic scaffolds (Zhang *et al.*, 2014), suggesting that the adaptation of organisms for EET to stationary electron acceptors is faster in the hybrid biomaterial than in the natural system. Thus, the initial lag-phase visualized by the monitored current production was expected to be shorter for the synthetic biofilm compared to the natural system. This was confirmed, for example, by the hourly incline in current density over 96 h which was calculated to be 0.0061 h^{-1} and 0.0095 h^{-1} for the natural and synthetic system, respectively. The 1.5-fold increased hourly incline for the synthetic biofilm confirms again the beneficial effect the agarose fibers provided that can be attributed to more efficient EET processes as discussed in section 4.2.1.

After 96 h, however, there is no significant improvement of the synthetic biofilm compared to the natural system. As mentioned above, complete coverage of a *S. oneidensis* biofilm on the surface on which it proliferates has been shown to be achieved after 20 h (Thormann *et al.*, 2004). However, biofilm development and adaptation to environmental conditions is an ongoing process and the improved performance of mature biofilms after long-term cultivation under BES conditions has been reported (Bridier *et al.*, 2013; Koch *et al.*, 2019; Dzofou Ngoumelah *et al.*, 2021). Consequently, it is possible that the natural biofilm has

matured to the point where the EET efficiency has become similar to that of the synthetic biofilm after 96 h.

4.3 Influence of hydrogel characteristics on current output

4.3.1 Improvement of current output based on abiotic supplements

This section discusses the improvement in current output by altering the characteristics of the biomaterial made from conventional agarose and embedded *S. oneidensis* cells according to Knoll *et al.* (2022). This approach was chosen to demonstrate the flexibility with which the synthetic matrix can be functionalized to achieve user-defined properties. The overall aim was to further improve the production of current density, and to this end two abiotic additives were initially tested. Before application of the enhanced biomaterials in the MEC reactor, the abiotic conductivity of the hydrogel scaffold was determined. As mentioned in section 4.2.1, agarose itself is non-conductive. However, when the hydrogel is fabricated from the ion-buffered solution (see section 2.1.4), an ionic conductivity of the hydrogel is achieved. In the following, the conductivity of three different hydrogels and one ion-buffered solution (0 % agarose) was determined (Figure 17). When 1.8 % agarose was added to the ion-buffered solution and a hydrogel was formed, an increase in conductivity was measured. The further addition of riboflavin did not result in a further increase compared to the hydrogel without additives, while the supplementation with riboflavin-functionalized CNFs resulted in the highest measured conductivity.

In general, conductivity is the rate at which an electric current passes through a material. A distinction can be made between the conductivity of aqueous solutions (i.e. electrolytes), in which current is transported by ions, and that of solids, in which current is transported by electrons. It is not possible to distinguish between the two in the experimental setup of the conductivity measurement carried out in this thesis. However, there is no report on the electrical conductivity in agarose hydrogels and therefore the measured conductivity of the 0 % agarose solution and the 1.8 % agarose hydrogel is most likely due to the ionic conductivity described previously (Yang *et al.*, 2011; Pomfret *et al.*, 2013; Moon *et al.*, 2015). Therefore, the measured difference in conductivity between 0 % agarose, i.e. the ion-

buffered solution, and 1.8 % agarose is consistent with reports in literature. As no increase in conductivity was observed with the addition of riboflavin, no contribution to the ionic or electrical conductivity of the biomaterial was assumed for this molecule.

However, the addition of CNFs resulted in an increase in conductivity. CNFs are promising nanomaterials for use as electronic components and, due to their unique mechanical and electrical properties, are being considered as an additive to improve electrical conductivity in composites (Tennent, 1987; Jong and Geus, 2000). It is therefore likely that the electrical conductivity provided by the CNFs is responsible for the increase in conductivity of the biomaterial. However, this is based on a simplified representation of the overall conductivity of the biomaterial, as factors such as adsorption of ions, dispersion of the CNFs in the composite matrix, temperature among others have a significant influence on the electrical and ionic conductivity. In order to elucidate the chemical and physical processes that contribute to the overall conductivity, electrochemical impedance spectroscopy (EIS) would have to be carried out (Musiani, 1990; Floudas, 2012; Aguedo *et al.*, 2020). Electrochemical impedance determines the AC resistance of electrochemical systems and is a standard method for gaining a better understanding of the electrochemical mechanisms that occur at the interphase between the electrode and the electrolyte, and is widely used to characterize, for example, MES electrodes after modification with various nanoparticles (Yu *et al.*, 2020; Cao *et al.*, 2021; Pu *et al.*, 2022; Tseng *et al.*, 2022). Therefore, EIS analysis could help to distinguish between the different physiochemical processes that influence the overall electrochemical behavior of the biomaterial. As the acquisition and interpretation of EIS data is not trivial, and as the focus of this work was on improving biological current production using the established biomaterial, it was not the aim of this work to investigate these physiochemical processes further.

Although no improvement in conductivity was measured after the addition of riboflavin, an increase in current density was observed in the riboflavin-enriched biomaterial compared to the material without riboflavin (Figure 18). Riboflavin is a soluble electron shuttle that, as described above, plays a central role in the EET processes (see section 1.2.2). The positive influence of riboflavin on the current production of *S. oneidensis* has been reported previously and is mainly related to increased biofilm formation (Edel *et al.*, 2021) and an increase in MET processes, as it acts as an additional electron shuttle (Marsili *et al.*, 2008;

Brutinel and Gralnick, 2012; Kotloski and Gralnick, 2013). However, the application of riboflavin in at least continuous processes is limited due to the constant loss of this expensive supplement from the fermentation broth (Arinda *et al.*, 2019). By embedding riboflavin in the biomaterial, its spatial proximity to the exoelectrogenic cells could be facilitated, thus allowing the compound to be immobilized in the biomaterial and implemented in continuous processes. In conclusion, since the addition of riboflavin did not improve the conductivity of the hydrogel scaffold, the observed current improvement can thus be related to the nature of riboflavin as an electron shuttle, promoting MET through the hydrogel channels towards the electrode. To rule out the possibility that riboflavin contributed to current production by shuttling electrons even in the absence of cells, a negative control was performed in which the hydrogel without cells but with added riboflavin was tested for current production in the MEC reactor (see section 6.2). Even after 48 h of MEC operation, no positive current was detected, indicating that the positive effect of riboflavin on current production is not abiotic in nature, but due to the influence of riboflavin on the EET process of the embedded cells.

In contrast, the addition of CNFs to the hydrogel resulted in an increase in conductivity and current density. Several factors could explain this beneficial effect of CNFs on the current production of *S. oneidensis*. First, the increase in conductivity could be related to an increase in electron transfer within the hydrogel scaffold, resulting in the aforementioned increase in current density. Potentially, the dispersion of CNFs in the hydrogel was sufficient to improve the overall electrical conductivity of the biomaterial, which in turn improved the biological EET rate. As mentioned above, EIS analysis could be used to gain a better understanding of the electrochemical processes that contribute to the conductivity and the current production of this biomaterial. However, the improvement of long-distance DET by the addition of nanoparticles has already been reported (Liang *et al.*, 2011; Yu *et al.*, 2011; Liu *et al.*, 2018), so the same could be assumed for the biomaterial established here. In addition, the functionalization immobilized the riboflavin molecules on the surface of the CNFs (Toshimitsu *et al.*, 2019). Riboflavin as a co-factor of the outer membrane cytochromes of *S. oneidensis* (see section 1.2.2) could additionally facilitate DET between organism and CNFs, resulting in an improved electrochemical interaction of *S. oneidensis* with the agarose scaffold, embedded CNFs and the electrode. Second, Sanchez *et al.* reported that reducing the diameter of the electrode material from micro- to nanoscale is beneficial solely because

the scaffold created is more suitable for *S. oneidensis* biofilm formation (Sanchez *et al.*, 2015). The CNFs are a nano-sized addition to the micro-sized agarose fibers, which could have improved colonization and therefore current production. In addition, it can be assumed that the CNFs, when evenly distributed in the agarose gel, simultaneously lead to an increase in the electroactive surface area on which the organisms can proliferate. Here it is conceivable that the nanofibers form a network along the agarose fibers and this network conducts the electrons to the electrode, thus enabling long-range DET throughout the agarose hydrogel and improving the overall current production of this biomaterial.

A schematic overview of the tested biomaterials and the proposed influence of the additives on the biological EET towards the electrode is given below (Figure 26). While *S. oneidensis* naturally forms rather thin biofilms performing mainly short-range DET in the initial start-up phase of 24 h, the biomaterial spatially fixed a multitude of cells on the electrode surface, providing an artificial scaffold that resulted in improved EET and, consequently, current production. The addition of riboflavin, as a co-factor of the outer membrane cytochromes of *S. oneidensis*, may have facilitated enhanced microbe-electrode interactions and, more importantly, the electron shuttle promoted MET throughout the biomaterial. Further, the addition of CNFs most likely enabled long-range DET throughout the hydrogel scaffold, which significantly enhanced the biological EET rate, resulting in a 9.1-fold improvement in current production compared to the natural system.

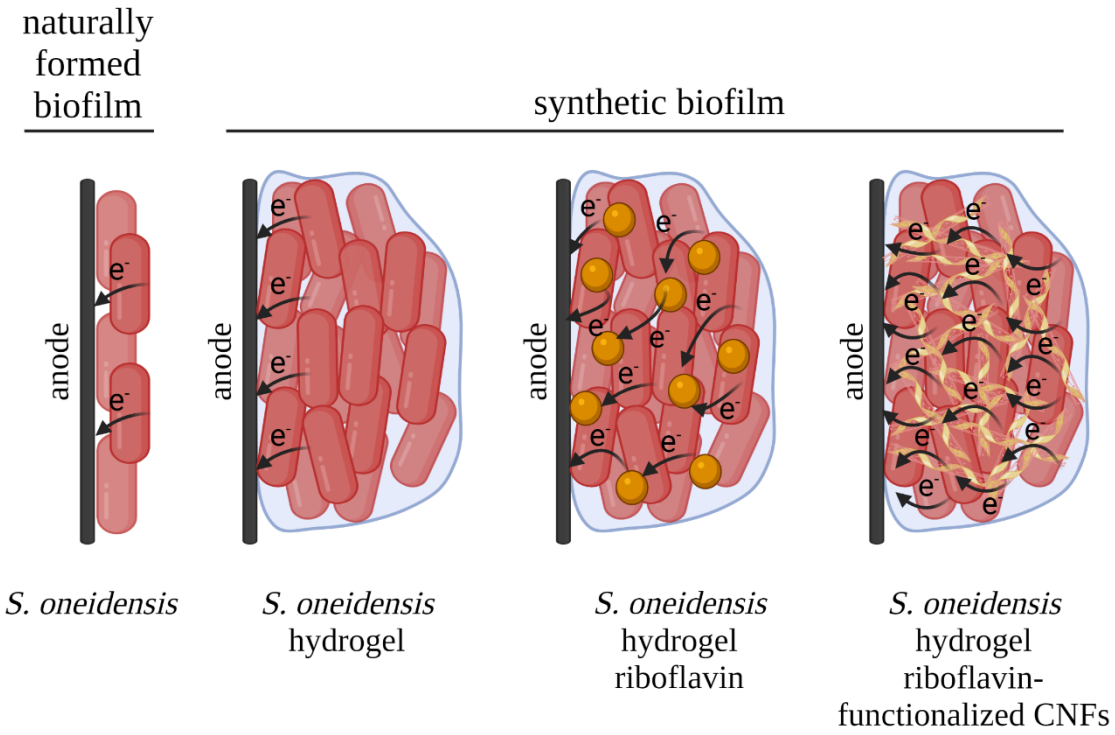

Figure 26: Proposed EET processes in natural and synthetic biofilms studied in this thesis. While *S. oneidensis* naturally forms rather thin biofilms performing mainly short-range DET in the start-up phase, the biomaterial spatially fixed a multitude of cells on the electrode surface and, additionally provided an artificial scaffold that resulted in improved EET and, consequently, current production. The addition of riboflavin, as a co-factor of the outer membrane cytochromes of *S. oneidensis*, may have facilitated enhanced microbe-electrode interactions and, additionally, the electron shuttle promoted MET throughout the biomaterial. Further, the addition of CNFs most likely enabled long-range DET throughout the hydrogel scaffold, which significantly enhanced the biological EET rate, resulting in a 9.1-fold improvement in current production compared to the natural system.

4.3.2 **Performance of novel hybrid biomaterial compared to literature**

The biomaterial presented in this thesis was not the first approach to improve current production by introducing a synthetic matrix for *S. oneidensis* to proliferate in, as described in section 1.4. To compare the current output of the biomaterial established in this thesis, the performance of reported biomaterial approaches from literature is given below (Table 11). For each study listed, the current or power density for MEC or MFC operation, respectively, is provided and an improvement factor was calculated if a natural system was also tested. However, the improvement factor is biased in such a way that it does not cover the native (dis)advantages of different materials. For example, carbon-based electrodes are generally considered to be more biocompatible than metal-based electrodes, so the reported

improvement factor achievable for metal-based electrodes is in most cases higher. Nevertheless, the improvement factor given for each study is an approach to facilitate partial comparability of different strategies. For a comprehensive overview, reference is made to a recent review comparing the technical advances of nearly 40 synthetic approaches. (Klein *et al.*, 2023).

In this context, Lin *et al.* (2012) demonstrated a 5-fold increase in the maximum current density to 65 mA m^{-2} 6 h after encapsulation of *S. oneidensis* in a phospholipid hydrogel formed from polyvinyl alcohol and poly(2-methacryloyloxyethyl phoshorylcholin-*co*-*n*-butyl metha-crylate-*co*-*p*-vinylphenylboronic acid-*co*-vinylferrocene) (PMBVF), compared to the natural system. The ferrocene groups of the PMBVF appeared to interact with the *c*-type cytochromes of *S. oneidensis* to promote EET throughout the hydrogel, whereas the polyvinyl alcohol was required to form the hydrogel scaffold (Lin *et al.*, 2012). Further, a matrix of polypyrrole and conductive micro-sized graphite resulted in an 11-fold increase in power production to 0.2 W m^{-2} compared to the natural biofilm matrix, due to the EET promoted by the graphite particles embedded in the polypyrrole (Yu *et al.*, 2011). This effect was similarly discussed above for the CNF addition and supports the assumption that long-range DET is indeed promoted by the addition of CNFs to the hydrogel scaffold of the biomaterial established in this thesis. As mentioned in section 1.4, the embedding in a PEDOT:PSS hydrogel matrix further resulted in a 20-fold improve in current production to 16 mA m^{-2} (Zajdel *et al.*, 2018). Further, the 3D-printing of a fully functional bio-anode from an alginate/cellulose hydrogel with embedded *S. oneidensis* cells and carbon black was reported to achieve a power output of 8.5 W m^{-2} (Freyman *et al.*, 2019). However, no negative control was performed in this study, so no improvement factor could be calculated. Recently, the successful fabrication of a biomaterial from conjugated polyelectrolytes, short CPE-K, and *S. oneidensis* has been demonstrated to significantly improve the current output to 0.2 A m^{-2} when applied to a gold electrode (McCuskey *et al.*, 2020) and 0.3 A m^{-2} when applied to a carbon paper electrode (Vázquez *et al.*, 2022). This was attributed to the conductive polymer matrix promoting long-range EET throughout the synthetic biofilm.

Table 11: Brief tabular overview of recently reported improvement approaches facilitating the application of different hybrid biomaterials with *S. oneidensis*. The hybrid biomaterial used is shortly described, the electrode material and the performance output either as power density (MFC) or current density (MEC) are given. Further, the improvement factor (IF) is given in comparison to the performance of the natural system.

Hybrid biomaterial	**Electrode**	**Output**	**IF**	**Reference**
Polypyrrole hydrogel spiked with micro-sized graphite	carbon cloth	0.2 W m^{-2}	11x	Yu *et al.*, 2011
Phospholipid polymer hydrogel formed from PMBVF and polyvinyl alcohol	indium tin oxide	65 mA m^{-2}	5x	Lin *et al.*, 2012
PEDOT:PSS multi-layered conductive bacterial composite	carbon felt	16 mA m^{-2}	20x	Zajdel *et al.*, 2018
3D printed bioanode from alginate/cellulose hydrogel with acetylene carbon black	carbon cloth	8.5 W m^{-3}	--	Freyman *et al.*, 2019
Self-assembly of conjugated polyelectrolyte CPE-K	carbon paper	0.3 A m^{-2}	5.7x	Vázquez *et al.*, 2022
Self-assembly of conjugated polyelectrolyte CPE-K	gold silicon wafer	0.2 A m^{-2}	151x	McCuskey *et al.*, 2020
Agarose hydrogel spiked with riboflavin-functionalized CNFs	Carbon felt	1.3 A m^{-2}	9.1x	This thesis

The observed current density of 1.3 A m^{-2} after 24 h for the biomaterial with riboflavin-CNFs and *S. oneidensis* is therefore higher than the other current density values listed above for different biomaterial applications. However, the normalisation of current and power values is highly dependent on the system and especially the electrode material used to test the optimisations, so no uniform normalisation is applied in literature. Consequently, the higher current density for the biomaterial developed here could be due to the reactor system chosen. While the other biomaterials listed in Table 11 were tested in reactor systems with small electrode surface areas (< 6 cm^2), the agarose-based biomaterial developed here was applied in a system optimised for current production (Golitsch, 2016) with a larger surface area of 16 cm^2. This greater surface area was chosen to allow for better comparability with potential upscaled systems in which the biomaterial may be used in the future. However, the improvement factor facilitated by the agarose biomaterial is very similar to the approaches performed with carbon-based electrodes. Nevertheless, the low-cost fabrication process and the flexible application technique established in this thesis offer a simplified handling of the hybrid material. Further, some of the improvement strategies listed below are based on the use of toxic monomers, such as the PEDOT:PSS composite, or on complicated manufacturing processes. In contrast, the biocompatibility of the agarose-based biomaterial facilitates a gentle embedding and manufacturing process. Besides, its low economic cost predetermines the biomaterial developed in this thesis as an excellent candidate for potential upscaling and industrial application.

4.4 Analysis of mixed species biomaterial

As a third potential enhancing supplement, a second exoelectrogenic organism was chosen to be embedded together with *S. oneidensis*. For this, *G. sulfurreducens* was selected as this organism, as mentioned in section 1.2.3, exhibits excellent performance in BES in terms of current production. This can mainly be attributed to the conductive cell appendages that allow the formation of highly conductive biofilm matrices formed by *G. sulfurreducens*. Further, syntrophic associations between microorganisms in electroactive biofilms have been reported to be a critical factor in the overall performance of these communities (Summers *et al.*, 2010; Dolfing, 2014; Wang *et al.*, 2016), and the syntrophic relationship between *S. oneidensis* and *G. sulfurreducens* has already been studied in detail in an anodic model biofilm (Prokhorova

et al., 2017). The addition of this organism to the biomaterial therefore corresponded to the addition of cells with a reportedly improved EET compared to *S. oneidensis*, contributing to the overall current production, as well as a network of conductive nanowires that could promote long-range DET throughout the hydrogel matrix, and further beneficial effects on the performance of *S. oneidensis* due to their previously reported syntrophic relationship.

Surprisingly, the current density with 4 A m^{-2} produced by the naturally formed biofilm of *S. oneidensis* and *G. sulfurreducens* was higher compared to the sprayed biomaterial with 2.5 A m^{-2} (Figure 19, A). As mentioned above, the spraying process implies a sudden acceleration of the organisms in the biomaterial, therefore it was first assumed that the conductive pili of *G. sulfurreducens* were damaged or detached from the cells during the spraying. The loss of these cell appendages, which are responsible for the efficient EET performed by *G. sulfurreducens*, could indeed have a negative impact on the performance of this organism. To exclude this possibility, the biomaterial was poured to protect the nanowires from harsh spray conditions. However, the monitored current density of the poured biomaterial was again lower compared to the natural system, thus, the spraying process itself did not seem to be the limiting factor here. In a next step, the biomaterial was supplemented with riboflavin-functionalized CNFs, as this addition gave the best performance improvement for the biomaterial in which only *S. oneidensis* was embedded. Further, the addition of CNFs appeared to promote long-range DET in the biomaterial with *S. oneidensis* (see section 4.3.1), so an improvement in EET and hence current density after the introduction was expected for the mixed species biomaterial as well. However, again, the current density achieved by the biomaterial was below that of the natural system.

This suggests that while the biohybrid material provided a better scaffold for embedding *S. oneidensis* in the initial start-up phase, the natural matrix produced in the initial 72 h by *G. sulfurreducens* could outperform the artificial matrix in its properties for optimized electricity production. The ability of *G. sulfurreducens* to form highly conductive biofilms therefore surpasses the agarose scaffold in its support of EET. This is underlined by the abundance of *G. sulfurreducens* in natural biofilms formed from mixed inoculums. When inoculated with a mixed inoculum, a complex consortium forms the biofilm on the electrode, and in the presence of acetate these communities are found to be dominated by

Geobacteraceae (Nevin *et al.*, 2008; Kiely *et al.*, 2011; Li *et al.*, 2020), highlighting the excellent ability of these organisms to form electroactive biofilm matrices.

As mentioned above, acetate was not added to the medium used in these experiments (see section 2.1.2.3), however, *S. oneidensis* metabolizes lactate to acetate and therefore a co-dependency of *G. sulfurreducens* with *S. oneidensis* is induced. Although unlikely, the possibility that the acetate production facilitated by *S. oneidensis* would be the limiting factor in the biomaterial, additional acetate supplementation was conducted in a last step. However, this approach resulted as all the other synthetic approaches in less current production compared to the natural system. Apparently, the dependence of *G. sulfurreducens* on acetate production by *S. oneidensis* is not the limiting factor for the biomaterial's current production. Consequently, the EET rate within the biomaterial appeared to be lower than in the natural biofilm and the artificial structure formed by agarose and riboflavin-functionalized CNFs did not support the EET process as efficiently as the natural matrix. In this context, it could be conceivable that the chosen ratio of *S. oneidensis* to *G. sulfurreducens* for embedding in the agarose hydrogel (see section 2.1.4) was not ideal for current production. As mentioned above, *G. sulfurreducens* was reported to dominate anodic biofilms, implying that the fixed ratio of 10 to 1 of *S. oneidensis* to *G. sulfurreducens* inhibited the optimal current production of this mixed species biomaterial compared to the natural system. Investigating different ratios and their influence on the current production of the biomaterial may provide insight into this. However, when comparing the performance of the mixed species biofilm with that of the *S. oneidensis* biofilms (Figure 20), it is evident that there was no significant difference between the current produced by the mixed species biomaterial (1.5 A m^{-2}) and the *S. oneidensis* biomaterial supplemented with riboflavin-functionalized CNFs (1.3 A m^{-2}). This suggests that the CNFs supported the EET and thus the current production of *S. oneidensis* in a similar manner as the nanowires provided by *G. sulfurreducens*.

Nevertheless, the further optimization of the biomaterial scaffold should be investigated in the future in order to achieve the same level of performance for the synthetic biofilm as for the natural biofilm formed by *S. oneidensis* and *G. sulfurreducens* to surpass the current limit in electricity production of 1.5 A m^{-2} found in this thesis. In this context, Suravaram *et al.* postulated the possibility of modifying the polysaccharide scaffold due to its exposed hydroxyl groups in the cross-linking unit between D-galactose and 3,6-dianhydro-L-

galactopyranose to improve the interface between *S. oneidensis* and the electrode. The authors first embedded gold nanoparticles in the agarose matrix and found, using transmission electron microscopy, that large aggregates of the nanoparticles were localized in the water pockets of the hydrogel matrix (Suravaram *et al.*, 2019). Nevertheless, this addition already resulted in a 30-fold improvement in the conductivity of the hydrogel, which is consistent with the finding of conductivity improvement after CNF addition in this thesis. However, modification of the agarose with 2-chloroethylamine promoted uniform dispersion of the gold nanoparticles and a further increase in conductivity was reported (Suravaram *et al.*, 2019). The application of this optimized agarose hydrogel was carried out by planktonic inoculation of *S. oneidensis* rather than embedding as done in this thesis, and a 10-fold improvement in current was observed (Suravaram *et al.*, 2019). This would be an interesting approach for improving the artificial scaffold for the mixed species biomaterial of this thesis, as the uniform distribution may better support the promotion of long-range DET along the agarose gel fibers.

Additionally, this section could provide insight into the possibility to spray oxygen sensitive organisms (Figure 19, A). The successful application of spraying in anoxic or argon atmospheres could even enable the transfer of this technique for embedding oxygen-intolerant organisms in the biomaterial. If positive effects can be achieved here, the concept of sprayable biofilm could similarly improve processes based on strict anaerobic organisms. This might be interesting for a process called bioelectrosynthesis, in which the organisms proliferate the cathode of an MESC (see section 1.1.2) as their energy and electron source, and in which such obligate anaerobic organisms are applied. Besides this, the introduction of a hydrogel equals a barrier to the harsh conditions that biofilms are exhibited to in environmental but also industrial processes. To investigate the beneficial effects of the biomaterial in this context, an application scenario was carried out in a coupled MEC-biogas system (see section 4.5).

4.5 Application of biomaterial for electrical anaerobic digestion processes

The biomaterial consisting of agarose hydrogel, *S. oneidensis* and *G. sulfurreducens* was in a next step investigated for its application in a MEC-biogas system. In biogas plants microorganisms are utilized for the degradation of organic waste stream to biogas, however,

this process is rather sensitive to an accumulation of organic acids which inhibits the methanogenesis. For optimization of this process, the introduction of an additional electron acceptor in the form of an MEC electrode has been suggested as organisms growing on the anode can metabolize the organic acids and therefore stabilize the biogas process (see section 1.3). However, under real process conditions the AD effluent due to its complexity and particle-rich composition was reported to negatively affect the stability of the implemented MEC, resulting in an inhibition of the anodic biofilm (Kretzschmar *et al.*, 2018). As shortly stated in the section above, the hydrogel itself forms a barrier between the harsh environmental conditions and the organisms. Therefore, the potential improvement of robust MEC performance after implementation of the biomaterial was investigated. For this, the current production of the mixed species biomaterial was once again compared to a naturally formed biofilm of *S. oneidensis* and *G. sulfurreducens*.

Interestingly, during the daily biomass addition, both systems first showed a rapid increase in current density to 0.4 mA cm^{-2} and 0.1 mA cm^{-2} for the natural and synthetic biofilm, respectively (Figure 21). As observed during the characterization of the mixed species biomaterial (see section 4.4), this improved performance of the natural biofilm was therefore expected. In this application scenario the natural biofilm outperforms the synthetic approach by about the same factor as found in the initial analysis of the mixed species biomaterial. However, during the daily addition of biomass, the current production of the natural biofilm was found to decrease to a value of about 0.25 mA cm^{-2}, while the current density of the biomaterial was monitored to increase to around 0.17 mA cm^{-2} (Figure 21, phase II). This difference could be due to the different stages that the organisms in the natural and synthetic biofilms were in at the time. While the organisms in the natural biofilm had been introduced and adapted to the BES conditions for over a week at this point, the microbes in the synthetic biomaterial were still in the initial growth phase, resulting in the observed increase in current density for the synthetic system compared to the decrease in current density for the natural system.

As mentioned in the result section, on day 10 a technical malfunction led to the potential contamination with oxygen of both systems. Correspondingly, the current density of both systems was found to drop drastically. This decline in current density could have several reasons. First, the organisms could have transferred their respiratory electrons to oxygen as

their terminal electron acceptor, therefore diminishing the electron flux to the anode. For example, this has been shown to limit the efficiency of MFCs due to oxygen crossover from the cathode to the anode compartment (Hays *et al.*, 2011). Second, the organisms might have been inhibited due to the oxygen exposure. Oxygen can act as an inhibitory and toxic agent (McCord *et al.*, 1971; Carlioz and Touati, 1986; Imlay, 2003) and the negative effects oxygen can have, for instance, on biogas processes is widely known (Shen and Guiot, 1996; Zitomer and Shrout, 1998; Botheju and Bakke, 2011). The same negative influence could be assumed for the anaerobic electroactive organisms in this system. This would also explain, why both systems were inhibited in their performance until day 17, on which both systems started to show an increase in current production. As the technical malfunction only occurred on day 10, it is unlikely that oxygen contamination was still inhibiting the biofilm one week after this event, and the increase may indicate that the biofilm required this time to recover.

Another possible explanation for this decrease of current could be the negative influence AD effluent has on the MEC performance as mentioned above (Kretzschmar *et al.*, 2018). In addition, it could be that the level of organic acids was rather low at that time, which would also result in reduced current production due to substrate limitations. AD occurs in simultaneous but metabolically distinct steps, including the hydrolysis of complex polymers to sugars, amino acids and long-chain fatty acids, which are in turn metabolized to VFA, H_2 and CO_2, before methanogenesis can take place (Weiland, 2010). As biomass was added during this phase, consisting of a mixture of freshly prepared maize silage and AD effluent from an active biogas community (see section 2.1.5.2), a high quantity of AD components, including organic acids, were introduced into the system at this time. Therefore, it seems unlikely that substrate limitations would be the reason for the decrease in current density. To elucidate which one of these factors resulted in the monitored decrease of current density, more detailed analyses of the effluent components as well as the gas composition present in the system must be carried out, however, due to time limitations these results are not further discussed in this thesis.

Nevertheless, the current production of both system increases from day 17 to 0.25 mA cm^{-2} and 0.4 mA cm^{-2} for the natural and synthetic biofilm, respectively (Figure 21, phase III). Here, the synthetic biofilm outperforms the natural system in terms of current density. Interestingly, the maximum current density was achieved by the natural system in the pre-

cultivation phase under conditions with synthetic medium. In contrary, the synthetic biofilm performed best in the non-optimal environment containing AD effluent. Although the natural biofilm of *S. oneidensis* and *G. sulfurreducens* outperformed the synthetic mixed species biomaterial when cultured in a defined medium, this result may indicate the potential advantage of the synthetic scaffold when the mixed species biofilm is applied in real process conditions. The monitored current density decreased again on day 30 for both systems, which could be attributed to the same potential reasons listed above for the initial decrease on day 10. Interestingly, the course of the current production of both the natural and the synthetic biofilm showed the same pattern during the experiment, which again underlines the comparability of the biomaterial with natural biofilms. In conclusion, the biomaterial resulted in the same maximum current density as the natural biofilm of around 0.4 mA cm^{-2} when exposed to the harsh environmental conditions of the AD effluent added in phase II. Moreover, the synthetic biofilm showed this improved current production compared to the natural system from day 23 to day 30, so that a stable current plateau was achieved here. In contrast, the natural system only reached this maximum current density immediately after the first addition of biomass for a short period of time, when the environment consisted mainly of the defined cultivation medium. Moreover, the one-week pre-cultivation phase was omitted in the synthetic system, which significantly shortened the start-up time. However, further analysis of all the parameters that contribute to the electrical AD process would be required to define more precisely the beneficial factors that the application of the biomaterial may have on these systems.

4.6 **Induced detachment of synthetic biofilms**

In the last part of this thesis, the detachment of the synthetic biofilm from the electrode was investigated to gain insight into the potential harvesting of the biomaterial. For this, negative currents were applied to two different electrode materials, namely graphite felt and graphite plate, and the detachment was visualized using OCT and video recording. In conclusion, the graphite felt resulted in partial detachment of parts of the biofilm, whereas the graphite plate resulted in complete detachment of the biomaterial as a whole. This difference might be attributed to the nature of the materials themselves. A graphite plate is a planar electrode material with a defined surface area, while graphite felt offers a three-dimensional specific

surface area that is described as being more favorable for the formation of electroactive biofilms (Guo *et al.*, 2015). The fibrous nature of the graphite felt might facilitate H_2 formation more abundant over the complex surface area compared to the graphite plate, resulting in the observed partial rather than the total detachment.

The targeted detachment of parts of the biofilm achieved at the graphite felt might therefore be applied for the user-defined introduction of new channels into the biomaterial. As already mentioned, for *G. sulfurreducens* biofilms the limit for acetate penetration was found to be 100 µm depth (Renslow *et al.*, 2013). The introduction of new channels to the biomaterial might therefore be beneficial for mass transfer of substrates, resulting in an increased performance of the biomaterial. The possibility that a more porous biofilm structure could be beneficial due to increased mass transfer has also been postulated for the cells embedded in the conjugated polyelectrolyte CPE-K (see section 4.3.2). Here, due to electrostatic repulsion the cells were stated to be less packed, allowing for better diffusion of substrate and metabolic products (Ren *et al.*, 2019).

In contrast, the total detachment implies the potential harvesting of the biomaterial as a whole. As briefly mentioned above, the transfer of the sprayed biomaterial to other systems, including bioelectrosynthesis in MESC (see section 4.4) could lead to similar beneficial effects. Here, sprayed biofilms containing methanogens, acetogens or knallgas bacteria as biocatalysts could improve the overall performance of these systems and the harvesting of the cathodic biofilm is often of interest due to the intracellular multicarbon compounds that are produce from CO_2 fixation (see section 1.1.2). For this application, the detachment experiment can provide another insight into the maximum number of electrons that can be supplied to a cathodic biofilm before the biomaterial would start to degrade. The formation of H_2 bubbles was visualized to begin at an applied current of -2 mA cm^{-2}, defining the maximum current that can be applied before biomaterial degradation occurred. From this value, the number of electrons can be calculated on the basis of the relation between amperes and coulombs, as follows. The application of one ampere is equivalent to the delivery of one coulomb per second, and one coulomb is defined as the delivery of 6.24 x 10^{18} electrons. This gives a maximum of 1.25 x 10^{20} electrons per second per square meter of electrode surface that can be supplied in this system before biomaterial degradation occurs. Using Avogadro's constant (N_A; 6.02 x 10^{23} mol^{-1}), this refers to 0.75 mol electrons per h and per

square meter electrode surface (mol h^{-1} m^{-2}). Based on this, the theoretical maximum amount of, for example, ethanol or biomass that can be produced from the CO_2 fixation of electrotrophic organisms in MESC systems can be calculated. Thereby, the number of electrons required to reduce CO_2 determines the productivity of these production processes. This can be derived from the oxidation state of the carbon in the individual molecules. For CO_2 and ethanol (C_2H_6O) the oxidation state can be deduced from the sum formula to be -IV and +II respectively, whereas in cellular biomass the oxidation state of carbon is reported to be approximately ±0 (Dick, 2014). Thus, 12 electrons are required to produce 1 mol ethanol, which is formed from 2 mol CO_2. Given the maximum electron supply of 0.75 mol h^{-1} m^{-2}, this results in a maximum productivity of 62 mmol ethanol h^{-1} m^{-2} that could be produced by the applied biomaterial in MESC processes. Biomass production, on the other hand, requires approximately 4 electrons to reduce 1 mol CO_2 (Dick, 2014), corresponding to a maximum production of 187 mmol biomass h^{-1} m^{-2}. This theoretical value assumes optimal conditions, such as all electrons being converted to the final product, which is unlikely to be achievable experimentally. However, the biomaterial could facilitate an increase in productivity, which has been reported to be between 5 mmol and 9 mmol ethanol h^{-1} m^{-2} for conversion by the organism *Clostridium ljungdahlii* in a MESC system (Li *et al.*, 2017; Romans-Casas *et al.*, 2023). Accordingly, the theoretical maximum given here is an indication of the extent to which the biomaterial could support the improvement of ethanol production before hydrogel degradation occurs.

4.7 Conclusion and outlook

The interaction between electroactive bacteria and the electrode in a MES is one of the key factors that influences the current outputs that can be generated in these systems. In this thesis, a novel biomaterial consisting of an agarose-hydrogel and *S. oneidensis* was designed and characterized that led to improved performance in terms of current production in the initial start-up phase of a MEC compared to the natural system. This improvement was stable for the first 72 h of MEC operation, but after this time point, no significant improvement could be found to be facilitated by the biomaterial. The addition of enhancing supplements to the synthetic biofilm resulted in a 6-fold increase for riboflavin, 9-fold increase for CNFs and 10-fold increase for *G. sulfurreducens*. These improvement factors are in line with other

reported improvements reported for the application of synthetic hydrogel scaffolds (Table 11). As high current densities are required for high space-time-yields and thus future commercialization of BES (Bartlett, 2008; Sleutels *et al.*, 2012), the biomaterial established in this thesis contributes to the necessary improvement of the biofilm-electrode interaction and consequently the current output. However, the natural biofilm formed by *S. oneidensis* and *G. sulfurreducens* was found to outperform the biomaterial in current production. Here, the natural scaffold provided by *G. sulfurreducens* appeared to outcompete the beneficial properties of the artificial agarose matrix. Therefore, prospective optimizations of the agarose polymer, such as modification of the exposed hydroxyl groups in the cross-linking units with 2-chloroethylamine for uniform dispersion of nanoparticles, as reported by Suravaram *et al.* (2019), should be considered to further improve performance of the biomaterial.

In addition, the spray application of the biomaterial was successfully established, which is a key factor for potential upscaling and industrial application. Prospectively, this will allow for the production of a ready-to-use biomaterial that can be sprayed onto a variety of different types of electrodes. By incorporating conductive nanoparticles, a fully functional 3D anode, as previously described in literature (Freyman *et al.*, 2019), could be fabricated from the agarose-based biomaterial, allowing for a rapid and low-cost fabrication of an electrode that can be incorporated into any BES setup. In order for hybrid biomaterials to be industrially applicable, it is essential that they are scalable and robust. These criteria are met by the biomaterial developed here, and although the robust upscaling needs to be experimentally verified in the future, the proof of concept has been achieved within the scope of this thesis.

Further, the application of the biomaterial in MEC biogas systems was investigated, for which the same maximum current density for the synthetic and the natural biofilm of *S. oneidensis* and *G. sulfurreducens* was found. This eliminated the need for the week-long pre-cultivation period required for natural biofilm, which means that the start-up time of BES reactors could be reduced. Further, the biomaterial allowed this maximum current density to be stabilized for almost a week, whereas the natural system only showed a peak in current production. Consequently, the biomaterial could be used to accelerate the start-up and potentially the overall performance of industrial BES biofilm processes in the future. Long-term analysis of a synthetic biofilm in such a coupled system, as well as detailed analysis of all relevant parameters, including VFA content, biogas composition and metagenomic

analysis of the biofilm community, would be essential to verify the improvement the biomaterial could provide to these application systems.

Moreover, not only *S. oneidensis* has been reported to form thin biofilms that limit the productivity of MES processes on electrodes. The same was found for model organisms currently being investigated for use in the bioelectrosynthesis process, including *C. ljungdalii*, *Sporomusa* spp. and *Acetobaterium woodii* among others (Nevin *et al.*, 2011; Logan *et al.*, 2019). Consequently, biofilm formation on cathodes was synthetically promoted prior to start-up or in the early stages of MESC operation (Kuroda and Watanabe, 1995; Nevin *et al.*, 2011; Su *et al.*, 2013; Philips *et al.*, 2017). Embedding these organisms in the agarose scaffold could facilitate the production of an electrotrophic synthetic biofilm, which in turn could improve the productivity of MESC processes in the same way that anodic current production has been improved in this thesis. The basis for this transfer of concept was provided in this thesis by demonstrating the possibility of spraying anaerobic organisms and providing the maximum number of electrons that can be provided before biomaterial degradation occurs as 0.75 mol electrons per h and per square meter of electrode surface. In conclusion, the incorporation of methanogens, acetogens and knallgas bacteria into the sprayable biofilm will be of particular interest due to the potential positive effect that the biomaterial could provide for these processes.

Finally, for future commercialization of the sprayable biofilm technique, it would be beneficial to develop a ready-to-use composite that can be stored for longer periods and applied at user-defined times. This could be facilitated by applying a technology currently used to commercialize probiotic bacteria to the synthetic biofilm. These probiotic bacteria are freeze-dried to produce easy-to-use components that are stable and flexible for applications in the food, feed or pharmaceutical industries (Champagne *et al.*, 1991; To and Etzel, 1997; Broeckx *et al.*, 2016). In this context, the encapsulation of the anaerobic bacteria *Bifidobacterium pseudocatenulatum* in agarose-based hydrogel particles, which were subsequently freeze-dried, was reported to exhibit viability levels required for commercial application (Alehosseini *et al.*, 2019). The application of this technique to the synthetic biofilm established in this thesis could therefore enable long-term storage of this biomaterial, resulting in a ready-to-use, sprayable biofilm that would facilitate easy implementation for future industrial application.

5 REFERENCES

Achinas, S., Achinas, V., and Euverink, G.J.W. (2020) Chapter 2 - Microbiology and biochemistry of anaerobic digesters: an overview. In *Bioreactors: Sustainable design and industrial applications in mitigation of GHG emissions.* Amsterdam: Elsevier, pp. 17–26.

Adhikari, R.Y., Malvankar, N.S., Tuominen, M.T., and Lovley, D.R. (2016) Conductivity of individual *Geobacter* pili. *RSC Adv.* **6** (10): 8354–8357.

Aguedo, J., Lorencova, L., Barath, M., Farkas, P., and Tkac, J. (2020) Electrochemical impedance spectroscopy on 2D nanomaterial MXene modified interfaces: application as a characterization and transducing tool. *Chemosensors* **8** (4): 127.

Alehosseini, A., Del Gomez Pulgar, E.-M., Fabra, M.J., Gómez-Mascaraque, L.G., Benítez-Páez, A., Sarabi-Jamab, M., *et al.* (2019) Agarose-based freeze-dried capsules prepared by the oil-induced biphasic hydrogel particle formation approach for the protection of sensitive probiotic bacteria. *Food Hydrocolloids* **87:** 487–496.

Angenent, L.T., Karim, K., Al-Dahhan, M.H., Wrenn, B.A., and Domíguez-Espinosa, R. (2004) Production of bioenergy and biochemicals from industrial and agricultural wastewater. *Trends in Biotechnology* **22** (9): 477–485.

Araki, C. (1956) Structure of the agarose constituent of agar-agar. *Bulletin of the Chemical Society of Japan* **29** (4): 543–544.

Arinda, T., Philipp, L.-A., Rehnlund, D., Edel, M., Chodorski, J., Stöckl, M., *et al.* (2019) Addition of riboflavin-coupled magnetic beads increases current production in bioelectrochemical systems via the increased formation of anode-biofilms. *Frontiers in Microbiology* **10:** 126.

Armisén, R. (1991) Agar and agarose biotechnological applications. In *International Workshop on Gelidium: Proceedings of the International Workshop on Gelidium,* pp. 157–166.

Bakonyi, P., Koók, L., Rózsenberszki, T., Kalauz-Simon, V., Bélafi-Bakó, K., and Nemestóthy, N. (2023) CO_2-refinery through microbial electrosynthesis (MES): A concise review on design, operation, biocatalysts and perspectives. *Journal of CO2 Utilization* **67:** 102348.

Baron, D., LaBelle, E., Coursolle, D., Gralnick, J.A., and Bond, D.R. (2009) Electrochemical measurement of electron transfer kinetics by *Shewanella oneidensis* MR-1. *Journal of Biological Chemistry* **284** (42): 28865–28873.

Bartlett, P.N. (2008) *Bioelectrochemistry: Fundamentals, experimental techniques and applications.* Chichester: Wiley.

Beblawy, S., Philipp, L.A., and Gescher, J. (2020) Accelerated electro-fermentation of acetoin in *Escherichia coli* by identifying physiological limitations of the electron transfer kinetics and the central metabolism. *Microorganisms* **8** (11): 1843.

Bhargavi, G., Venu, V., and Renganathan, S. (2018) Microbial fuel cells: recent developments in design and materials. *IOP Conference Series: Materials Science and Engineering* **330** (1): 12034.

Biffinger, J.C., Pietron, J., Ray, R., Little, B., and Ringeisen, B.R. (2007) A biofilm enhanced miniature microbial fuel cell using *Shewanella oneidensis* DSP10 and oxygen reduction cathodes. *Biosensors and Bioelectronics* **22** (8): 1672–1679.

Biffinger, J.C., Ray, R., Little, B.J., Fitzgerald, L.A., Ribbens, M., Finkel, S.E., and Ringeisen, B.R. (2009) Simultaneous analysis of physiological and electrical output changes in an operating microbial fuel cell with *Shewanella oneidensis*. *Biotechnology and Bioengineering* **103** (3): 524–531.

Bird, L.J., Kundu, B.B., Tschirhart, T., Corts, A.D., Su, L., Gralnick, J.A., *et al.* (2021) Engineering wired life: Synthetic biology for electroactive bacteria. *ACS Synthetic Biology* **10** (11): 2808–2823.

Bo, T., Zhu, X., Zhang, L., Tao, Y., He, X., Li, D., and Yan, Z. (2014) A new upgraded biogas production process: Coupling microbial electrolysis cell and anaerobic digestion

in single-chamber, barrel-shape stainless steel reactor. *Electrochemistry Communications* **45:** 67–70.

Botheju, D., and Bakke, R. (2011) Oxygen effects in anaerobic digestion – A review. *The Open Waste Management Journal* **4** (1): 1–19.

Bridier, A.A., Desmond, E., Madigou, C., and Bouchez, T. (2013) Adaptation of sessile and planktonic microbial communities in BES. In *BioMicroWorld 2013: V International Conference on Environmental, Industrial and Applied Microbiology*.

Broeckx, G., Vandenheuvel, D., Claes, I.J.J., Lebeer, S., and Kiekens, F. (2016) Drying techniques of probiotic bacteria as an important step towards the development of novel pharmabiotics. *International Journal of Pharmaceutics* **505** (1-2): 303–318.

Brutinel, E.D., and Gralnick, J.A. (2012) Shuttling happens: soluble flavin mediators of extracellular electron transfer in *Shewanella*. *Appl Microbiol Biotechnol* **93** (1): 41–48.

Bursac, T., Gralnick, J.A., and Gescher, J. (2017) Acetoin production via unbalanced fermentation in *Shewanella oneidensis*. *Biotechnology and Bioengineering* **114** (6): 1283–1289.

Caccavo, F., Lonergan, D.J., Lovley, D.R., Davis, M., Stolz, J.F., and McInerney, M.J. (1994) *Geobacter sulfurreducens* sp. nov., a hydrogen- and acetate-oxidizing dissimilatory metal-reducing microorganism. *Applied and Environmental Microbiology* **60** (10): 3752–3759.

Canfield, D.E., Kristensen, E., and Thamdrup, B. (2005) Thermodynamics and Microbial Metabolism. In *Advances in Marine Biology: Aquatic Geomicrobiology.* London: Elsevier Academic Press, pp. 65–94.

Canstein, H. von, Ogawa, J., Shimizu, S., and Lloyd, J.R. (2008) Secretion of flavins by *Shewanella* species and their role in extracellular electron transfer. *Applied and Environmental Microbiology* **74** (3): 615–623.

Cao, B., Zhao, Z., Peng, L., Shiu, H.Y., Ding, M., Song, F., *et al.* (2021) Silver nanoparticles boost charge-extraction efficiency in *Shewanella* microbial fuel cells. *Science* **373** (6561): 1336–1340.

Carlioz, A., and Touati, D. (1986) Isolation of superoxide dismutase mutants in *Escherichia coli*: is superoxide dismutase necessary for aerobic life? *The EMBO Journal* **5** (3): 623–630.

Cerrillo, M., Viñas, M., and Bonmatí, A. (2016) Removal of volatile fatty acids and ammonia recovery from unstable anaerobic digesters with a microbial electrolysis cell. *Bioresource Technology* **219:** 348–356.

Cerrillo, M., Viñas, M., and Bonmatí, A. (2018) Anaerobic digestion and electromethanogenic microbial electrolysis cell integrated system: Increased stability and recovery of ammonia and methane. *Renewable Energy* **120:** 178–189.

Champagne, C.P., Gardner, N., Brochu, E., and Beaulieu, Y. (1991) The freeze-drying of lactic acid bacteria: A review. *Canadian Institute of Food Science and Technology Journal* **24** (3-4): 118–128.

Chang, I.S., Jang, J.K., Gil, G.C., Kim, M., Kim, H.J., Cho, B.W., and Kim, B.H. (2004) Continuous determination of biochemical oxygen demand using microbial fuel cell type biosensor. *Biosensors and Bioelectronics* **19** (6): 607–613.

Chen, W., Liu, Z., Hou, J., Zhou, Y., Lou, X., and Li, Y. (2018) Enhancing performance of microbial fuel cells by using novel double-layer-capacitor-materials modified anodes. *International Journal of Hydrogen Energy* **43** (3): 1816–1823.

Chen, Y.-P., Zhao, Y., Qiu, K.-Q., Chu, J., Lu, R., Sun, M., *et al.* (2011) An innovative miniature microbial fuel cell fabricated using photolithography. *Biosensors and Bioelectronics* **26** (6): 2841–2846.

Cohen, B. (1931) The bacterial culture as electrical half-cell. *Journal of Bacteriology* **21** (1): 18–19.

Costerton, J.W., Lewandowski, Z., Caldwell, D.E., Korber, D.R., and Lappin-Scott, H.M. (1995) Microbial biofilms. *Annual Review of Microbiology* **49** (1): 711–745.

Dheilly, A., Linossier, I., Darchen, A., Hadjiev, D., Corbel, C., and Alonso, V. (2008) Monitoring of microbial adhesion and biofilm growth using electrochemical impedancemetry. *Applied Microbiology and Biotechnology* **79** (1): 157–164.

Dick, J.M. (2014) Average oxidation state of carbon in proteins. *Journal of the Royal Society Interface* **11** (100): 20131095.

Ding, W., Cheng, S., Yu, L., and Huang, H. (2017) Effective swine wastewater treatment by combining microbial fuel cells with flocculation. *Chemosphere* **182:** 567–573.

Dolch, K., Wuske, J., and Gescher, J. (2016) Genomic barcode-based analysis of exoelectrogens in wastewater biofilms grown on anode surfaces. *Journal of Microbiology and Biotechnology* **26** (3): 511–520.

Dolfing, J. (2014) Syntrophy in microbial fuel cells. *The ISME Journal* **8** (1): 4–5.

Donlan, R.M. (2002) Biofilms: microbial life on surfaces. *Emerging infectious diseases* **8** (9): 881–890.

Dzofou Ngoumelah, D., Harnisch, F., and Kretzschmar, J. (2021) Benefits of age-improved resistance of mature electroactive biofilm anodes in anaerobic digestion. *Environmental Science and Technology* **55** (12): 8258–8266.

Edel, M., Philipp, L.A., Lapp, J., Reiner, J., and Gescher, J. (2022) Electron transfer of extremophiles in bioelectrochemical systems. *Extremophiles* **26** (3): 31.

Edel, M., Sturm, G., Sturm-Richter, K., Wagner, M., Ducassou, J.N., Couté, Y., *et al.* (2021) Extracellular riboflavin induces anaerobic biofilm formation in *Shewanella oneidensis*. *Biotechnology for Biofuels* **14** (1): 1–14.

ElMekawy, A., Hegab, H.M., Mohanakrishna, G., Elbaz, A.F., Bulut, M., and Pant, D. (2016) Technological advances in CO_2 conversion electro-biorefinery: A step toward commercialization. *Bioresource Technology* **215:** 357–370.

Filman, D.J., Marino, S.F., Ward, J.E., Yang, L., Mester, Z., Bullitt, E., *et al.* (2019) Cryo-EM reveals the structural basis of long-range electron transport in a cytochrome-based bacterial nanowire. *Communications Biology 2019 2:1* **2** (1): 1–6.

Flemming, H.C., and Wingender, J. (2010) The biofilm matrix. *Nature Reviews Microbiology* **8** (9): 623–633.

Flemming, H.C., Wingender, J., Szewzyk, U., Steinberg, P., Rice, S.A., and Kjelleberg, S. (2016) Biofilms: an emergent form of bacterial life. *Nature Reviews Microbiology* **14** (9): 563–575.

Floudas, G. (2012) Chapter 2.32 - Dielectric Spectroscopy. In *Polymer science: A comprehensive reference.* Amsterdam: Elsevier Science, pp. 825–845.

Flynn, J.M., Ross, D.E., Hunt, K.A., Bond, D.R., and Gralnick, J.A. (2010) Enabling unbalanced fermentations by using engineered electrode-interfaced bacteria. *mBio* **1** (5).

Fonseca, B.M., Paquete, C.M., Neto, S.E., Pacheco, I., Soares, C.M., and Louro, R.O. (2013) Mind the gap: cytochrome interactions reveal electron pathways across the periplasm of *Shewanella oneidensis* MR-1. *Biochemical Journal* **449** (1): 101–108.

Förster, A.H., Beblawy, S., Golitsch, F., and Gescher, J. (2017) Electrode-assisted acetoin production in a metabolically engineered *Escherichia coli* strain. *Biotechnology for Biofuels* **10** (1): 65.

Franks, A.E., Nevin, K.P., Glaven, R.H., and Lovley, D.R. (2010) Microtoming coupled to microarray analysis to evaluate the spatial metabolic status of *Geobacter sulfurreducens* biofilms. *The ISME Journal* **4** (4): 509–519.

Franks, A.E., Nevin, K.P., Jia, H., Izallalen, M., Woodard, T.L., and Lovley, D.R. (2009) Novel strategy for three-dimensional real-time imaging of microbial fuel cell communities: monitoring the inhibitory effects of proton accumulation within the anode biofilm. *Energy and Environmental Science* **2** (1): 113–119.

Freguia, S., Teh, E.H., Boon, N., Leung, K.M., Keller, J., and Rabaey, K. (2010) Microbial fuel cells operating on mixed fatty acids. *Bioresource Technology* **101** (4): 1233–1238.

Freyman, M.C., Kou, T., Wang, S., and Li, Y. (2019) 3D printing of living bacteria electrode. *Nano Research* **13** (5): 1318–1323.

Fujii, T., Yano, T., Kumagai, H., and Miyawaki, O. (2000) Scaling analysis of the concentration dependence on elasticity of agarose gel. *Bioscience, Biotechnology, and Biochemistry* **64** (8): 1618–1622.

Gescher, J.S., Cordova, C.D., and Spormann, A.M. (2008) Dissimilatory iron reduction in *Escherichia coli*: identification of CymA of *Shewanella oneidensis* and NapC of *E. coli* as ferric reductases. *Molecular microbiology* **68** (3): 706–719.

Global Footprint Network (2022) *National Footprint and Biocapacity Accounts:* York University Ecological Footprint Initiative & Global Footprint Network, available online at https://data.footprintnetwork.org, last checked 24.04.2023.

Golitsch, F. (2016) *Entwicklung bioelektrochemischer Systeme für die Untersuchung von elektrodenabhängigen Konversionsprozessen.* Karlsruhe.

Golitsch, F., Bücking, C., and Gescher, J. (2013) Proof of principle for an engineered microbial biosensor based on *Shewanella oneidensis* outer membrane protein complexes. *Biosensors and Bioelectronics* **47:** 285–291.

Gu, Y., Srikanth, V., Salazar-Morales, A.I., Jain, R., O'Brien, J.P., Yi, S.M., *et al.* (2021) Structure of *Geobacter* pili reveals secretory rather than nanowire behaviour. *Nature* **597** (7876): 430–434.

Guo, K., Prévoteau, A., Patil, S.A., and Rabaey, K. (2015) Engineering electrodes for microbial electrocatalysis. *Current Opinion in Biotechnology* **33:** 149–156.

Hackbarth, M., Jung, T., Reiner, J.E., Gescher, J., Horn, H., Hille-Reichel, A., and Wagner, M. (2020) Monitoring and quantification of bioelectrochemical *Kyrpidia spormannii* biofilm development in a novel flow cell setup. *Chemical Engineering Journal* **390:** 124604.

Hartshorne, R.S., Reardon, C.L., Ross, D., Nuester, J., Clarke, T.A., Gates, A.J., *et al.* (2009) Characterization of an electron conduit between bacteria and the extracellular

environment. *Proceedings of the National Academy of Sciences of the United States of America* **106** (52): 22169–22174.

Hays, S., Zhang, F., and Logan, B.E. (2011) Performance of two different types of anodes in membrane electrode assembly microbial fuel cells for power generation from domestic wastewater. *Journal of Power Sources* **196** (20): 8293–8300.

Herbert-Guillou, D., Tribollet, B., Festy, D., and Kiéné, L. (1999) *In situ* detection and characterization of biofilm in waters by electrochemical methods. *Electrochimica Acta* **45** (7): 1067–1075.

Hiegemann, H., Littfinski, T., Krimmler, S., Lübken, M., Klein, D., Schmelz, K.G., *et al.* (2019) Performance and inorganic fouling of a submergible 255 L prototype microbial fuel cell module during continuous long-term operation with real municipal wastewater under practical conditions. *Bioresource Technology* **294:** 122227.

Hindatu, Y., Annuar, M.S., and Gumel, A.M. (2017) Mini-review: Anode modification for improved performance of microbial fuel cell. *Renewable and Sustainable Energy Reviews* **73:** 236–248.

Horneck, G. (2001) Bacterial spores survive simulated meteorite impact. *Icarus* **149** (1): 285–290.

Hou, H., Li, L., Cho, Y., Figueiredo, P. de, and Han, A. (2009) Microfabricated microbial fuel cell arrays reveal electrochemically active microbes. *PLOS ONE* **4** (8): e6570.

Hu, Y., Rehnlund, D., Klein, E., Gescher, J., and Niemeyer, C.M. (2020) Cultivation of exoelectrogenic bacteria in conductive DNA nanocomposite hydrogels yields a programmable biohybrid materials system. *ACS Applied Materials & Interfaces* **12** (13): 14806–14813.

Humphrey, A.E., and Lee, S.E. (1992) Industrial fermentation: Principles, processes, and products. In *Riegel's Handbook of Industrial Chemistry:* Springer, Dordrecht, pp. 916–986.

Imlay, J.A. (2003) Pathways of oxidative damage. *Reviews in Microbiology* **57** (1): 395–418.

International Energy Agency (2019) *World electricity final consumption by sector, 1974 - 2019:* International Energy Agency (IEA), available online at https://www.iea.org/data-and-statistics/charts/world-electricity-final-consumption-by-sector-1974-2019, last checked 23.04.2023.

Ivars-Barceló, F., Zuliani, A., Fallah, M., Mashkour, M., Rahimnejad, M., and Luque, R. (2018) Novel applications of microbial fuel cells in sensors and biosensors. *Applied Sciences* **8** (7): 1184.

Jiang, H., Halverson, L.J., and Dong, L. (2015) A miniature microbial fuel cell with conducting nanofibers-based 3D porous biofilm. *Journal of Micromechanics and Microengineering* **25** (12): 125017.

Jiang, X., Hu, J., Fitzgerald, L.A., Biffinger, J.C., Xie, P., Ringeisen, B.R., and Lieber, C.M. (2010) Probing electron transfer mechanisms in *Shewanella oneidensis* MR-1 using a nanoelectrode platform and single-cell imaging. *Proceedings of the National Academy of Sciences of the United States of America* **107** (39): 16806–16810.

Johansson, B.G. (1972) Agarose gel electrophoresis. *Scandinavian Journal of Clinical and Laboratory Investigation* **124** (sup124): 7–19.

Jones, A.-A.D., and Buie, C.R. (2019) Continuous shear stress alters metabolism, mass-transport, and growth in electroactive biofilms independent of surface substrate transport. *Scientific Reports* **9** (1): 2602.

Jong, K.P. de, and Geus, J.W. (2000) Carbon nanofibers: Catalytic synthesis and applications. *Catalysis Reviews* **42** (4): 481–510.

Jourdin, L., and Burdyny, T. (2021) Microbial electrosynthesis: Where do we go from here? *Trends in Biotechnology* **39** (4): 359–369.

Kadier, A., Kalil, M.S., Rai, P.K., Kumar, S.S., Abdeshahian, P., Sivagurunathan, P., *et al.* (2019) *Microbial Electrolysis Cells (MECs): Chapter 12 - A promising and green*

approach for bioenergy and biochemical production from waste resources. Hoboken: John Wiley & Sons.

Kadier, A., Simayi, Y., Abdeshahian, P., Azman, N.F., Chandrasekhar, K., and Kalil, M.S. (2016) A comprehensive review of microbial electrolysis cells (MEC) reactor designs and configurations for sustainable hydrogen gas production. *Alexandria Engineering Journal* **55** (1): 427–443.

Kadier, A., Simayi, Y., Kalil, M.S., Abdeshahian, P., and Hamid, A.A. (2014) A review of the substrates used in microbial electrolysis cells (MECs) for producing sustainable and clean hydrogen gas. *Renewable Energy* **71:** 466–472.

Kaur, A., Kim, J.R., Michie, I., Dinsdale, R.M., Guwy, A.J., and Premier, G.C. (2013) Microbial fuel cell type biosensor for specific volatile fatty acids using acclimated bacterial communities. *Biosensors and Bioelectronics* **47:** 50–55.

Kemmler, A., Wünsch, A., and Burret, H. (2021) *Entwicklung des Bruttostromverbrauchs bis 2030: Berechnungsergebnisse aus dem Szenario 1:* Bundesministerium für Wirtschaft und Energie (BMWi), available online at https://www.prognos.com/de/projekt/entwicklung-des-bruttostromverbrauches-bis-2030, last checked 23.04.2023.

Kerisit, S., Rosso, K.M., Dupuis, M., and Valiev, M. (2007) Molecular computational investigation of electron-transfer kinetics across cytochrome−iron oxide interfaces. *The Journal of Physical Chemistry C* **111** (30): 11363–11375.

Kerzenmacher, S. (2017) Engineering of Microbial Electrodes. In *Bioelectrosynthesis.* Cham: Springer, pp. 135–180.

Khodadadi Yazdi, M., Taghizadeh, A., Taghizadeh, M., Stadler, F.J., Farokhi, M., Mottaghitalab, F., *et al.* (2020) Agarose-based biomaterials for advanced drug delivery. *Journal of Controlled Release* **326:** 523–543.

Kiely, P.D., Regan, J.M., and Logan, B.E. (2011) The electric picnic: synergistic requirements for exoelectrogenic microbial communities. *Current Opinion in Biotechnology* **22** (3): 378–385.

Klapper, I., Rupp, C.J., Cargo, R., Purvedorj, B., and Stoodley, P. (2002) Viscoelastic fluid description of bacterial biofilm material properties. *Biotechnology and Bioengineering* **80** (3): 289–296.

Klein, E.M., Knoll, M.T., and Gescher, J. (2023) Microbe-Anode Interactions: Comparing the impact of genetic and material engineering approaches to improve the performance of microbial electrochemical systems (MES). *Microbial Biotechnology*.

Knoll, M.T., Fuderer, E., and Gescher, J. (2022) Sprayable biofilm – Agarose hydrogels as 3D matrix for enhanced productivity in bioelectrochemical systems. *Biofilm* **4:** 100077.

Koch, C., and Harnisch, F. (2016) Is there a specific ecological niche for electroactive microorganisms? *ChemElectroChem* **3** (9): 1282–1295.

Koch, C., Huber, K.J., Bunk, B., Overmann, J., and Harnisch, F. (2019) Trophic networks improve the performance of microbial anodes treating wastewater. *NPJ Biofilms and Microbiomes* **5** (1): 27.

Kopeček, J., and Yang, J. (2007) Hydrogels as smart biomaterials. *Polymer International* **56** (9): 1078–1098.

Kotloski, N.J., and Gralnick, J.A. (2013) Flavin electron shuttles dominate extracellular electron transfer by *Shewanella oneidensis*. *mBio* **4** (1): e00553-12.

Koul, Y., Devda, V., Varjani, S., Guo, W., Ngo, H.H., Taherzadeh, M.J., *et al.* (2022) Microbial electrolysis: a promising approach for treatment and resource recovery from industrial wastewater. *Bioengineered* **13** (4): 8115–8134.

Kretzschmar, J., Böhme, P., Liebetrau, J., Mertig, M., and Harnisch, F. (2018) Microbial electrochemical sensors for anaerobic digestion process control - Performance of electroactive biofilms under real conditions. *Chemical Engineering and Technology* **41** (4): 687–695.

Krieg, T., Sydow, A., Schröder, U., Schrader, J., and Holtmann, D. (2014) Reactor concepts for bioelectrochemical syntheses and energy conversion. *Trends in Biotechnology* **32** (12): 645–655.

Kumar, G.G., Sarathi, V.G., and Nahm, K.S. (2013) Recent advances and challenges in the anode architecture and their modifications for the applications of microbial fuel cells. *Biosensors and Bioelectronics* **43** (1): 461–475.

Kuroda, M., and Watanabe, T. (1995) CO_2 reduction to methane and acetate using a bio-electro reactor with immobilized methanogens and homoacetogens on electrodes. *Energy Conversion and Management* **36** (6-9): 787–790.

Li, F., Wang, L., Liu, C., Wu, D., and Song, H. (2018) Engineering exoelectrogens by synthetic biology strategies. *Current Opinion in Electrochemistry* **10:** 37–45.

Li, S., Cheng, C., Thomas, A., Li, S., Thomas Functional Materials, A., and Cheng, C. (2017) Carbon-based microbial-fuel-cell electrodes: From conductive supports to active catalysts. *Advanced Materials* **29** (8): 1602547.

Li, T., Zhou, Q., Zhou, L., Yan, Y., Liao, C., Wan, L., *et al.* (2020) Acetate limitation selects *Geobacter* from mixed inoculum and reduces polysaccharide in electroactive biofilm. *Water Research* **177:** 115776.

Liang, P., Wang, H., Xia, X., Huang, X., Mo, Y., Cao, X., and Fan, M. (2011) Carbon nanotube powders as electrode modifier to enhance the activity of anodic biofilm in microbial fuel cells. *Biosensors and Bioelectronics* **26** (6): 3000–3004.

Light, S.H., Su, L., Rivera-Lugo, R., Cornejo, J.A., Louie, A., Iavarone, A.T., *et al.* (2018) A flavin-based extracellular electron transfer mechanism in diverse Gram-positive bacteria. *Nature 2015 523:7562* **562** (7725): 140–144.

Lin, W.C., Coppi, M.V., and Lovley, D.R. (2004) *Geobacter sulfurreducens* can grow with oxygen as a terminal electron acceptor. *Applied and Environmental Microbiology* **70** (4): 2525–2528.

Lin, X., Nishio, K., Konno, T., and Ishihara, K. (2012) The effect of the encapsulation of bacteria in redox phospholipid polymer hydrogels on electron transfer efficiency in living cell-based devices. *Biomaterials* **33** (33): 8221–8227.

Liu, H., Grot, S., and Logan, B.E. (2005) Electrochemically assisted microbial production of hydrogen from acetate. *Environmental Science and Technology* **39** (11): 4317–4320.

Liu, P., Liang, P., Jiang, Y., Hao, W., Miao, B., Wang, D., and Huang, X. (2018) Stimulated electron transfer inside electroactive biofilm by magnetite for increased performance microbial fuel cell. *Applied Energy* **216:** 382–388.

Liu, X., Wu, W., and Gu, Z. (2015) Poly (3,4-ethylenedioxythiophene) promotes direct electron transfer at the interface between *Shewanella loihica* and the anode in a microbial fuel cell. *Journal of Power Sources* **277:** 110–115.

Liu, X.-W., Sun, X.-F., Huang, Y.-X., Sheng, G.-P., Wang, S.-G., and Yu, H.-Q. (2011) Carbon nanotube/chitosan nanocomposite as a biocompatible biocathode material to enhance the electricity generation of a microbial fuel cell. *Energy and Environmental Science* **4** (4): 1422.

Lloyd, J.R., Leang, C., Hodges Myerson, A.L., Coppi, M.V., Cuifo, S., Methe, B., *et al.* (2003) Biochemical and genetic characterization of PpcA, a periplasmic *c*-type cytochrome in *Geobacter sulfurreducens*. *Biochemical Journal* **369** (1): 153–161.

Logan, B.E. (2009) Exoelectrogenic bacteria that power microbial fuel cells. *Nature Reviews Microbiology* **7** (5): 375–381.

Logan, B.E., Call, D., Cheng, S., Hamelers, H.V.M., Sleutels, T.H.J.A., Jeremiasse, A.W., and Rozendal, R.A. (2008) Microbial electrolysis cells for high yield hydrogen gas production from organic matter. *Environmental Science and Technology* **42** (23): 8630–8640.

Logan, B.E., Hamelers, B., Rozendal, R., Schröder, U., Keller, J., Freguia, S., *et al.* (2006) Microbial fuel cells: Methodology and technology. *Environmental Science and Technology* **40** (17): 5181–5192.

Logan, B.E., and Rabaey, K. (2012) Conversion of wastes into bioelectricity and chemicals by using microbial electrochemical technologies. *Science* **337** (6095): 686–690.

Logan, B.E., Rossi, R., Ragab, A., and Saikaly, P.E. (2019) Electroactive microorganisms in bioelectrochemical systems. *Nature Reviews Microbiology* **17** (5): 307–319.

Lovley, D.R. (2011) Powering microbes with electricity: direct electron transfer from electrodes to microbes. *Environmental Microbiology Reports* **3** (1): 27–35.

Lovley, D.R. (2012) Electromicrobiology. *Annual Review of Microbiology* **66:** 391–409.

Lovley, D.R. (2017) Electrically conductive pili: Biological function and potential applications in electronics. *Current Opinion in Electrochemistry* **4** (1): 190–198.

Lovley, D.R., and Holmes, D.E. (2020) Protein nanowires: The electrification of the microbial world and maybe our own. *Journal of Bacteriology* **202** (20).

Lovley, D.R., and Nevin, K.P. (2013) Electrobiocommodities: powering microbial production of fuels and commodity chemicals from carbon dioxide with electricity. *Current Opinion in Biotechnology* **24** (3): 385–390.

Lovley, D.R., and Phillips, E.J. (1988) Novel mode of microbial energy metabolism: organic carbon oxidation coupled to dissimilatory reduction of iron or manganese. *Applied and Environmental Microbiology* **54** (6): 1472–1480.

Lovley, D.R., and Walker, D.J. (2019) Geobacter protein nanowires. *Frontiers in Microbiology* **10:** 2078.

Malvankar, N.S., Lau, J., Nevin, K.P., Franks, A.E., Tuominen, M.T., and Lovley, D.R. (2012) Electrical conductivity in a mixed-species biofilm. *Applied and Environmental Microbiology* **78** (16): 5967–5971.

Malvankar, N.S., and Lovley, D.R. (2012) Microbial nanowires: a new paradigm for biological electron transfer and bioelectronics. *ChemSusChem* **5** (6): 1039–1046.

Malvankar, N.S., Vargas, M., Nevin, K.P., Franks, A.E., Leang, C., Kim, B.C., *et al.* (2011) Tunable metallic-like conductivity in microbial nanowire networks. *Nature Nanotechnology* **6** (9): 573–579.

Marsili, E., Baron, D.B., Shikhare, I.D., Coursolle, D., Gralnick, J.A., and Bond, D.R. (2008) *Shewanella* secretes flavins that mediate extracellular electron transfer. *Proceedings of the National Academy of Sciences of the United States of America* **105** (10): 3968–3973.

McCord, J.M., Keele, B.B., and Fridovich, I. (1971) An enzyme-based theory of obligate anaerobiosis: the physiological function of superoxide dismutase. *Proceedings of the National Academy of Sciences of the United States of America* **68** (5): 1024–1027.

McCuskey, S.R., Su, Y., Leifert, D., Moreland, A.S., Bazan, G.C., McCuskey, S.R., *et al.* (2020) Living bioelectrochemical composites. *Advanced Materials* **32** (24): 1908178.

McLean, J.S., Wanger, G., Gorby, Y.A., Wainstein, M., McQuaid, J., Ishii, S.I., *et al.* (2010) Quantification of electron transfer rates to a solid phase electron acceptor through the stages of biofilm formation from single cells to multicellular communities. *Environmental Science and Technology* **44** (7): 2721–2727.

McMillan, D.G.G., Marritt, S.J., Butt, J.N., and Jeuken, L.J.C. (2012) Menaquinone-7 is specific cofactor in tetraheme quinol dehydrogenase CymA. *Journal of Biological Chemistry* **287** (17): 14215–14225.

Mohanakrishna, G., Kalathil, S., and Pant, D. (2017) *Microbial Fuel Cell: Reactor design for bioelectrochemical systems.* Cham: Springer, pp. 209-227.

Moon, W.G., Kim, G.-P., Lee, M., Song, H.D., and Yi, J. (2015) A biodegradable gel electrolyte for use in high-performance flexible supercapacitors. *ACS Applied Materials and Interfaces* **7** (6): 3503–3511.

Morgan-Sagastume, F., Larsen, P., Nielsen, J.L., and Nielsen, P.H. (2008) Characterization of the loosely attached fraction of activated sludge bacteria. *Water Research* **42** (4-5): 843–854.

Musiani, M.M. (1990) Characterization of electroactive polymer layers by electrochemical impedance spectroscopy (EIS). *Electrochimica Acta* **35** (10): 1665–1670.

Myers, C.R., and Nealson, K.H. (1988) Bacterial manganese reduction and growth with manganese oxide as the sole electron acceptor. *Science (New York, N.Y.)* **240** (4857): 1319–1321.

Nagar, E., and Schwarz, R. (2015) To be or not to be planktonic? Self-inhibition of biofilm development. *Environmental Microbiology* **17** (5): 1477–1486.

Neal, A.L., Rosso, K.M., Geesey, G.G., Gorby, Y.A., and Little, B.J. (2003) Surface structure effects on direct reduction of iron oxides by *Shewanella oneidensis*. *Geochimica et Cosmochimica Acta* **67** (23): 4489–4503.

Nevin, K.P., Hensley, S.A., Franks, A.E., Summers, Z.M., Ou, J., Woodard, T.L., *et al.* (2011) Electrosynthesis of organic compounds from carbon dioxide is catalyzed by a diversity of acetogenic microorganisms. *Applied and Environmental Microbiology* **77** (9): 2882–2886.

Nevin, K.P., Richter, H., Covalla, S.F., Johnson, J.P., Woodard, T.L., Orloff, A.L., *et al.* (2008) Power output and columbic efficiencies from biofilms of *Geobacter sulfurreducens* comparable to mixed community microbial fuel cells. *Environmental Microbiology* **10** (10): 2505–2514.

Nevin, K.P., Woodard, T.L., Franks, A.E., Summers, Z.M., and Lovley, D.R. (2010) Microbial electrosynthesis: feeding microbes electricity to convert carbon dioxide and water to multicarbon extracellular organic compounds. *mBio* **1** (2): e00103-10.

Nosek, D., Jachimowicz, P., and Cydzik-Kwiatkowska, A. (2020) Anode modification as an alternative approach to improve electricity generation in microbial fuel cells. *Energies* **13** (24): 6596.

O'Toole, G., Kaplan, H.B., and Kolter, R. (2003) Biofilm formation as microbial development. *Annual Reviews in Microbiology* **54** (1): 49–79.

Okamoto, A., Hashimoto, K., Nealson, K.H., and Nakamura, R. (2013) Rate enhancement of bacterial extracellular electron transport involves bound flavin semiquinones. *Proceedings of the National Academy of Sciences of the United States of America* **110** (19): 7856–7861.

Okamoto, A., Nakamura, R., Nealson, K.H., and Hashimoto, K. (2014) Bound flavin model suggests similar electron-transfer mechanisms in *Shewanella* and *Geobacter*. *ChemElectroChem* **1** (11): 1808–1812.

Otero, F.J., Chan, C.H., and Bond, D.R. (2018) Identification of different putative outer membrane electron conduits necessary for Fe(III) citrate, Fe(III) oxide, Mn(IV) oxide, or electrode Reduction by *Geobacter sulfurreducens*. *Journal of Bacteriology* **200** (19): e00347-18.

Palma-Delgado, V., Gescher, J., and Sturm, G. (2020) *Microbial Electrochemical Technologies: Electrode-assisted fermentations: Their limitations and future research directions.* Boca Raton: CRC Press, pp. 85–96.

Pandey, P., Shinde, V.N., Deopurkar, R.L., Kale, S.P., Patil, S.A., and Pant, D. (2016) Recent advances in the use of different substrates in microbial fuel cells toward wastewater treatment and simultaneous energy recovery. *Applied Energy* **168:** 706–723.

Paquete, C.M. (2020) Electroactivity across the cell wall of Gram-positive bacteria. *Computational and Structural Biotechnology Journal* **18:** 3796–3802.

Park, S.G., Rajesh, P.P., Sim, Y.U., Jadhav, D.A., Noori, M.T., Kim, D.H., *et al.* (2022) Addressing scale-up challenges and enhancement in performance of hydrogen-producing microbial electrolysis cell through electrode modifications. *Energy Reports* **8:** 2726–2746.

Philipp, L.A., Edel, M., and Gescher, J. (2020) Genetic engineering for enhanced productivity in bioelectrochemical systems. *Advances in Applied Microbiology* **111:** 1–31.

Philips, J., Rabaey, K., Lovley, D.R., and Vargas, M. (2017) Biofilm formation by *Clostridium ljungdahlii* is induced by sodium chloride stress: Experimental evaluation and transcriptome analysis. *PLOS ONE* **12** (1): e0170406.

Pomfret, R., Sillay, K., and Miranpuri, G. (2013) Investigation of the electrical properties of agarose gel: characterization of concentration using nyquist plot phase angle and the implications of a more comprehensive *in vitro* model of the brain. *Annals of Neurosciences* **20** (3): 99–107.

Potter, M.C. (1911) Electrical effects accompanying the decomposition of organic compounds. *Proceedings of the Royal Society of London. Serie B, containing Papers of a Biological Character* **84** (571): 260–276.

Prokhorova, A., Sturm-Richter, K., Doetsch, A., and Gescher, J. (2017) Resilience, dynamics, and interactions within a model multispecies exoelectrogenic-biofilm community. *Applied and Environmental Microbiology* **83** (6).

Pu, K.B., Gao, J.Y., Cai, W.F., Chen, Q.Y., Guo, K., Huang, Y., *et al.* (2022) A new modification method of metal substrates via candle soot to prepare effective anodes in air-cathode microbial fuel cells. *Journal of Chemical Technology and Biotechnology* **97** (1): 189–198.

Rabaey, K., and Rozendal, R.A. (2010) Microbial electrosynthesis - revisiting the electrical route for microbial production. *Nature Reviews Microbiology* **8** (10): 706–716.

Rabaey, K., and Verstraete, W. (2005) Microbial fuel cells: novel biotechnology for energy generation. *Trends in Biotechnology* **23** (6): 291–298.

Reguera, G., Nevin, K.P., Nicoll, J.S., Covalla, S.F., Woodard, T.L., and Lovley, D.R. (2006) Biofilm and nanowire production leads to increased current in *Geobacter sulfurreducens* fuel cells. *Applied and Environmental Microbiology* **72** (11): 7345–7348.

Ren, L., McCuskey, S.R., Moreland, A., Bazan, G.C., and Nguyen, T.-Q. (2019) Tuning *Geobacter sulfurreducens* biofilm with conjugated polyelectrolyte for increased performance in bioelectrochemical system. *Biosensors and Bioelectronics* **144:** 111630.

Renslow, R.S., Babauta, J.T., Dohnalkova, A.C., Boyanov, M.I., Kemner, K.M., Majors, P.D., *et al.* (2013) Metabolic spatial variability in electrode-respiring *Geobacter sulfurreducens* biofilms. *Energy and Environmental Science* **6** (6): 1827–1836.

Renslow, R.S., Majors, P.D., McLean, J.S., Fredrickson, J.K., Ahmed, B., and Beyenal, H. (2010) *In situ* effective diffusion coefficient profiles in live biofilms using pulsed-field gradient nuclear magnetic resonance. *Biotechnology and Bioengineering* **106** (6): 928–937.

Ringeisen, B.R., Henderson, E., Wu, P.K., Pietron, J., Ray, R., Little, B., *et al.* (2006) High power density from a miniature microbial fuel cell using *Shewanella oneidensis* DSP10. *Environmental Science and Technology* **40** (8): 2629–2634.

Romans-Casas, M., Perona-Vico, E., Dessì, P., Bañeras, L., Balaguer, M.D., and Puig, S. (2023) Boosting ethanol production rates from carbon dioxide in MES cells under optimal solventogenic conditions. *Sci Total Environ* **856** (1): 159124.

Rozendal, R.A., Hamelers, H.V.M., and Buisman, C.J.N. (2006a) Effects of membrane cation transport on pH and microbial fuel cell performance. *Environmental Science and Technology* **40** (17): 5206–5211.

Rozendal, R.A., Hamelers, H.V.M., Euverink, G.J., Metz, S.J., and Buisman, C.J. (2006b) Principle and perspectives of hydrogen production through biocatalyzed electrolysis. *International Journal of Hydrogen Energy* **31** (12): 1632–1640.

Sahle-Demessie, E., and Tadesse, H. (2011) Kinetics and equilibrium adsorption of nano-TiO_2 particles on synthetic biofilm. *Surface Science* **605** (13-14): 1177–1184.

Sanchez, D., Jacobs, D., Gregory, K., Huang, J., Hu, Y., Vidic, R., and Yun, M. (2015) Changes in carbon electrode morphology affect microbial fuel cell performance with *Shewanella oneidensis* MR-1. *Energies* **8** (3): 1817–1829.

Sauer, K., Camper, A.K., Ehrlich, G.D., Costerton, J.W., and Davies, D.G. (2002) *Pseudomonas aeruginosa* displays multiple phenotypes during development as a biofilm. *Journal of Bacteriology* **184** (4): 1140–1154.

Sauer, K., Stoodley, P., Goeres, D.M., Hall-Stoodley, L., Burmølle, M., Stewart, P.S., and Bjarnsholt, T. (2022) The biofilm life cycle: expanding the conceptual model of biofilm formation. *Nature Reviews Microbiology* **20** (10): 608–620.

Savla, N., Anand, R., Pandit, S., and Prasad, R. (2020) Utilization of Nanomaterials as Anode Modifiers for Improving Microbial Fuel Cells Performance. *Journal of Renewable Materials* **8** (12): 1581–1605.

Schindelin, J., Arganda-Carreras, I., Frise, E., Kaynig, V., Longair, M., Pietzsch, T., *et al.* (2012) Fiji: an open-source platform for biological-image analysis. *Nature Methods* **9** (7): 676–682.

Schröder, U. (2011) Discover the possibilities: microbial bioelectrochemical systems and the revival of a 100-year–old discovery. *Journal of Solid State Electrochemistry* **15** (7-8): 1481–1486.

Schrope, M. (2001) Which way to energy utopia? *Nature* **414** (6865): 682–684.

Serwer, P., and Hayes, S.J. (1986) Exclusion of spheres by agarose gels during agarose gel electrophoresis: dependence on the sphere's radius and the gel's concentration. *Analytical Biochemistry* **158** (1): 72–78.

Shen, C.F., and Guiot, S.R. (1996) Long-term impact of dissolved O_2 on the activity of anaerobic granules. *Biotechnology and Bioengineering* **49** (6): 611–620.

Sleutels, T.H., Hamelers, H.V., Rozendal, R.A., and Buisman, C.J. (2009) Ion transport resistance in Microbial Electrolysis Cells with anion and cation exchange membranes. *International Journal of Hydrogen Energy* **34** (9): 3612–3620.

Sleutels, T.H.J.A., Heijne, A. ter, Buisman, C.J.N., and Hamelers, H.V.M. (2012) Bioelectrochemical systems: an outlook for practical applications. *ChemSusChem* **5** (6): 1012–1019.

Stein, N.E., Hamelers, H.M., van Straten, G., and Keesman, K.J. (2012) On-line detection of toxic components using a microbial fuel cell-based biosensor. *Journal of Process Control* **22** (9): 1755–1761.

Stewart, P.S. (2003) Diffusion in biofilms. *Journal of Bacteriology* **185** (5): 1485–1491.

Strathmann, M., Griebe, T., and Flemming, H.-C. (2000) Artificial biofilm model – a useful tool for biofilm research. *Applied Microbiology and Biotechnology* **54** (2): 231–237.

Strathmann, M., Griebe, T., and Flemming, H.-C. (2001) Agarose hydrogels as EPS models. *Water Science and Technology* **43** (6): 169–175.

Sturm, G., Richter, K., Doetsch, A., Heide, H., Louro, R.O., and Gescher, J. (2015) A dynamic periplasmic electron transfer network enables respiratory flexibility beyond a thermodynamic regulatory regime. *The ISME Journal* **9** (8): 1802.

Sturm-Richter, K., Golitsch, F., Sturm, G., Kipf, E., Dittrich, A., Beblawy, S., *et al.* (2015) Unbalanced fermentation of glycerol in *Escherichia coli* via heterologous production of an electron transport chain and electrode interaction in microbial electrochemical cells. *Bioresource Technology* **186:** 89–96.

Su, M., Jiang, Y., and Li, D. (2013) Production of acetate from carbon dioxide in bioelectrochemical systems based on autotrophic mixed culture. *Journal of Microbiology and Biotechnology* **23** (8): 1140–1146.

Summers, Z.M., Fogarty, H.E., Leang, C., Franks, A.E., Malvankar, N.S., and Lovley, D.R. (2010) Direct exchange of electrons within aggregates of an evolved syntrophic coculture of anaerobic bacteria. *Science* **330** (6009): 1413–1415.

Sun, J.-Z., Peter Kingori, G., Si, R.-W., Zhai, D.-D., Liao, Z.-H., Sun, D.-Z., *et al.* (2015) Microbial fuel cell-based biosensors for environmental monitoring: a review. *Water Science and Technology* **71** (6): 801–809.

Suravaram, S.K., Smith, D.K., Parkin, A., and Chechik, V. (2019) Conductive gels based on modified agarose embedded with gold nanoparticles and their application as a conducting support for *Shewanella oneidensis* MR-1. *ChemElectroChem* **6** (23): 5876–5879.

Sydow, A., Krieg, T., Mayer, F., Schrader, J., and Holtmann, D. (2014) Electroactive bacteria--molecular mechanisms and genetic tools. *Applied Microbiology and Biotechnology* **98** (20): 8481–8495.

Tang, T.-C., An, B., Huang, Y., Vasikaran, S., Wang, Y., Jiang, X., *et al.* (2021) Materials design by synthetic biology. *Nature Reviews Materials* **6** (4): 332–350.

Tennent, H.G. (1987) Carbon fibrils, method for producing same and compositions containing same: US Patent (4,663,230): Elsevier BV, p. 255.

Thauer, R.K., Jungermann, K., and Decker, K. (1977) Energy conservation in chemotrophic anaerobic bacteria. *Bacteriological Reviews* **41** (1): 100–180.

Thevenot, D.R., Tóth, K., Durst, R.A., and Wilson, G.S. (1999) Electrochemical biosensors: Recommended definitions and classification. *Pure and Applied Chemistry* **71** (12): 2333–2348.

Thormann, K.M., Saville, R.M., Shukla, S., Pelletier, D.A., and Spormann, A.M. (2004) Initial phases of biofilm formation in *Shewanella oneidensis* MR-1. *Journal of Bacteriology* **186** (23): 8096–8104.

To, B.C.S., and Etzel, M.R. (1997) Spray drying, freeze drying, or freezing of three different lactic acid bacteria species. *Journal of Food Science* **62** (3): 576–578.

Tominaka, S., Ohta, S., Obata, H., Momma, T., and Osaka, T. (2008) On-chip fuel cell: micro direct methanol fuel cell of an air-breathing, membraneless, and monolithic design. *Journal of the American Chemical Society* **130** (32): 10456–10457.

Torres, C.I., Kato Marcus, A., and Rittmann, B.E. (2008) Proton transport inside the biofilm limits electrical current generation by anode-respiring bacteria. *Biotechnology and Bioengineering* **100** (5): 872–881.

Torres, C.I., Marcus, A.K., Lee, H.S., Parameswaran, P., Krajmalnik-Brown, R., and Rittmann, B.E. (2010) A kinetic perspective on extracellular electron transfer by anode-respiring bacteria. *FEMS microbiology reviews* **34** (1): 3–17.

Toshimitsu, F., Ishimaru, W., and Nakashima, N. (2019) Individual solubilization behavior of single-walled carbon nanotubes by riboflavin (vitamin B2) in water and its analyses using regression approach and computational simulations. *Bulletin of the Chemical Society of Japan* **92** (10): 1679–1683.

Trivedi, T.J., Srivastava, D.N., Rogers, R.D., and Kumar, A. (2012) Agarose processing in protic and mixed protic–aprotic ionic liquids: dissolution, regeneration and high conductivity, high strength ionogels. *Green Chemistry* **14** (10): 2831.

Tseng, C.-P., Liu, F., Zhang, X., Huang, P.-C., Campbell, I., Li, Y., *et al.* (2022) Solution-deposited and patternable conductive polymer thin-film electrodes for microbial bioelectronics. *Advanced Materials* **34** (13): 2109442.

Vázquez, R.J., McCuskey, S.R., Quek, G., Su, Y., Llanes, L., Hinks, J., *et al.* (2022) Conjugated polyelectrolyte/bacteria living composites in carbon paper for biocurrent generation. *Macromolecular Rapid Communications* **43** (16): 2100840.

Vellingiri, A., Song, Y.E., Munussami, G., Kim, C., Park, C., Jeon, B.H., *et al.* (2019) Overexpression of *c*-type cytochrome, CymA in *Shewanella oneidensis* MR-1 for enhanced bioelectricity generation and cell growth in a microbial fuel cell. *Journal of Chemical Technology and Biotechnology* **94** (7): 2115–2122.

Venkateswaran, K., Moser, D.P., Dollhopf, M.E., Lies, D.P., Saffarini, D.A., MacGregor, B.J., *et al.* (1999) Polyphasic taxonomy of the genus *Shewanella* and description of *Shewanella oneidensis* sp. nov. *International Journal of Systematic Bacteriology* **49** (2): 705–724.

Wagner, M., and Horn, H. (2017) Optical coherence tomography in biofilm research: A comprehensive review. *Biotechnology and Bioengineering* **114** (7): 1386–1402.

Wang, D., Pan, J., Xu, M., Liu, B., Hu, J., Hu, S., *et al.* (2021) Surface modification of *Shewanella oneidensis* MR-1 with polypyrrole-dopamine coating for improvement of power generation in microbial fuel cells. *Journal of Power Sources* **483:** 229220.

Wang, F., Craig, L., Liu, X., Rensing, C., and Egelman, E.H. (2023) Microbial nanowires: type IV pili or cytochrome filaments? *Trends in Microbiology* **31** (4): 384–392.

Wang, F., Gu, Y., O'Brien, J.P., Yi, S.M., Yalcin, S.E., Srikanth, V., *et al.* (2019) Structure of microbial nanowires reveals stacked hemes that transport electrons over micrometers. *Cell* **177** (2): 361-369.

Wang, L.-Y., Nevin, K.P., Woodard, T.L., Mu, B.-Z., and Lovley, D.R. (2016) Expanding the diet for DIET: Electron donors supporting direct interspecies electron transfer (DIET) in defined co-cultures. *Frontiers in Microbiology* **7:** 236.

Wang, N., and Wu, X.S. (1997) Preparation and characterization of agarose hydrogel nanoparticles for protein and peptide drug delivery. *Pharmaceutical Development and Technology* **2** (2): 135–142.

Weiland, P. (2010) Biogas production: current state and perspectives. *Applied Microbiology and Biotechnology* **85** (4): 849–860.

Wentland, E.J., Stewart, P.S., Huang, C.T., and McFeters, G.A. (1996) Spatial variations in growth rate within *Klebsiella pneumoniae* colonies and biofilm. *Biotechnology Progress* **12** (3): 316–321.

Wichterle, O., and Lím, D. (1960) Hydrophilic gels for biological use. *Nature* **185** (4706): 117–118.

Wingender, J., Neu, T.R., and Flemming, H.-C. (1999) What are bacterial extracellular polymeric substances? In *Microbial Extracellular Polymeric Substances:* Springer, Berlin, Heidelberg, pp. 1–19.

Xiao, Y., Zhang, E., Zhang, J., Dai, Y., Yang, Z., Christensen, H.E.M., *et al.* (2017) Extracellular polymeric substances are transient media for microbial extracellular electron transfer. *Science Advances* **3** (7): e1700623.

Xu, K.D., Stewart, P.S., Xia, F., Huang, C.T., and McFeters, G.A. (1998) Spatial physiological heterogeneity in *Pseudomonas aeruginosa* biofilm is determined by oxygen availability. *Applied and Environmental Microbiology* **64** (10): 4035–4039.

Xu, S., Jangir, Y., and El-Naggar, M.Y. (2016) Disentangling the roles of free and cytochrome-bound flavins in extracellular electron transport from *Shewanella oneidensis* MR-1. *Electrochimica Acta* **198:** 49–55.

Yang, H., Zhou, M., Liu, M., Yang, W., and Gu, T. (2015a) Microbial fuel cells for biosensor applications. *Biotechnology Letters* **37** (12): 2357–2364.

Yang, N., Hafez, H., and Nakhla, G. (2015b) Impact of volatile fatty acids on microbial electrolysis cell performance. *Bioresource Technology* **193:** 449–455.

Yang, Y., Hu, H., Zhou, C.-H., Xu, S., Sebo, B., and Zhao, X.-Z. (2011) Novel agarose polymer electrolyte for quasi-solid state dye-sensitized solar cell. *Journal of Power Sources* **196** (4): 2410–2415.

Yu, Y.Y., Wang, Y.Z., Fang, Z., Shi, Y.T., Cheng, Q.W., Chen, Y.X., *et al.* (2020) Single cell electron collectors for highly efficient wiring-up electronic abiotic/biotic interfaces. *Nature Communications* **11** (1): 1–10.

Yu, Y.-Y., Chen, H.-L., Yong, Y.-C., Kim, D.-H., and Song, H. (2011) Conductive artificial biofilm dramatically enhances bioelectricity production in *Shewanella*-inoculated microbial fuel cells. *Chemical Communications* **47** (48): 12825–12827.

Yu, Z., Leng, X., Zhao, S., Ji, J., Zhou, T., Khan, A., *et al.* (2018) A review on the applications of microbial electrolysis cells in anaerobic digestion. *Bioresource Technology* **255:** 340–348.

Zacharoff, L., Chan, C.H., and Bond, D.R. (2016) Reduction of low potential electron acceptors requires the CbcL inner membrane cytochrome of *Geobacter sulfurreducens*. *Bioelectrochemistry* **107:** 7–13.

Zajdel, T.J., Baruch, M., Méhes, G., Stavrinidou, E., Berggren, M., Maharbiz, M.M., *et al.* (2018) PEDOT:PSS-based multilayer bacterial-composite films for bioelectronics. *Scientific Reports* **8** (1): 1–12.

Zarrintaj, P., Manouchehri, S., Ahmadi, Z., Saeb, M.R., Urbanska, A.M., Kaplan, D.L., and Mozafari, M. (2018) Agarose-based biomaterials for tissue engineering. *Carbohydrate Polymers* **187:** 66–84.

Zhang, Y., and Angelidaki, I. (2014) Microbial electrolysis cells turning to be versatile technology: recent advances and future challenges. *Water Research* **56:** 11–25.

Zhang, Y., Ng, C.K., Cohen, Y., and Cao, B. (2014) Cell growth and protein expression of Shewanella oneidensis in biofilms and hydrogel-entrapped cultures. *Molecular BioSystems* **10** (5): 1035–1042.

Zitomer, D.H., and Shrout, J.D. (1998) Feasibility and benefits of methanogenesis under oxygen-limited conditions. *Waste Management* **18** (2): 107–116.

6 APPENDIX

6.1 Supplementary tables

Table S1: Total current over 24 h for short-term experiments regarding *S. oneidensis* biofilms. The current is given without normalization to the surface area of the electrode (16 cm^2).

experiment	**total current [mA after 24 h]**			**mean**	**deviation**
	replicate 1	replicate 2	replicate 3		
cell densities					
0.79 x 10^7	0.15	0.15	0.13	0.14	0.01
1.99 x 10^7	0.23	0.23	0.22	0.23	0.00
3.98 x 10^7	0.26	0.31	0.24	0.27	0.03
5.98 x 10^7	0.43	0.39	0.34	0.39	0.04
7.97 x 10^7	0.40	0.40	0.39	0.40	0.01
gel height					
1.25 mm	0.61	0.59	0.44	0.55	0.08
2.50 mm	0.40	0.63	0.57	0.53	0.10
3.75 mm	0.26	0.34	0.41	0.34	0.06
5.00 mm	0.26	0.31	0.24	0.27	0.03
additives					
planktonic control	0.18	0.21	0.31	0.23	0.05
sprayed biofilm, 1.8 %	0.39	0.62	0.46	0.49	0.09
sprayed biofilm, 0 %	0.09	0.09	--	0.09	0.00
poured biofilm	0.40	0.63	0.57	0.53	0.10
sprayed biofilm 1.85 µM riboflavin	1.59	1.37	1.45	1.47	0.09
sprayed biofilm 1.85 µM riboflavin 0.2 % CNFs	1.97	2.24	2.14	2.12	0.11

Table S2: *p*-values for the performed unpaired *t*-test of the current of *S. oneidensis* biofilms regarding the cell number per mL gel (Figure 11, A) in the first 24 h. Values are marked for $p < 0.1$, $p < 0.05$ and $p < 0.01$.

experiment	unpaired *t*-test			
cell number (Figure 11, A)	1.99×10^7	3.98×10^7	5.98×10^7	7.98×10^7
0.79×10^7	1.64×10^{-4}	3.27×10^{-3}	9.33×10^{-4}	1.89×10^{-6}
1.99×10^7		0.099	4.17×10^{-3}	7.41×10^{-7}
3.98×10^7			0.022	2.48×10^{-3}
5.98×10^7				0.774

Table S3: *p*-values for the performed unpaired *t*-test of the current of *S. oneidensis* biofilms with various gel heights (Figure 11, B) in the first 24 h and after different time points for analysis of performance after the initial start-up phase (Figure 16). Values are marked for $p < 0.1$, $p < 0.05$ and $p < 0.01$.

experiment	unpaired *t*-test				
gel height (Figure 11, B)	3.75 mm	2.5 mm	1.25 mm	**experiment after start-up (Figure 16)**	
5 mm	0.206	0.019	8.62×10^{-3}	24 h	0.094
3.75 mm	--	0.071	0.038	48 h	0.044
2.5 mm	--	--	0.866	72 h	0.055
				96 h	0.206

Table S4: *p*-values for the performed unpaired *t*-test of the current of *S. oneidensis* biofilms regarding sprayed, poured and planktonic inoculation (Figure 14, B and Figure 15) as well as improved hydrogels with riboflavin, CNFs or *G. sulfurreducens* as additives (Figure 18). Values are marked for $p < 0.1$, $p < 0.05$ and $p < 0.01$.

experiment / **additives (Figure 14, B; Figure 15; Figure 18)**	unpaired *t*-test					
	sprayed biofilm, 1.8 %	sprayed biofilm, 0%	poured biofilm	sprayed biofilm riboflavin	sprayed biofilm riboflavin CNFs	sprayed biofilm *Geobacter* addition
planktonic control	0.027	0.057	0.018	7.72×10^{-5}	2.68×10^{-5}	0.012
sprayed biofilm, 1.8 %	--	0.018	0.692	4.42×10^{-4}	9.14×10^{-5}	0.018
sprayed biofilm, 0 %			0.015	4.77×10^{-4}	2.73×10^{-4}	9.57×10^{-3}
poured biofilm	--		--	5.47×10^{-4}	1.05×10^{-4}	0.019
sprayed biofilm riboflavin	--		--	--	3.10×10^{-3}	0.132
sprayed biofilm riboflavin CNFs	--	--	--	--	--	0.593

Table S5: *p*-values for the performed unpaired *t*-test of the conductivity of the agarose hydrogel with various additives. (Figure 17). Values are marked for $p < 0.1$, $p < 0.05$ and $p < 0.01$.

experiment **conductivity (Figure 17)**	unpaired *t*-test		
	1.8 % agarose	1.8 % agarose riboflavin	1.8 % agarose riboflavin CNFs
0 % agarose	0.079	0.068	0.027
1.8 % agarose	--	0.939	0.071
1.8 % agarose riboflavin	--	--	0.054

Table S6: Total current over 72 h for experiments regarding *S. oneidensis* and *G. sulfurreducens* biofilms (Figure 19). The current is given without normalization to the surface area of the electrode (16 cm^2). For Figure 20 the mean current density was calculated after 24 h as well and the values are marked with * accordingly.

experiment	**total current [mA after 72 h]**			**mean**	**deviation**
	replicate 1	replicate 2	replicate 3		
planktonic control	5.54	7.15	--	6.35	0.81
sprayed biofilm, argon atmosphere	3.43	5.52	2.86	3.94	1.15
sprayed biofilm, argon atmosphere (start-up)	1.96*	3.39*	1.87*	2.41*	0.70*
sprayed biofilm anoxic atmosphere	3.54	2.41	--	2.97	0.56
poured biofilm	2.76	3.09	--	2.93	0.17
sprayed biofilm riboflavin, CNFs	2.32	3.40	2.13	2.62	0.56
sprayed biofilm acetate addition	1.83	--	--	--	--

6.2 MEC performance of abiotic hydrogel with riboflavin

The addition of riboflavin to the biomaterial resulted in an increase in current density compared to the biomaterial without riboflavin (Figure 18). To exclude the possibility that current production due to abiotic electron transfer from riboflavin towards the electrode contributed to this increase, a negative control with an abiotic hydrogel with no cells but the same amount of riboflavin was performed. No positive current could be measured over 48 h of MEC operation which underlines that the positive impact of riboflavin is not due to an abiotic reaction.

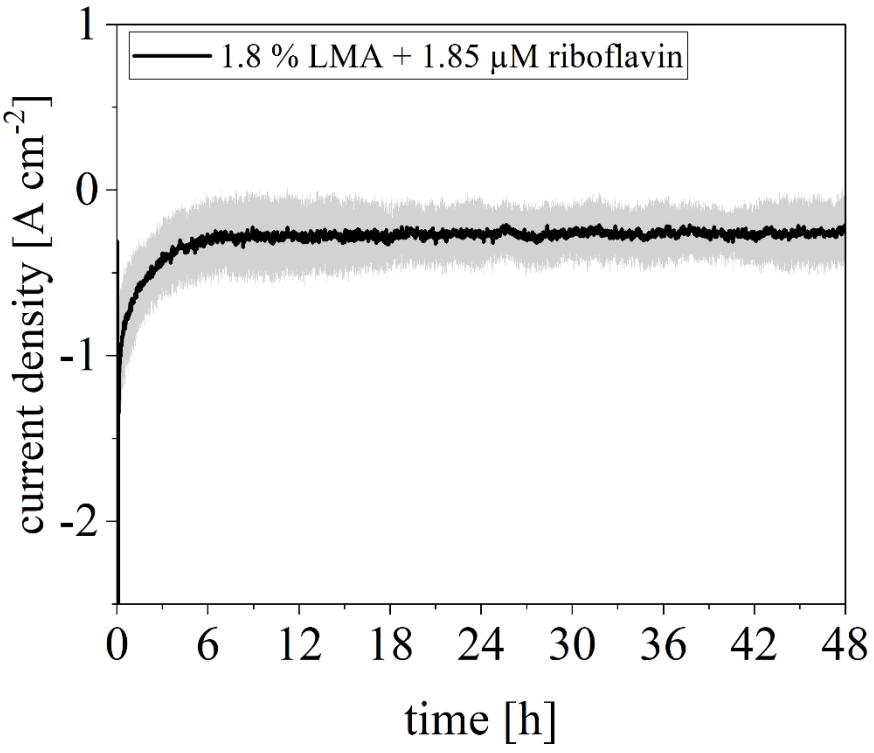

Figure S1: Current density of abiotic hydrogel (1.8 % low melt agarose, LMA) with 1.85 µM riboflavin. After 48 h of MEC operation, no positive current was monitored. Therefore, no abiotic electron transfer from riboflavin towards the electrode took place and the positive impact of riboflavin on the current production (Figure 18) of the biomaterial is not due to an abiotic effect.

6.3 Establishment of active biogas community

As mentioned in section 2.1.5.1, a biogas producing community was established as part of this thesis. After about 4 weeks, stable biogas production was observed. Given below is an excerpt from the gas analysis of this active community over 800 h including one feeding event (Figure S2). This confirmed that an active biogas community could be established with a gas production rate of about 11 mL h^{-1} and a CH_4 to CO_2 ratio of about 60 to 40.

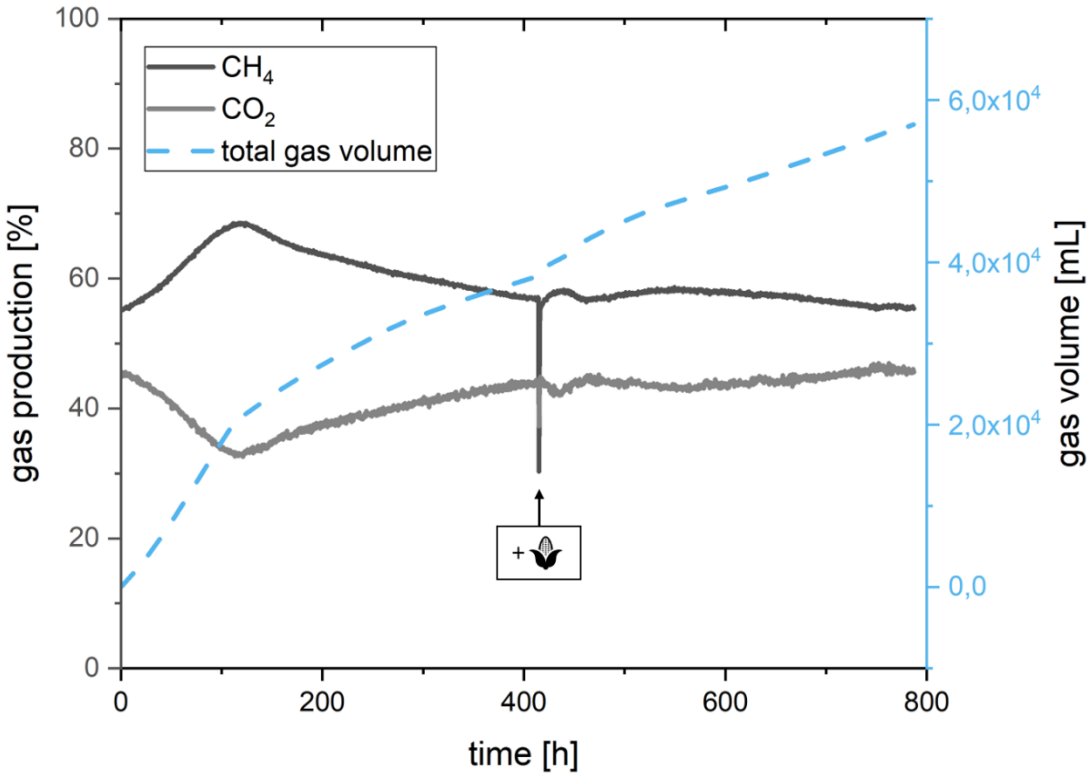

Figure S2: Biogas production of active biogas community. An excerpt of gas analysis including gas production ratio of CO_2 and CH_4 and gas volume is shown including one feeding event (maize symbol). Gas production was verified with a production rate of about 11 mL h^{-1} and a CH_4 to CO_2 ratio of about 60 to 40 for this time period.

6.4 **Detachment of biomaterial – OCT and video time lapse**

To visualize the detachment process of the biomaterial from the graphite felt and the graphite plate, a time-lapse video was recorded. The corresponding detachment videos are available at the following DOI: https://doi.org/10.15480/882.8701.

ACKNOWLEDGMENTS

"If I have seen further, it is by standing on the shoulders of giants." Isaac Newton

Even though during endless (especially late-evening) lab work you sometimes think that the doctoral thesis is the biggest solo project you have ever started, this work has been made possible mainly by the support of so many great people.

First of all, dear Johannes, I would like to thank you! Thank you for your unconditional support over the last 3 ¾ years, for the idea of the sprayable biofilm and your confidence and trust that I would somehow get it implemented, your patience during my countless train journeys, the opportunities to go out in the world to present my research and of course for your scientific input, which always provided the right impetus to push my work forward! And in the end, thank you for dragging me to Hamburg with you.

Dear AG Gescher! You are the greatest bunch of people I could have imagined for this time. The support, the backing and the friendship cannot be taken for granted and I am infinitely grateful that I was allowed to share this time with you.

To my MJLK'N office: you guys have been awesome and each and every one of you has grown way too close to my heart!

Janek, thanks for the original Biber Brüder, the most instructive and best project partner-/friendship I can imagine, your wacky pirate music taste, excursions to farms with minimal preparation from our side and your disposition, which in the end survived every single stupid saying on my part.

Lukas, thank you for calling out my (and your) bullshit talk, your enthusiasm for science, the exciting discussions about literally everything, your legendary birthday party, the "let's jump into the harbor basin" action, your incredibly clear, detached, endlessly funny manner and your friendship! And thank you for proofreading this thesis as quickly and helpfully as humanly possible!

Kerstin, thank you for the unexpected, best roomie I couldn't have wished for better! Thank you for the most relaxed morning routine in the world, the shared enthusiasm for yoga, your

“innere Mitte” while searching for exactly that together, for Momo and Michi, for several successful Big City Wednesdays and simply you!

Niko, thank you for your late but completely successful arrival in Team Biber, for your patience when the duo became an unbeatable trio, your super-nice manner and the indispensable image of you chilling at home with your milk carton.

Laura, thank you for your humor, for the shared hatred of the cold and for the discussions about everything and anything. Jonas, thank you for game nights, your music taste including the infamous “Brüllschal” and for opening your family home to us. Miri, thank you for helping me so much in the first months in the lab, for not getting annoyed by my questions and for your productive, sometimes chaotic energy. Leonie, thank you for being the organized, enthusiastic engineer that you are, and for sharing chaotic trips to Lübeck and elsewhere with me. René, thank you for sharing science and sauna/yoga enthusiasm in equal measure. Edi, thank you for your wonderful nature and for being such an amazing co-author. Benni, thank you for the retreat discussions and your unconventional, funny manner. Carmen, thank you for your scientific and bubbly energy. Petra, thank you for being such an incredibly helpful and kind soul. Sigi, thank you for the short but wonderful lab-cooperation, for always having everyone's back and for your sense of humor, with which you managed to keep the chaotic bunch of us under control.

I would also like to thank all the students I had the pleasure of supervising for their help in the lab. Special thanks to Emely, Vivi and Su-Bin, who luckily all came back in one way or another. Thank you so much! Many thanks also to my cooperation partners from KIT, ZSW and UVT Bremen.

Many, many thanks to everyone outside the lab who not only put up with my sometimes deeply stressed nature, but also did everything they could to get me through this time. A special thank you to my Knittelsheimer crew for more than 20 years of friendship! Thank you for every chaotic trip, for your unbelievable willingness to visit me up here as often as possible, and for the fact that we have been together for so long, cheering each other on no matter where we are. You are incredible! Mailin, thank you for the amazing friendship that has fortunately grown out of the shortest time anyone has ever lived together, for the endless

long-distance support after I moved up north, for our trip to Italy, for every laugh in the silliest situations and so much more! I am so lucky to have you. Phillip, thank you for your support, especially at the beginning of this thesis, your humor and taste in music, and for sharing the chaotic life of a doctoral student in a similar but different situation.

Last but not least, a massive thank you to my family! Daniel, thank you for sharing science between chemist and biologist (and annoying everyone at family dinners with discussions about it), for your endless, very inspiring enthusiasm for new hobbies, for sharing music and for being a fantastic brother. Anika, thank you for your incredibly nice and kind nature and your laugh. I'm happy to call you part of our family. Special thanks to my parents for always having my back and giving me the best support network anyone could ask for. Thank you, Dad, for sharing your wisdom and your wine in equal parts and showing me how to keep a cool head in almost any situation. Thank you, Mum, for your endless support, your warm understanding and just the right amount of sympathetic chaotic-ness that I was lucky enough to inherit from you. You both, more than anyone, have made me who I am and I am so grateful for your support and love!